Dissertation

submitted to the

Combined Faculties for the Natural Sciences and for Mathematics

of the Ruperto-Carola University of Heidelberg, Germany

for the degree of

Doctor of Natural Sciences

Presented by

M.Sc. Mircea Tric

Born in Temeschwar

Oral-examination: 24.10.2017

Optical in-line biosensor for long-term continuous glucose monitoring and control in cell culture

Referees: Prof. Dr. Stefan Wölfl   (1. supervisor)

Prof. Dr. Tobias Werner   (2. supervisor)

Abstract

Monitoring important process variables such as glucose in real-time is a major goal of bioprocess engineering, because it allows process control, which is not only essential for product quality and yield, but also important for the documentation and understanding of the production process and therefore relates to risk management [1].

This thesis deals with the development, thorough characterization and application of a disposable, optical in-line biosensor for monitoring and control of glucose in suspension cell culture. The in-line sensor, developed in this thesis, utilizes a commercially available oxygen sensor, that is coated with a crosslinked glucose oxidase (GOD) enzyme layer. The sensitivity of the sensor was tuned by the addition of a hydrophilic perforated diffusion membrane, to customize the dynamic range in order to meet the desired specifications. The biosensor was modelled in order to gain crucial insights into the internal concentration profile of the enzyme deactivating by-product hydrogen peroxide. The one-dimensional biosensor model revealed that the turnover rate of the enzyme GOD plays a crucial role for the functional stability of the biosensor in combination with the internal hydrogen peroxide accumulation. This insight was utilized to optimize the glucose biosensor for long-term continuous glucose monitoring over typical cell culture durations. A comprehensive biosensor characterization was performed to study the applicability and limitations of the developed biosensor for cell culture. Hereby, it was demonstrated that the sensor is sterilisable with beta, gamma and UV irradiation and is only subject to minor cross sensitivity to oxygen in combination with a reference oxygen sensor.

The presented optical biosensor provides information in real-time and was therefore used in combination with a reference oxygen sensor to control the glucose level continuously in CHO cell culture with an automated feeding systems. It was found that the sialylation of the hyperglycosylated erythropoietin analog Darbepoetin alfa, could be significantly increased through continuous glucose feeding by retaining a high glucose level during the production phase of the cell culture. Therefore, the developed biosensor provides a valuable tool for optimizing culture conditions in biotechnological applications.

Zusammenfassung

Die Überwachung von wichtigen Prozess-Variablen (z.B. Glukose) in Echtzeit, ist ein bedeutendes Ziel der Bioprozesstechnik. Es erlaubt eine lückenlose Prozesskontrolle, die nicht nur für die Produktqualität und Produktausbeute essentiell ist, sondern auch für die Dokumentationsanforderungen und das Verstehen des Produktionsprozesses. Somit ist es auch für das Risikomanagement relevant [1].

Diese Dissertation beschäftigt sich mit der Entwicklung und umfassenden Charakterisierung, sowie Anwendung eines optischen 'in-line' Biosensors für die Messung und Regelung von Glukose in Suspensionszellkulturen. Der 'in-line' Sensor basiert auf einem kommerziell erhältlichen Sauerstoffsensor, der mit einer quervernetzten Enzymschicht aus Glukose-Oxidase beschichtet ist. Die Sensitivität und damit der Messbereich des Sensors wurde mittels einer hydrophilen Diffusionsmembran an die jeweilige Messanforderung angepasst. Ein eindimensionales Biosensormodell wurde für die Simulationen entwickelt und ermöglichte einen Einblick in das interne Konzentrationsprofil der Substrate und des toxischen Nebenprodukts Wasserstoffperoxid. Die Modellsimulationen ergaben, dass neben der Wasserstoffperoxid-Konzentration, die Umsatzrate des Enzyms (GOD) eine wesentliche Rolle für die Sensorstabilität spielt. Aufgrund dieser wichtigen Erkenntnis, konnte der Glukosesensor hinsichtlich seiner Funktionsstabilität für die kontinuierliche Glukosemessung für die typische Dauer einer Zellkultur optimiert werden. Des Weiteren konnte gezeigt werden, dass der Sensor mit Beta-, Gamma- und UV-Strahlung sterilisierbar ist und nur eine geringe Querempfindlichkeit zu Sauerstoff aufweist, wenn gleichzeitig ein Referenz-Sauerstoffsensor verwendet wird.

Die Kombination aus einem Biosensor und einem Sauerstoff-Referenzsensor wurde in Zellkulturexperimenten eingesetzt, um den Glukoselevel in Fed-Batch CHO Zellkulturen konstant zu halten. Bei diesen Versuchen zeigte sich, dass die Produktqualität des rekombinanten Produkts Darbepoetin Alfa signifikant verbessert werden konnte, wenn der Glukoselevel auf einem hohen Niveau gehalten wurde. Der entwickelte Glukose-Biosensor stellt somit ein nützliches Werkzeug für die Zellkulturoptimierung im Bereich der Biotechnologie dar.

Table of contents

1   INTRODUCTION

In the biotechnological industry, mammalian cell culture is an important tool for the production of biological therapeutics, such as recombinant proteins, for a variety of applications. A consistent product quality at industrial titers, however, requires tight monitoring and control of crucial environmental parameters during the cell culture process [1–4]. Therefore, the U.S. Food and Drug Administration (FDA) published the Process Analytical Technology (PAT) guidance for industry in 2004 in order to encourage manufacturers to introduce innovative systems that improve the manufacturing process and quality control [4]. In this respect, a "continuous real time quality assurance" is needed to enhance the process understanding and the product quality through timely measurements using on-, in- or at-line sensors [4].

While the in-line measurement of process parameters, such as pH and oxygen, is already state-of-the-art, the continuous monitoring of the important metabolite glucose, remains a challenge [5]. In many cases, the labor intensive and delayed offline measurement of glucose is still the default method [6], since reliable glucose biosensors for long term monitoring applications over the typical cell culture durations have proved to be elusive so far [7]. For single-use bioreactor (SUB) systems, which are emerging in recent years [8], additional requirements are imposed, such as disposability, low cost and non-invasive measurement [9]. Furthermore, the sensors are preferably preinstalled and gamma irradiated in the SUB system [7, 10].

In this thesis, the development of an optical in-line biosensor for continuous long-term glucose monitoring in single-use bioreactors and cell culture plates is described that fulfills the above-mentioned requirements. Furthermore, a comprehensive characterization of the glucose biosensor is outlined and augmented by a one-dimensional computer model that provides insight into the limited biosensor life-time. Finally, the influence of different constant glucose levels and the implication of nutrient availability and waste products on the product quality of Darbepoetin alfa is presented. Therefore, the developed glucose biosensor was applied for continuous glucose monitoring during CHO fed-batch culture to maintain a constant glucose level.

In this introduction, an overview of the applied sensors is given, followed by a description of cell metabolism and cell culture strategies as well as their consequences. Finally, the goals of this thesis are outlined.

1.1 Sensors

Oxygen, pH and glucose levels are of utmost importance for animal cell culture processes and were measured during this work. In following sections, the working principle of the applied pH and oxygen sensors is outlined, followed by the description of the glucose biosensor, which contains either an oxygen or a pH sensor as a transducer.

1.2 Optical oxygen and pH sensors

Luminescence based optical sensors (Figure 1) offer important advantages over electrochemical sensors, because they are flexible, more rugged, easy to miniaturize and are capable of multiplexing [11–13]. In addition, optical sensors can be operated non-invasively through transparent surfaces without contamination risks and are inexpensive, which makes them suitable for single-use applications. Drawbacks, on the other hand, are a non-linear response and photo bleaching [11]. The latter, however, can be overcome by using life-time rather than intensity measurements [14]. Optical sensors are operated with glass fibers or polymer optical fibers (POF), which guide the excitation light to the dye and the fluorescence light back to the detector (e.g. photomultiplier tube) [14].

Figure 1 Optical pH and oxygen sensors

(A) Optical oxygen sensors in different sizes. (B) pH sensors in a 24-well plate. Both figures were kindly provided by PreSens GmbH.

1.2.1 Photoluminescence

In general, photoluminescence is generated when a luminescent molecule is excited through light absorption and subsequently relaxes to the initial unexcited state by emitting energy in form of photons [12]. The optical sensors applied during the course of this thesis entail a photoluminescent dye (luminophore) inside a carrier matrix, which can be excited through absorption of blue or green light from a light-emitting diode (LED). In the absorption process, the luminophore transits from the ground singlet state (S_0) to an excited singlet state (e.g. S_1 or S_2) [12]. This absorption process is illustrated in the Jablonski diagram (Figure 2).
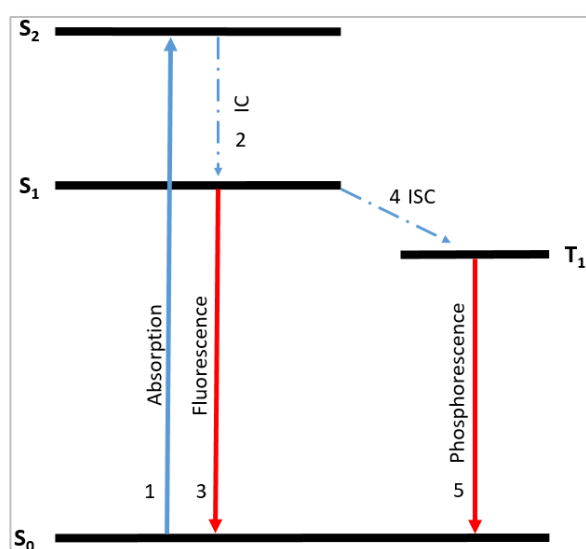
Figure 2 Jablonski diagram

(1) Absorption of excitation light. (2) Internal conversion (IC) between excited molecular states with the same spin quantum number. (3) Fluorescence: Radiative relaxation between states with the same spin quantum number. (4) Inter system crossing (ISC): transition from a singlet to a triplet state. (5) Phosphorescence: Radiative relaxation between states with differing spin quantum number. Figure adapted from literature[11].

Eventually, the excited molecules relax through nonradiative internal conversion, from higher electronic states to the S_1 state by kinetic energy exchange with the surrounding (heat dissipation) [11]. From the S_1 state, the excited molecules can relax to the former ground state S_0 by emission of light, termed fluorescence [12]. Fluorescence occurs with no change in the spin quantum number (multiplicity) and therefore relatively fast (around 10^{-8} s) [12]. Hence, the life-time of fluorescent molecules (the average time the excited molecule remains in the excited state) is very short.

In the case of phosphorescence, a nonradiative intersystem crossing (ISC) from the excited singlet state S_1 to the triplet state T_1 occurs (Figure 2), in which the spin quantum number is changed [11]. In many cases phosphorescent indicators are combined with heavy atoms in a complex to enhance the probability for intersystem crossing (ISC) [12, 15]. The excited molecules emit light during the transition to the ground state, termed phosphorescence. The life-time of phosphorescent dyes (phosphorophores) are much higher (> 10^{-6} s) compared to fluorophores, because the

transition to the ground state requires a spin reverse, which is quantum mechanically prohibited [15]. Because of the long life-time of the excited phosphorophores, non-radiative deactivation processes (quenching) plays an important role and is therefore discussed in the following section.

1.2.2 Photoluminescence based oxygen sensors

Oxygen sensors are needed in the biotechnological industry in order to continuously monitor and control the dissolved oxygen (DO) concentration during cell culture [16]. In contrast to amperometric oxygen sensors such as the Clark electrode, fluorescence based oxygen sensors do not consume oxygen and are easily miniaturized [11]. The oxygen sensitive luminescent dye is embedded in a highly oxygen permeable polymer (e.g. polysiloxane derivatives), which prevents a luminophore leakage and ensures a high oxygen solubility and diffusion rate. Oxygen indicators are for example organometallic complexes (e.g. platinum and palladium porphyrins [12]), which possess a good sensitivity due to a high quantum yield and a long life-time (100-770 µs) [11, 12]. The detection of the oxygen related quenching process, can be performed via intensity or life-time measurement [11].

1.2.2.1 Oxygen sensor principle

In the excited state, the luminophore can be quenched through collision with oxygen in a process called collisional dynamic quenching [11]. The luminophore thereby returns from its excited state to the ground state, while conversely oxygen is transferred from its ground state (triplet $^3O_2$) to the excited state (singlet $^1O_2$) (Figure 3). This non-radiative energy transfer between the two colliding molecules leads to a decrease in luminescence intensity [15]. The mean life-time of a luminophore consist of many excited molecules with varying life-times, of which those with the longest life-time possess the highest quenching probability [14]. Hence, the collisional quenching process affects also the mean life-time of a luminophore. The degree of quenching is described by the Stern-Volmer equation (Equation 1). It displays the correlation between the quencher concentration $[O_2]$ and the luminescence intensity ratio (I_0/I) or decay time ratio (τ_0/τ) between the non-quenched and quenched luminophores.

$$\frac{I_0}{I} = \frac{\tau_0}{\tau} = 1 + K_{SV} \cdot [O_2]$$

Equation 1

K_{SV} describes the overall quenching constant (Stern-Volmer constant), which reflects the sensitivity of the oxygen sensor (see Figure 4). However, the Stern-Volmer equation in its linear form, only applies to luminophores with a homogenous environment. For luminophores embedded in a polymeric film, such as the sensor developed in this thesis, the Stern-Volmer constant varies, which leads to a non-linear relationship [11].
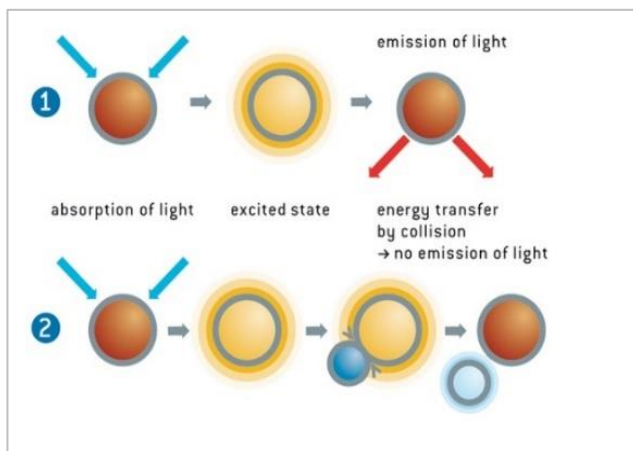
Figure 3 Dynamic quenching process

(1) Excitation and emission of light of a luminophore without oxygen. (2) Dynamic quenching of an excited luminophore through collision with oxygen. Figure 3 was kindly provided by PreSens GmbH.
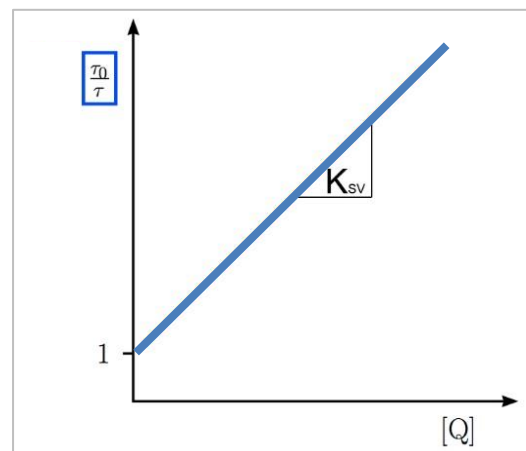
Figure 4 Stern-Volmer plot

Gives the relation between the quencher concentration [Q] and the life-time ratio of luminophores without and with a quencher. Figure 4 was adapted from literature [17].

In the case of the applied oxygen sensor, the luminescence intensity can be used to determine the oxygen concentration according to Equation 1. This approach is however flawed by variations in the intensity and sensitivity of the light source and the detector in addition to varying dye concentrations, caused by leaching and photobleaching [11]. For life-time measurements, ageing light sources and inhomogeneous indicator layers are negligible [11]. Hence, the life-time measurement technique is advantageous and was therefore used during this thesis.

1.2.2.2 Life-time measurement

The life-time of excited luminophores can be measured either in time domain or frequency domain mode [18]. In time domain mode, the emission intensity is measured over time and the decay time is calculated from the intensity slope [12]. In the frequency domain mode, intensity modulated light is used for the excitation of the luminophore. The decay time of the excited luminophore causes a time delay in the emitted light, which results in a detectable phase angle shift between the excitation and the emission light (Figure 5) [12]. The excitation life-time τ is connected to the phase angle θ by the following equation:

$$tan\theta = 2\pi \cdot f_{mod} \cdot \tau \qquad \text{Equation 2}$$

where f_{mod} is the sinusoidal modulated frequency [14]. Equation 2 can be combined with the Stern-Volmer equation (Equation 1), where the decay time is a function of the quencher concentration. This leads to the following expression, through which the wanted oxygen concentration can be derived from the detected phase angle shift:

$$tan\theta = 2\pi \cdot f_{mod} \cdot \frac{\tau_0}{1 + K_{SV} \cdot [O_2]} \qquad \text{Equation 3}$$

The optical sensor is operated with light guided through an optical fiber from a light emitting diode (LED) to the sensor [19]. A digital-analogue converter generates sine modulated voltages that are converted into modulated currents for the LED [19]. The luminophore in the optical sensor is then excited through filters and the luminescence emission is guided back through the optical fiber to a photodiode. The captured signal is then digitized by an analogue-digital converter [19].

Figure 5 Life-time measurement principle

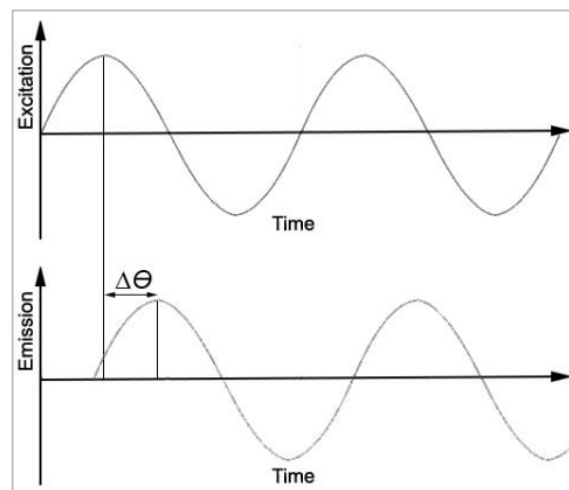*Phase shift ($\Delta\theta$) between the sinusoidal modulated excitation and emission light. The phase shift is measured and can then be converted into the given oxygen partial pressure according to Equation 3. Figure 5 was adapted from literature [20].*

1.2.3 Photoluminescence based pH sensors

Since the first fiber-optic pH sensor was developed by Peterson in 1980 [21], a number of approaches based on the absorption of different pH sensitive dyes ranging from phenol red to bromothymol blue [22, 23] was developed. Today, the most common fiber-optic pH sensors, as the one applied in this thesis, use fluorescent molecules like 1-hydroxypyrene-3,6,8-trisulphate (HPTS) or derivatives of fluorescein as the indicator dye [24].

1.2.3.1 pH sensor principle

Since the life-time of fluorophores is very short (cf. section 1.2.1 Photoluminescence), the phase angle shift measurement of the applied pH indicator dye requires a second (reference) dye with a life-time in the µs range. The reference dye is used to receive a combined total life-time, that is increased compared to the pure indicator dye [19]. The combination of two luminescent dyes, which differ significantly in luminescence life-times, enables an internally referenced measurement with the Dual Lifetime Referencing (DLR) method. The indicator dye is sensitive to the analyte and changes its luminescence property due to protonation or deprotonation, while the reference dye is inert (Figure 6) [19]. The total luminescence life-time is a combination of the life-time of both dyes. The sensitive matrix is excited with sine modulated light through an optical fiber. The emitted light from the luminophores is also a sine function, but its phase angle is shifted due to the emission delay caused by the luminophore life-times (τ) [11]. The DLR method can be applied when a fluorophore and a second luminophore are combined in a matrix such that their absorption and emission bands overlap [19]. In this case, they can be excited and measured at the same wavelength by the same photodetector [19]. While the phase angle shift of the analyte sensitive fluorophore is negligible ($\theta_{Ind} \approx 0$), the inert luminophore provides a significant but constant reference signal (θ_{Ref}) [19]. The intensity of the fluorophore (A_{Ind}) is altered by the analyte, whereas the intensity of the luminophore (A_{Ref}) remains constant [11]. The resulting phase shift is a mixed signal (θ_m), which depends on the intensity ratio of the constant luminophore and the pH sensitive fluorophore [19] (see Equation 4, Figure 7).

$$\cot \theta_m = \frac{A_{Ref} \cdot \cos \theta_{Ref} + A_{Ind}}{A_{Ref} \cdot \sin \theta_{Ref}} = \cot \theta_{Ref} + \frac{A_{Ind}}{A_{Ref} \cdot \sin \theta_{Ref}} \qquad \text{Equation 4}$$
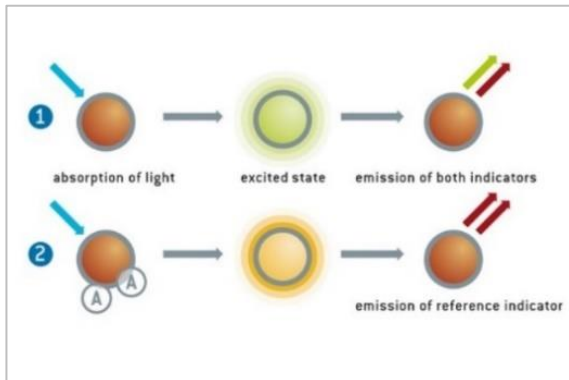
Figure 6 pH sensor principle

(1) Excitation and emission of light by the unprotonated indicator molecule. (2) Excitation and emission of the protonated indicator dye. Figure 6 was kindly provided by PreSens GmbH.
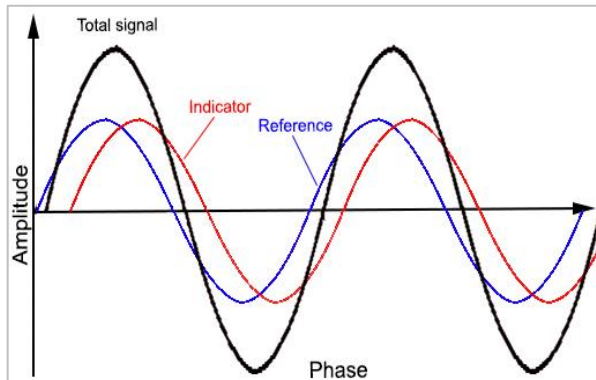
Figure 7 Superposition of indicator and reference amplitude

The final signal results from a superposition of the indicator signal and the reference signal. This graph was adapted from literature [19].

Since the intensity of the fluorophore is analyte dependent, the overall phase angle shift is influenced by the analyte concentration. The DLR method generates a more reliable signal, because it is independent of variations in temperature, the light source or the detector, due to the ratiometric approach [11].

1.3 Glucose biosensors

The term "biosensor" refers to as analytical devices that consist of a biological recognition element (e.g. enzymes, antibodies etc.) which is sensitive to a specific analyte, and a transducer (e.g. electrode, optrode etc.) which translates the resulting recognition event (physico-chemical change) into an electrical signal (see Figure 8) [25].
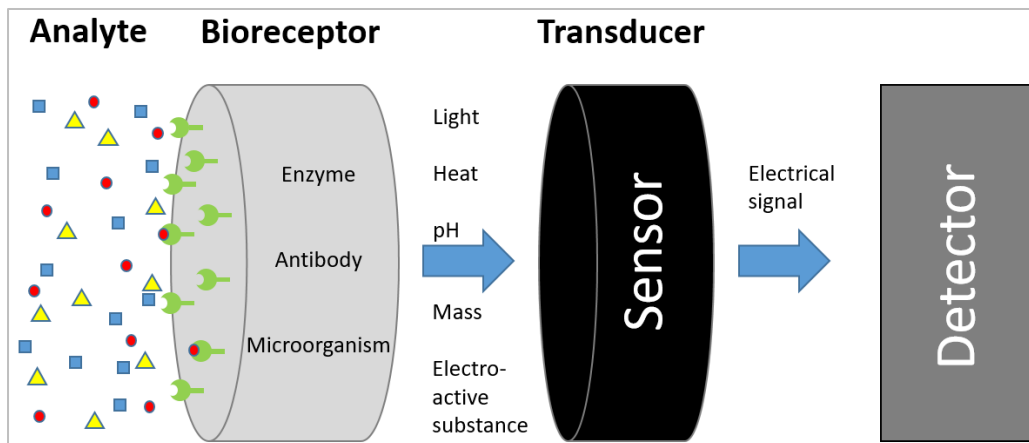
Figure 8 Schematic of a biosensor

The analyte of interest binds to a specific biological recognition element, which triggers physico-chemical change that is translated into an electrical signal by the underlying transducer. Figure 8 was adapted from literature [15].

Since the invention of the first biosensor by Leyland C. Clark in 1962 [13], amperometric biosensors have been the predominant sensor type, especially in the field of glucose measurement, whereas optical techniques found their niche rather in research and development [25]. By 2013, the biosensor market was already worth over 13 billion US dollars with 85 % of the world biosensor market share covered by glucose biosensors [25]. Because the number of cases and the prevalence of diabetes has been steadily increasing [26], it is reasonable to assume, that the glucose biosensor market value will increase further in the future [25, 27]. Besides medicine, biosensors have also found their application in environmental monitoring and defense, as well as food and process control [25, 28]. Because of their high portability, low cost, ease of use and possibility to be miniaturized, biosensors gained ground compared to classical analytical methods and are important for *in situ* continuous monitoring [29].

Biosensors display a good sensitivity and specificity due to the biological receptor [30]. A classic example for a potent bioreceptor is the enzyme glucose-oxidase (GOD), which was already used by Leland C. Clark in order to manufacture the first electrochemical biosensor [25]. In current research, GOD is still the preferred enzyme over glucose dehydrogenase [13, 31], due to its unique features, which are discussed in detail in the next section.

1.3.1 Glucose-oxidase

Glucose-oxidase (ß-D-glucose: oxygen 1-oxidoreductase, EC 1.1.3.4) was first isolated in Aspergillus niger [31], but can also be found in some insects, where the accumulation of hydrogen peroxide serves as an anti-bacterial and anti-fungal agent [32]. In the food industry, it is used where the presence of oxygen can pose a threat on taste and shelf life (e.g. mayonnaise) [32], as well as for the production of gluconic acid [31]. Furthermore, it is widely applied for D-glucose determination in fermentation processes, and as a diagnostic agent for the determination of blood glucose levels in medicine [28, 32]. Because of the outstanding stability of immobilized GOD (over 95% after 16 months [33]), the enzyme is utilized in most glucose biosensors.

The glycoprotein consists of two homodimeric subunits with the coenzyme flavin adenine dinucleotide (FAD) that is utilized as an electron carrier [34]. The coenzyme FAD is noncovalently bound at the active site [32]. The molecular weight is reported to fall in the range of 155.000 ± 5000 Da of which 10-17 % (w/w) are carbohydrates [34]. Glucose-oxidase belongs to the oxidoreductases and utilizes oxygen as the natural electron acceptor in the specific oxidation of ß-D-glucose to D-glucono-δ-lactone [31]. The reaction can be divided into two steps. First, a reductive step, where the substrate is oxidized and the enzyme is reduced, and then a second step, where GOD is oxidized into its initial form. This process is described in the following equations:

$$\text{ß-D-Glucose} + \text{GOD-FAD} \rightarrow \text{ß-D-Glucono-δ-lactone} + \text{GOD-FADH}_2 \quad \text{Equation 5}$$

$$\text{GOD-FADH}_2 + O_2 \rightarrow \text{GOD-FAD} + H_2O_2 \quad \text{Equation 6}$$

$$\text{ß-D-Glucono-δ-lactone} + H_2O \rightarrow \text{Gluconic acid} \quad \text{Equation 7}$$
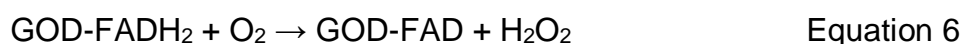
GOD-FAD and GOD-FADH$_2$ refer to the oxidized and reduced glucose oxidase, respectively. Gluconic acid and H$_2$O$_2$ are by-products of the reaction, of which hydrogen peroxide is an enzyme-deactivating agent, compromising the enzyme stability [35, 36]. Hydrogen peroxide is a strong oxidizer at low pH and decomposes into hydroxyl radicals (*OH). Therefore, it is toxic to biological active compounds like enzymes or cells, if it occurs in high concentrations [37]. It is suggested that the

irreversible inactivation of the glucose oxidase due to hydrogen peroxide, involves the modification of certain methionine residues located at or near the active site [37]. Interestingly, a strong inhibition of glucose oxidase only occurs, if glucose is present and thus the enzyme is in its reduced state [35]. This phenomenon is attributed to the conformational change of the enzyme in its reduced state, which exposes oxidation sensitive methionine to hydrogen peroxide [34, 35].

The reaction product D-glucono-δ-lactone hydrolyzes spontaneously to gluconic acid and thereby reduces the pH [31]. The pH optimum for GOD is reported to be around pH 5-6 [38]. The decomposition of hydrogen peroxide occurs very slowly [32], but can be enhanced dramatically by the catalytic activity of the enzyme catalase (see Equation 8), which is usually contained in GOD powder as an impurity:

$$2\ H_2O_2 \rightarrow 2\ H_2O + O_2 \qquad\qquad \text{Equation 8}$$

The enzyme kinetic can be described by the Michealis-Menten equation [39]:

$$R_i = \frac{V_{max}}{(1+\frac{K_G}{G}+\frac{K_O}{O})} \qquad\qquad \text{Equation 9}$$

where G and O are the concentration of glucose and oxygen, respectively. K_G and K_O represent the Michaelis-Menten constants for glucose and oxygen. V_{max} denotes the maximum reaction velocity and R_i the enzyme velocity at given glucose and oxygen concentrations.

Two different glucose sensor types are established in biotechnological processes that rely on GOD as the biological recognition element. The most widely used sensor type is the electrochemical sensor, followed by the optical sensor [13]. Both sensor types, as well as their advantageous and drawbacks are presented in the following sections.

1.3.2 Amperometric glucose biosensors

The invention of the first oxygen electrode by Leland C. Clark in 1954 [40] laid the foundation for the development of the first glucose biosensor introduced by Clark and Lyons in 1962 [41]. This biosensor used GOD in combination with a Clark electrode (a platinum cathode with a negative potential versus a Ag/AgCl electrode) that measured the oxygen consumption according to the following equation [41, 42]:

$$O_2 + 4H^+ + 4e^- \rightarrow 2H_2O \qquad \text{Equation 10}$$

Later, an anodic method (platinum electrode at +0.6 V versus a Ag/AgCl electrode) was established in order to measure the hydrogen peroxide production rather than the oxygen consumption [41]:

$$H_2O_2 \rightarrow O_2 + 2H^+ + 2e^- \qquad \text{Equation 11}$$

Since then, glucose biosensors have been steadily improved. While in the first biosensor generation, oxygen was employed as the electron acceptor (Figure 38), it was replaced by an artificial mediator (e.g. ferricyanide) in the second-generation [32].
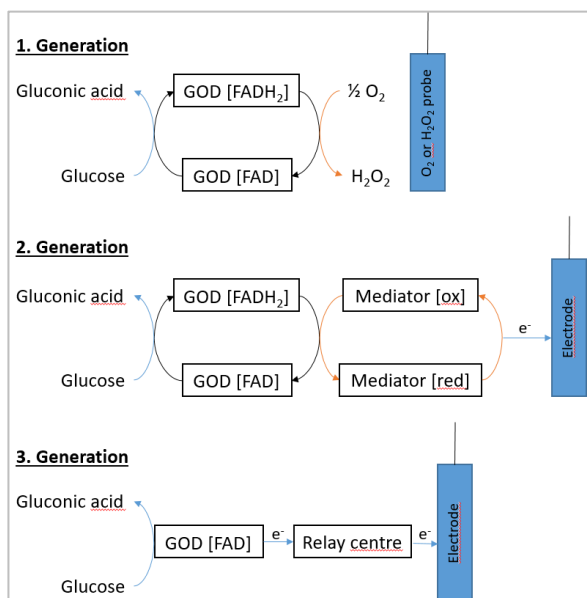
Figure 9 Overview of the amperometric glucose biosensor development

A constant potential is applied and a current is measured, which is proportional to the analyte concentration. Figure 9 was adapted from literature [41]

The mediator shuttles electrons between the electrode and the FAD center of the enzyme to overcome the oxygen limitation problem and to minimize the interference from other chemical species [32]. Despite this improvement, interferences and leakage of the toxic mediators remained an issue [43] which spurred the development of a third generation of glucose biosensors, which is subject of current research. Here, the electrons are directly transferred from the enzyme to the electrode (e.g. via carbon nanotubes) [31].

While the selectivity improved in the third biosensor generation, due to a reduction of the operating potential, the challenge of establishing an efficient direct electron transfer route still remains [41]. Electrochemical sensors offer a fast response time and a wide dynamic range, but feature some characteristic drawbacks like electromagnetic interference [44]. Fiber optic biosensors represent an alternative to amperometric sensors and are discussed in the following section.

1.3.3 Optical glucose biosensors

An alternative to amperometric biosensors are optical enzymatic biosensors, that rely on a measurable change of a luminescent dye upon interaction with an enzymatic substrate or product. Optical glucose biosensors offer considerable advantages over amperometric biosensors, since optical sensors can be operated non-invasively through a transparent surface, which is an important feature to avoid contamination risks. In addition, the biosensor signal of optical sensors is not influenced by an electrode drift [45].

The most common optical sensing methods involve the measurement of the oxygen consumption or the pH change due to gluconic acid production [11]. Both optical biosensor types are described in more detail in the following sections.

1.3.3.1 Oxygen consumption based optical glucose biosensor

In this section, optical glucose biosensors that are based on the measurement of the oxygen consumption in the sensor are introduced. The biosensor consists of an optical oxygen transducer that is coated with an GOD crosslinked enzyme layer and covered by a thin diffusion layer (see Figure 10). The diffusion layer separates the enzyme layer from the sample and its permeability determines the diffusion rate of glucose and oxygen into the biosensor [5]. Glucose and oxygen are consumed in the enzyme layer to gluconic acid and hydrogen peroxide according to Equation 5 to Equation 7. The oxygen consumption is tracked by the optical transducer, which is sensitive to the oxygen partial pressure inside the biosensor. The diffusion rate of glucose and oxygen through the diffusion layer determines the dynamic range of the biosensor [5]. Since the diffusion rate is influenced by the diffusion gradient, the response of the glucose biosensor depends on the glucose and the oxygen level in the sample [5]. The signal is inversely proportional to the glucose concentration and directly proportional to the

oxygen level in the sample [5]. Optical glucose biosensors suffer from cross sensitivity to oxygen, which requires an additional oxygen reference sensor under fluctuating oxygen conditions [46]. A typical configuration of an optical biosensor in combination with a reference oxygen sensor is illustrated in Figure 10. The resulting signal (ΔpO_2) is the difference in partial pressure between the oxygen reference signal and the signal from the oxygen transducer in the glucose biosensor (see Figure 11).
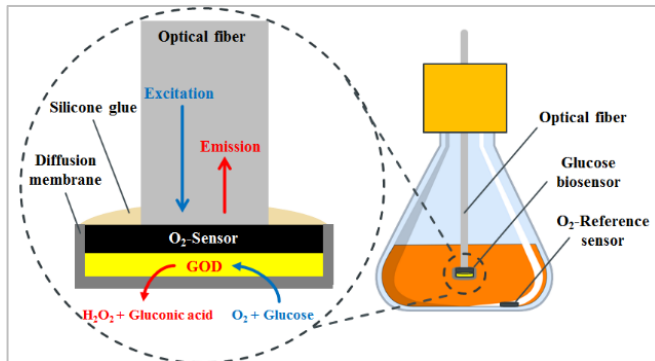
Figure 10 Optical glucose biosensor scheme

The oxygen probe acts as a transducer for the enzyme glucose oxidase. The enzyme GOD is immobilized on top of the oxygen probe and covered by a thin diffusion layer which tunes the dynamic range. Figure 10 was attained from literature [5].
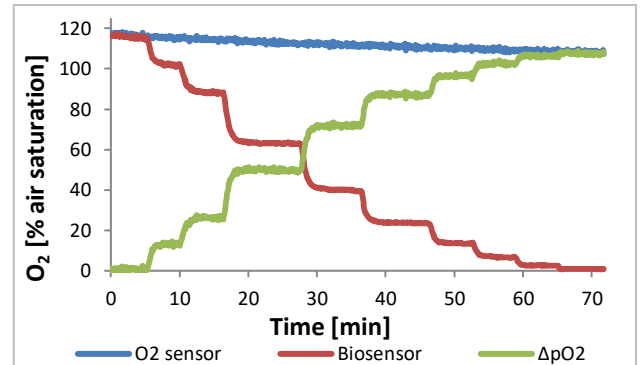
Figure 11 Biosensor signal

Measurement signal of a glucose biosensor and an oxygen reference sensor including the resulting signal difference (ΔpO_2).

1.3.3.2 pH based glucose biosensor

In this section, optical glucose biosensors that are based on the measurement of the pH change inside the biosensor are introduced.

A fluorescent pH sensitive transducer, as described in section 1.2.3 (Photoluminescence based pH sensors), can be utilized to build a glucose biosensor, when coated with an GOD enzyme layer that converts glucose into a weak acid according to Equation 5 to Equation 7 [5]. Therefore, the glucose level is measured indirectly through the pH change inside the biosensor [11]. This method requires a low capacity buffer environment [13] and is cross sensitive to pH [11], which is rather unsuitable for cell culture.

1.4 Non-enzymatic optical glucose sensors

Enzymatic biosensors offer a high selectivity and sensitivity because of the biological recognition element [28], but suffer on the other hand from drawbacks related to the enzyme stability [13, 40, 47]. Much work has therefore been devoted in the past, in order to develop stable non-enzymatic sensors for continuous glucose monitoring that rely on synthetic materials [40, 48]. In the following sections, a short overview of non-enzymatic glucose biosensors is given with respect to advantages and disadvantages.

1.4.1 Affinity binding sensors

The working principle of affinity based optical glucose sensors, relies on changes in luminescence due to a recognition event between glucose and e.g. a glucose binding protein (GBP) [49]. For this purpose, the GBP can be labelled with a fluorophore (e.g. (6-bromo-acetyl-2-dimethylaminonaphthalene (Badan)) close to the glucose binding site, which is sensitive to changes in polarity [50]. The consequence of the glucose binding event is a conformational change of GBP, which alters the polarity in the environment of the fluorophore and thus enables the detection of glucose [49]. In contrast to enzymes like GOD, GBPs do not oxidize the glucose molecule [13]. Hence, this sensing method neither consumes glucose nor oxygen, and is therefore not influenced by varying ambient oxygen levels. GBP based sensors proved to be fairly specific to glucose, but cover only a low dynamic range, unless the GBP is genetically modified [13, 50].

Another approach, uses concanavalin A (Con A), which binds to carbohydrates [51]. The measurement principle relies on the competitive binding between glucose and a labelled carbohydrate like dextran [13]. Therefore, the described sensing method is not influenced by varying ambient oxygen levels. However, Con A is toxic, not very specific to glucose and the sensor signal is described to be only slowly reversible [13].

1.4.2 Chemically binding sensors

Boronic acid sensors, which represent chemically binding sensors, utilize boronic acid as a molecular receptor that is capable of reversible binding to cis-1,2 diols like in glucose [40]. The resulting covalent complex is a ring cyclic ester. The boronic acid

undergoes thereby a conformational transformation from a trigonal to an anionic tetrahedral form [13]. This leads to a change in the pka of boronic acid and consequently the optical property of an attached luminophore, which can be utilized to detect the glucose concentration [13]. The advantages of the boronic acid sensor is a non-invasive measurement, with no influence from varying oxygen levels. The drawbacks on the other hand are reported to be a low selectivity for glucose over other sugars, as well as a strong pH dependency [13].

1.5 Analyte determination during cell culture

Different methods can be applied to analyze a cell culture sample. Samples can be extracted for off-line or at-line analyzation, which however bears a potential contamination risk. Alternatively, a direct analysis in real-time through on-line or in-line sensors can be applied. The on-line measurement is performed by either continuous automated sampling or by means of a bypass, in which the sample analysis is performed. For in-line analysis, the sample is measured by an integrated system (e.g. pH sensor) [4]. On-line and in-line sensors offer many advantages, because sampling steps are obsolete and automated process control becomes possible in real-time.

1.6 Cell metabolism

The most important carbon energy sources for cells are glucose and glutamine. In this section, the metabolism of both nutrients is discussed.

1.6.1 Glucose metabolism

Glucose enters the cytosol through glucose transporters and is metabolized in the glycolysis pathway, where it is converted to pyruvate via a series of metabolic reactions outlined in Figure 12.
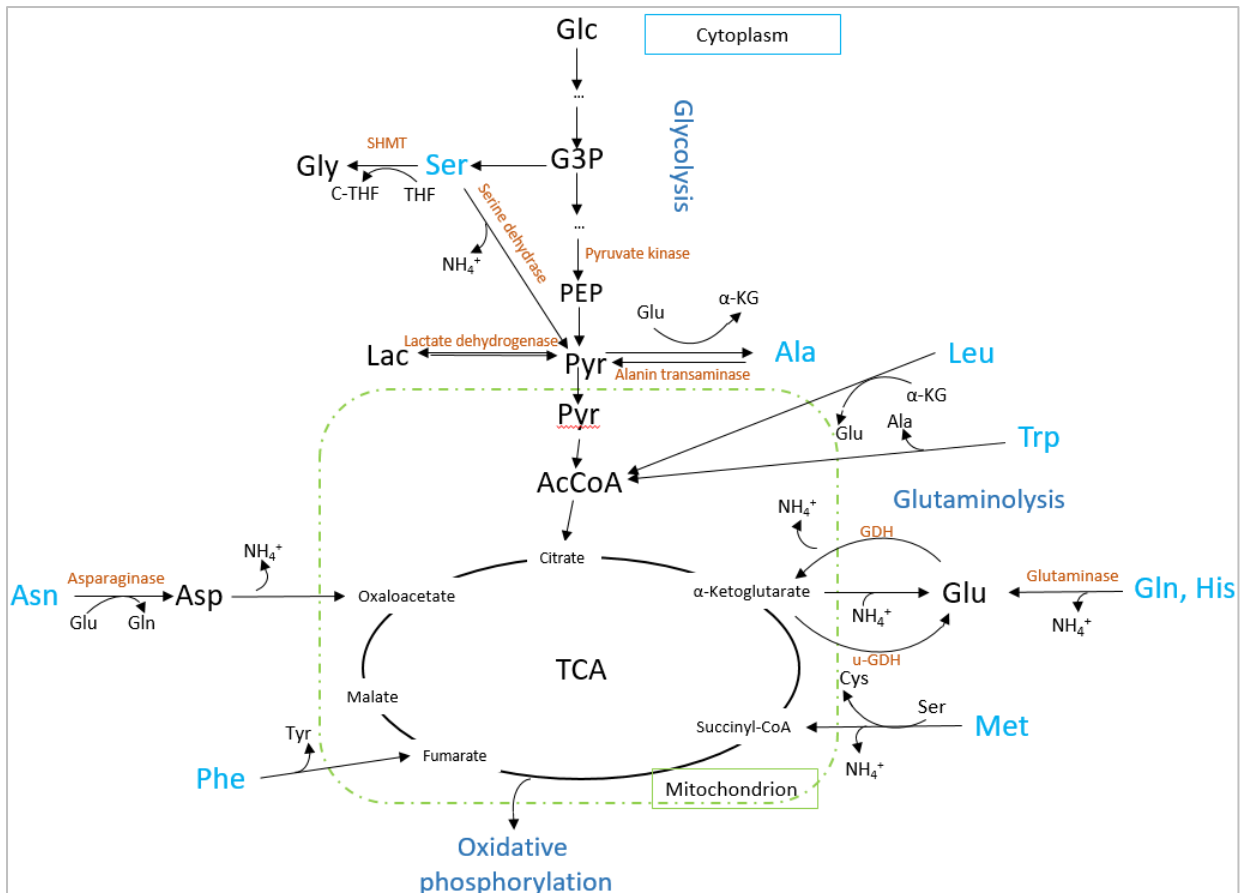
Figure 12 Overview of glucose and amino acid metabolism

Schematic representation of the metabolic pathways for important amino acids and glucose degradation. This graph was adapted from several literature sources [52–54].

Glycolysis generates energy that is stored in the reduction potential of two ATP and two NADH molecules respectively (see Equation 12).

$$\text{Glucose} + 2\ \text{ADP} + 2\ \text{NAD}^+ + 2\ \text{Phosphate} \rightarrow 2\ \text{Pyruvate} + 2\ \text{ATP} + 2\ \text{NADH} + 2\ \text{H}^+ + 2\ \text{H}_2\text{O}$$

Equation 12
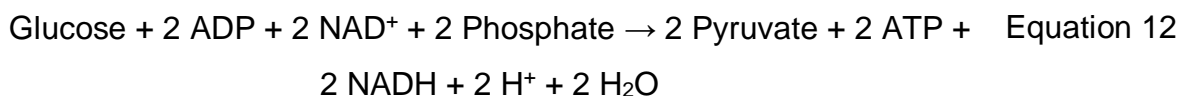
Under aerobic conditions, pyruvate is introduced into the tricarboxylic acid (TCA) cycle after decarboxylation and binding to coenzyme A [55]. The resulting molecule acetyl-CoA is processed further through a series of metabolic reactions during which NADH and $FADH_2$ are generated. The reduced co-enzymes are needed for the creation of a proton gradient by means of the electron transport chain, in a series of electron transfers to the final acceptor oxygen. The ATP-synthase utilizes the proton gradient to generate approximately 34 molecules of net ATP [55].

Under anaerobic conditions, pyruvate is processed to lactate (see Equation 13).
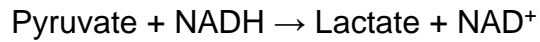
$$\text{Pyruvate} + \text{NADH} \rightarrow \text{Lactate} + \text{NAD}^+ \qquad \text{Equation 13}$$

Many mammalian cell lines applied in cell culture production are cancerous, and possess an altered metabolism, which is characterized by a modified gene expression or altered enzyme activity [56]. Additionally, more nutrient transporters are expressed, which increase the nutrient uptake like glucose and glutamine [57]. Although the oxidative phosphorylation generates much more energy (in form of ATP), most cancer cells convert a majority of glucose to lactate even in the presence of sufficient oxygen (see Figure 13) [58]. This is known as aerobic glycolysis, or the Warburg effect [59, 60]. Lactate is produced predominantly during the growth phase, because then the energy requirement of the cells is high [61]. In addition to glucose, 15 % of glutamine can also be converted to lactate [62]. Excess of lactate leads to cellular and extracellular acidification [62] that can inhibit cell growth [63]. In cell culture, lactate is sometimes consumed later in the stationary phase [61].
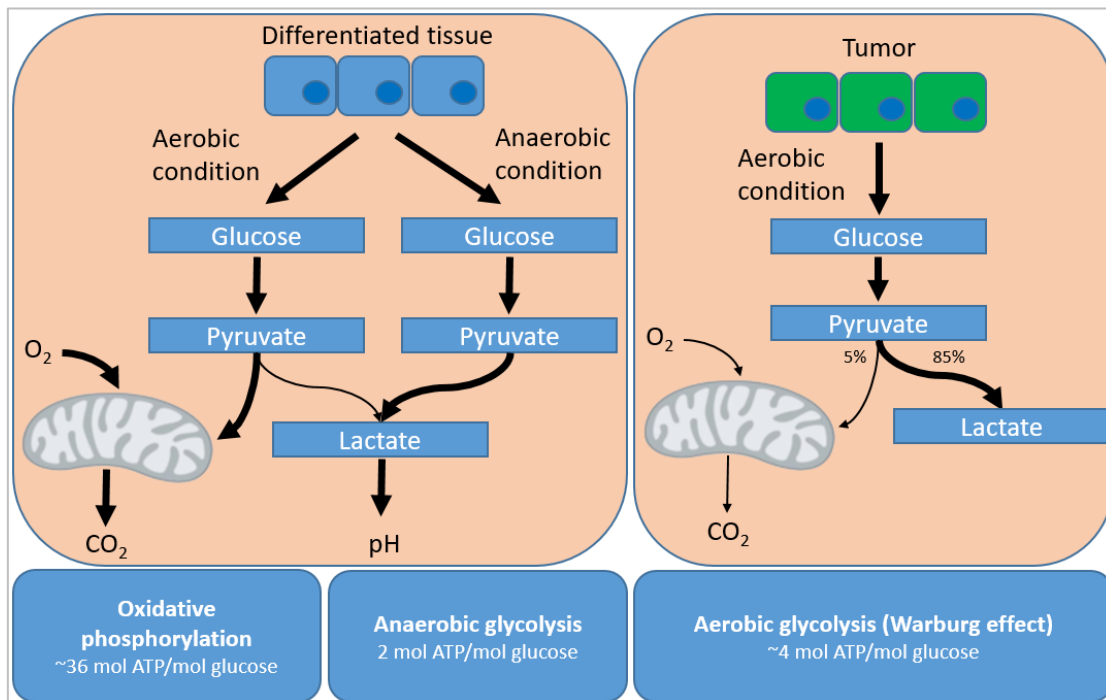

Figure 13 Cancer cell metabolism

Comparison of metabolism in differentiated tissue and tumor cells. This scheme was adapted from literature [60].

In cancerous cells, glucose is required to a great extend in order to generate carbohydrate building blocks for anabolic metabolism (e.g. nucleic acid) through the pentose phosphate pathway [56].

1.6.2 Glutamine metabolism

Amino acids are the precursor molecules for proteins and thus needed for cell growth, maintenance [64] and product generation. The amino acid consumption rate depends on the environment of the cell, among others things [64]. Glutamine is the most important amino acid for proliferating cancer cells, since it can be used for energy generation and biosynthesis [56, 58]. It enters the cell through one of many glutamine transporters and is metabolized mainly in the mitochondrion [56], where it is converted by glutaminase to glutamate and ammonia (see Figure 12) [58]. Glutamate can be converted to α-ketoglutarate, in a reaction called glutaminolysis, through two different pathways [65]. The first pathway uses the glutamate dehydrogenase, which yields a second ammonia molecule (deamination reaction) [56]. The second pathway is predominant in CHO cells [66] and uses an aminotransferase in order to transfer the amino-group to pyruvate or oxaloacetate and yield alanine or aspartate in a reaction termed transamination (see Figure 12) [56]. Between 35 % and 50 % of alanine is generated due to transamination of glutamate in a glutamine rich medium [66]. α-ketoglutarate is then introduced into the TCA cycle in order to replenish intermediates (see Figure 12), known as anaplerosis [67]. Thus, glutamine can be metabolized in the TCA cycle instead of glucose, while glucose is used in many cancer cells in order to generate lactate [58]. However, glutamine can also be used for lactate production [56] or synthesis of amino acids. At least 50 % of the non-essential amino acids for protein synthesis can be generated from glutamine [68]. Furthermore, glutamine is involved in the synthesis of uridine diphosphate N-acetylglucosamine (UDP-GlcNAc), which is required for protein glycosylation and proper ER-Golgi trafficking [58].

According to Street et al., a predominant portion of the accumulated ammonia created by CHO cells, is generated by the glutaminase catalyzed reaction [66]. However, glutamine is chemically labile. Hence, some ammonia is not generated by glutamine metabolism, but from pH dependent chemical degradation [56].

1.7 Cell culture

In this section, different cell culture strategies to improve the product quality of CHO cells are described, including the effect of different cell culture conditions and medium compositions.

1.7.1 Chinese hamster ovary (CHO) cell culture

About 70 % of all pharmaceutical drugs produced in animal cell lines are generated in Chinese Hamster Ovary (CHO) cells [69]. Their rigorous growth, high product titer and the ease of adaption to serum free suspension culture make them the primary production cell line for industrial cultivation in a variety of bioreactor formats [70]. Even though CHO cells are not able to express the α 2,6 sialyltransferase enzyme, which attaches sialic acid in a α 2,6 linkage [71], CHO cells are able to excrete proteins with sufficient post transcriptional modifications [72], e.g. folding and "human like" N-linked glycosylation [70]. The elevated cell proliferation property, however, leads to substantial glucose and glutamine consumption and thus to a high lactate and ammonium ion accumulation [72]. This, in turn, can cause growth inhibition and a decreased cell viability in addition to impaired product quality [73].

Typically, animal cells undergo four stages during their cultivation. The lag phase is the first stage, during which the cells adapt to the new environment without significant cell growth [61]. It is followed by the exponential growth phase, in which the cell density increases exponentially until the stationary phase is reached, where the cell density remains approximately constant. Since the protein expression is increased during the stationary phase [74], it is referred to as the production phase. In this work, the culture process was interrupted immediately after the cells entered the death phase, where the cell viability decreases due to the accumulation of toxic waste products or a lack of nutrients [61].

1.7.2 Influence of pH, temperature and DO on the product quality

For many cell culture products like antibodies and erythropoietin derivatives, the glycosylation and sialylation of the expressed protein is a crucial quality criterion. In this respect, the pH is an important parameter in cell culture, since it has a significant

influence on the macroheterogenity of glycoproteins [75–79]. For monoclonal antibodies, the differences in glycosylation between two cell cultures at pH 6.8 and pH 7.8 amounted about 50 % [79].

Another important physical parameter is the cell culture temperature, which can be lowered in order to increase the productivity of cells [74, 80, 81]. However, a cell culture temperature below 32 C was demonstrated to have a negative effect on the sialylation of erythropoietin (EPO) [78].

Controversial effects have been reported for the dissolved oxygen concentration [70], which might also influence the sialylation [78]. Generally, the impact of the parameters mentioned above seem to vary depending on the cell line and the expressed glycoprotein [79].

1.7.3 Medium composition and consequences

Although the average glucose level in mammalian blood is relatively modest (e.g. 5.5 mM in human blood [82]), the glucose levels in a common, serum free, chemically defined CHO cell culture medium is about 45 mM. Thereby, it is ensured that a sufficient amount of glucose is available for cell growth and recombinant protein production throughout the cell culture process. However, the consequence of excess glucose levels is reported to be an elevated lactate production due to an inefficient glucose metabolism [63]. A high lactate concentration above 20 mM is considered to be toxic for mammalian cells and inhibits cell growth due to the increase in osmolarity and decrease in pH [56]. Furthermore, it is believed that lactate negatively influences the production rate [74] and the glycosylation of glycoproteins [79]. Low glucose levels, on the other hand, are a hazard for cell growth and more importantly the glycosylation pattern of the glycoprotein [83], because glucose is a precursor for glycans. A negative influence on the sialylation is reported at glucose levels below 0.7 mM [84].
Similarly, low glutamine (< 0.1 mM) concentrations can also have a negative effect on cell growth [58], since glutamine is crucial during the growth phase for most production cell lines, because it is a major nitrogen and energy source [56, 58]. Furthermore, glutamine is a precursor for the synthesis of uridine diphosphate N-acetylglucosamine (UDP-GlcNAc), which is important for proper glycosylation of recombinant proteins

[84]. Glutamine can degrade spontaneously with time into ammonia and pyrrolidonecarboxylic acid in an irreversible first order reaction [56]:

$$[Gln]_t = [Gln]_0 * e^{-k*t}$$

<div align="right">Equation 14</div>

$[Gln]_t$ denotes the glutamine concentration at time t, while $[Gln]_0$ denotes the initial glutamine concentration, and *k* is the first order reaction rate. The reaction rate increases with temperature and pH [56]. Because of the lability of glutamine, it is added in the beginning of the cell culture in relatively high quantities ranging from 2 to 5 mM [56]. The consequence of a high glutamine supplementation, however, is an increased ammonia concentration, which is caused by its spontaneous degradation and glutamine metabolism (glutaminolysis) [63]. For mammalian cell cultures, ammonia levels over 4 mM have been reported to have an inhibitory effect on cell growth and to influence the terminal sialylation of many recombinant proteins [56, 79, 85, 86]. However, the critical ammonia concentration varies in different cell lines and even under different culture conditions [56]. Ammonia may be detoxified by the transamination reaction during which the α-amino group of glutamate is transferred to pyruvate or oxaloacetate to generate alanine or aspartate, while the activity of glutamate dehydrogenase is reduced in order to prevent an ammonia release from glutamate [56]. Thus, a high ammonia level leads to a lower specific excretion rate of ammonia and an increased specific excretion rate of alanine [56].

Two plausible explanations for the negative effect of ammonia on sialylation are suggested in literature. One suggests that an increase in the UDP-GlcNAc formation leads to a competitive inhibition of the CMP-NeuAc transport into the Golgi, a precursor needed for sialylation (see Figure 15) [63]. The second hypothesis focuses on the fact that under physiological conditions, about 1 % of the total ammonia concentration is in its NH_3 form [56]. NH_3 is a small hydrophobic molecule that can diffuse freely through the cell membrane and organelles to equilibrate the ammonia gradient, while the ammonium ion (NH_4^+) competes with other cations for active transport through the cell membrane by carrier proteins like Na^+/K^+-ATPase (see Figure 14) [56].

With a pka of 9.3 at 37°C, ammonia acts as a base and is quickly protonated to its ionic form (NH_4^+) [56]. This leads to an alkalinisation of the cellular environment and acidic organelles like the Golgi [56]. A pH change in the Golgi is assumed to impair the enzyme activity of sialyltransferase, leading to less sialylation [79, 87]. The second explanation is supported by the finding that the pH has a significant influence on the macroheterogenity of glycoproteins [75–79].
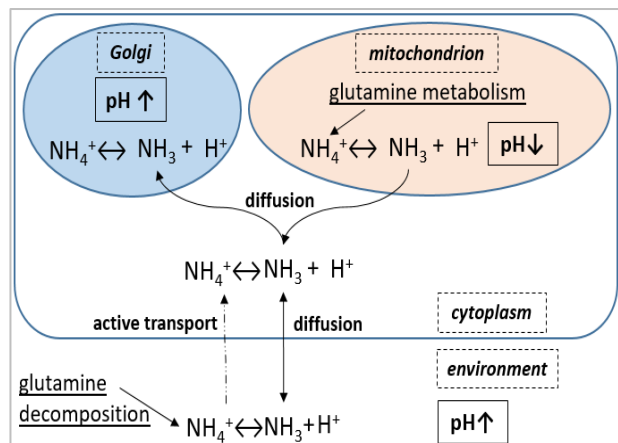

Figure 14 Influence of ammonia on the intercellular pH

Ammonium ions (NH_4^+) are produced due to amino acid metabolism in the mitochondrion and by decomposition of glutamine in an aqueous solution. This scheme was adapted from literature [56].

1.7.4 Cell culture strategies against ammonia and lactate accumulation

As described in the previous section (see section 1.7.3, Medium composition and consequences), the accumulation of waste products like ammonia and lactate have negative effects on cell growth and the product quality in mammalian cell culture. Many strategies for overcoming the accumulation of ammonia and lactate have been reported. The methods are ranging from substitution of glutamine by glutamine derivatives or other amino acids (e.g. Ala-L-Gln) [56], to substitution of glucose through sugar alternatives (e.g. galactose, mannose, fructose or other sugars) [74, 88, 89]. Unfortunately, these approaches can limit the availability of important glycan precursors and thereby impact the glycosylation quality [89]. Other strategies focus on discontinuous low glucose and glutamine feeding regime [58], which results in fluctuating nutrient levels and a potential risk of nutrient depletion, because of varying cell growth rates.

For lack of a reliable in-line glucose sensor, a pH based continuous glucose feeding in order to control the lactate accumulation during the exponential growth phase of CHO culture, was successfully demonstrated by M. Gagnon et al. [74]. This approach lead to lower lactate accumulation and thus higher monoclonal antibody titers, with similar

N-linked glycosylation of the product, compared to batch cell culture [74]. This method is however cross sensitive to pH and can therefore be influenced by other pH active compounds like ammonia. Furthermore, it is only applicable for low glucose levels below 1 mM [74], because then, CHO cells are forced to consume lactate, which leads to a measurable pH change.

A more cost intense approach is the removal of ammonia and lactate through a complex perfusion bioreactor, which results in a higher product purification effort [89]. The benefits and drawbacks of other cell culture operation modes are described in detail in the following sections.

1.7.5 Cell culture operation modes

Two types of cell culture strategies, batch and fed-batch, are routinely applied in the industry [90]. The batch culture mode is the simplest cultivation method, because the medium is not supplemented with nutrients after inoculation. The depletion of nutrients can be prevented in the fed-batch mode, by feeding nutrients like glucose during the cell culture process. In this section the advantages and disadvantages of both, batch and the fed-batch cell culture operation mode is discussed.

1.7.5.1 Batch culture:

Under a batch culture mode, a fixed amount of cell culture medium is propounded without subsequent addition of nutrients. The advantage of the batch format is its simplicity, as it can easily be applied in any type of bioreactor with no need for real-time measurement of metabolites. However, nutrient limitations can occur, which can cause a premature termination of the exponential growth phase and the transition into the stationary phase, where the lack of nutrients is accompanied by the accumulation of toxic by-products like ammonia and lactate and can cause incomplete product glycosylation [83], as discussed in section 1.7.3 (Medium composition and consequences).

1.7.5.2 Fed-batch culture:

The fed-batch mode is a common choice for large-scale protein production, because the stationary phase of mammalian cells can be prolonged during cell culture through nutrient feeding (e.g. amino acids, vitamins, glucose) in order to increase the product titer [61, 91]. Feeding during cell culture can also prevent lactate accumulation [61, 89]. In contrast to perfusion reactors, where the nutrients, waste products and excreted proteins are continuously exchanged with fresh medium through a permeable membrane [9], the processing complexity and the downstream costs of fed-batch cultures are much lower [89]. Careful monitoring and real-time control of important cell culture parameters is crucial for drug release and regulatory submission [61]. However, the lack of stable sensors often prevents the use of in-line sensors for real-time continuous measurement and control of important parameters, such as glucose. Stepwise addition of nutrients is a simple alternative, but neglects variations in nutrient requirements during cell culture [61]. Hence, a continuous monitoring and control is needed in order to meet the exact nutrient requirements [61] and to optimize the product quality for glycoproteins like Darbepoetin alfa.

1.8 Glycosylation of proteins

The biological activity and the pharmacokinetic behavior of therapeutic glycoproteins (e.g. Darbepoetin alfa, monoclonal antibodies, etc.) depends on their proper posttranslational modifications [92]. Herein, glycosylation plays an important role due to its influence on activity, stability, solubility, half-life, immunogenicity and inhibition of proteolysis [70, 89, 93]. The depletion of nutrients, more particularly glucose and glutamine, has a negative effect on glycosylation [79, 94, 95] and sialylation [95] through a lack of activated monosaccharide precursors needed for the glycosylation process [89, 96]. Monosaccharides are activated in the cytosol and subsequently transported by sugar-specific transporters [89]. The nucleotide sugar uridine diphosphate N-acetylglucosamine (UDP-GlcNAc) is the first sugar in the oligosaccharide synthesis and relies on glucosamine phosphate, which is formed from glutamine, and UTP, which depends on the availability of glucose [70]. UDP-GlcNAc is also important for the terminal sialylation of glycans, because it is the precursor for 5'-monophospho-N-acetylneuraminic acid (CMP-NeuAc), which is needed for the

attachment of sialic acid groups [89]. Low UDP-GlcNAc levels are associated with less sialylation [89], which is a quality criterion for recombinant proteins such as Darbepoetin alfa. On the other hand, elevated UDP-GlcNAc has also been reported to decrease sialylation through competitive inhibition of the CMP-NeuAc transport into the Golgi (see Figure 15) [63, 97]. The sugar nucleotides UDP-
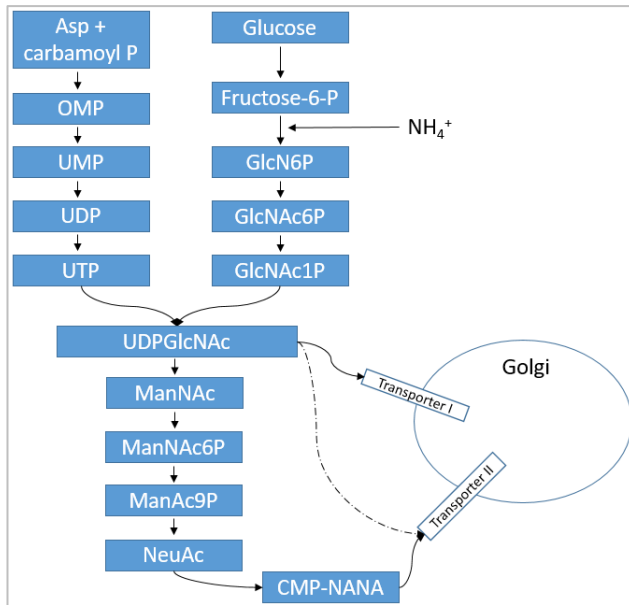

Figure 15 UDP-GlcNAc and CMP-NANA formation in the cytoplasm

A high concentration of ammonium increases the level of UDP-GlcNAc. Ammonium inhibits synthesis/transport of CMP-NANA, the precursor for sialylation. The dashed line represents the inhibition of the CMP-NANA transporter. This scheme was adapted from literature [63].

N-acetylglucosamine (UDP-GlcNAc) and UDP-N-acetylgalactosamine (UDP-GNAc) are formed in the cytoplasm of the cell by amination of fructose-6-P with ammonium or glutamine yielding glucosamine-6-P [56]. This reaction is catalyzed by the enzyme glutamine-6-phosphate transaminase orglucosamine-6-P deaminase [56]. Glucosamine-6 is acetylated and then activated by UTP to generate UDP-N-acetyl-glucosamine (UDP-GlcNAc) [56]. CMP-NANA, a precursor for sialylation, is formed by a series of enzymatic reactions from UDP-

GlcNAc before it is introduced into the Golgi [63]. There are two types of glycosylation's, N-linked and O-linked glycosylation. In the former, the glycan is bound to asparagine, while in the latter it is bound to serine or threonine [89]. N-linked glycosylation is accomplished by a complex pathway in the endoplasmic reticulum (ER) and Golgi. A series of enzymatic steps lead to a variety of glycan structures and branching termed microheterogeneity (see Figure 16) [70]. This variety results in different isoforms with varying numbers of terminal sialylations per protein. Variations in glycan occupancies can also occur and are called macroheterogeneity [70]. The first step in the assembly of asparagine-linked (N-linked) glycans involves the formation of a precursor oligosaccharide on a lipid carrier Dol-P (dolichyl pyrophosphate) [70].

The N-glycan precursor is then transferred co-translationally in a second step to the nascent protein by the oligosaccharyltransferase (OST) complex [70]. The asparagine-linked oligosaccharide is added to a specific asparagine-X-serine/threonine (Asn-X-Ser/Thr) site, where the amino acid X stands for any amino acid, except proline [70]. Further trimming and addition of saccharides is performed mainly in the Golgi, where also branching occurs into e.g. triantennary and tetraantennary [70].
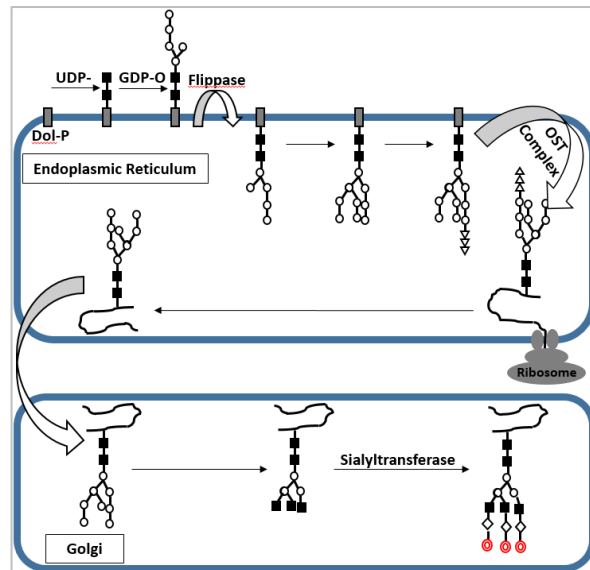
Figure 16 Synthesis of N-linked glycans

The glycans are first synthesized on dolichol-phosphate (Dol-P) in the cytoplasmic site of the ER. Further elongation and trimming occurs in the Golgi. This scheme was adapted from literature [70].

The glycosyltransferase enzymes are influenced by pH, intracellular nucleotide sugars, temperature, enzyme levels and Golgi transit time [63, 98, 99]. In O-linked glycosylation, individual sugars are added to the oxygen of serine or threonine as nucleotide sugar substrates by glycosyltransferases in the Golgi [100]. In contrast to N-linked glycosylation, O-linked glycosylation is less common in biotherapeutic proteins [89]. The terminal sugar for N-linked and O-linked glycans is usually sialic acid (N-acetylneuraminic acid) [70]. Variability in the resulting glycosylation pattern can be caused by the host cell type itself [79], but also by the cell culture environment. The influence of temperature, pH, dissolved oxygen concentration, nutrients and by-products, are discussed in section 1.7.2 (Influence of pH, temperature and DO on the product quality).

1.8.1 Darbepoetin alfa

Darbepoetin alfa is a hyperglycosylated recombinant human erythropoietin (rHuEPO) analogue, which was glycoengineered in order to enhance the in-vivo activity and the half-life of the therapeutic protein [93]. The aim of the performed glycoengineering was to improve patient compliance by less frequent administration needed to maintain the hemoglobin levels [93]. Two additional consensus sequences for N-linked carbohydrates were added into the peptide backbone. Hence, Darbepoetin alfa carries

five N-linked and one O-linked glycosylation sites [101]. This increases the serum half-life by a factor of three [101], which is mainly a result of the additional terminal sialic acids [102]. The recombinant HuEPO derivative is used for treating patients with anemia from chronic kidney disease, cancer and HIV [93]. The therapeutic recombinant protein stimulates erythrocyte proliferation and differentiation (erythropoiesis) in the bone marrow of patients [103].

Darbepoetin isoforms differ in the degree of sialylation and can therefore be separated due to their varying charge (e.g. by isoelectric focusing gel or capillary electrophoresis). The amount of different Darbepoetin isoforms resulting from the production in mammalian cell culture is between 25 to 30 [103]. However, only six to eight isoforms remain in the final product due to their high number of sialic acidic groups, which is the main quality criterion for Darbepoetin alfa [103].

1.9 Goals of this thesis

Although the first glucose biosensor dates back to the 1960's, reliable glucose sensors with a long-term functional stability for in-line monitoring in bioreactors have proven to be elusive so far. Thus, for most biotechnological applications, the glucose biosensors available on the market did not prevail offline measurement methods [9].

The main goal of this work was to develop an optical in-line biosensor for long-term continuous glucose monitoring in suspension cell culture. This includes a subsequent thorough characterization of the biosensor concerning its functional stability and the performance under different bioreactor conditions. An additional important objective, was the development of a computational biosensor model, that sheds light into the limited biosensor life-time, and contributes to the understanding of the underlying interrelation between different sensor layers, their permeability and kinetic features.

The developed glucose biosensor was finally applied for in-line continuous glucose monitoring and control in bioreactors during CHO cell culture to investigate the influence of different constant glucose levels on the sialylation of the highly glycosylated recombinant protein Darbepoetin alfa. The particular aim was to improve the product quality by enhancing its sialylation through a continuously controlled glucose level in fed-batch culture.

2 MATERIAL AND METHODS

The experimental section gives an overview of the materials and instruments used in the course of this thesis, followed by protocols for the manufacturing process of various glucose biosensors and their application in cell culture experiments in different types of bioreactors. Furthermore, the method for the determination of the diffusion coefficients for the applied biosensor materials is outlined.

2.1 Materials

2.1.1 Cell lines

A CHO production cell line for Darbepoetin alfa was kindly provided by the Steinbeis Transferzentrum für Angewandte Biologische Chemie (Mannheim, Germany).

Table 1 Applied cell lines

Cell line	Species	Tissue/Cell type
rCHO C6000	Cricetulus griseus	Ovar/Epithel
Jurkat wild type	Human	T-Lymphocyte

2.1.2 Solutions and buffers

All buffers and solutions were prepared in deionized water and stored at room temperature, unless otherwise mentioned.

2.1.2.1 Phosphate buffered saline (PBS)

PBS was prepared from NaCl (8.0 g), KCl (0.2 g), KH_2PO_4 (0.2 g) and $Na_2HPO_4 \times 7\ H_2O$ (1.14 g), mixed with 1.8 L of deionized water. The pH was adjusted to 7.2 with 0.1 M hydrochloric acid before 200 mL of deionized water was added.

2.1.2.2 Glucose stock solution

A 1 M glucose stock solution was prepared by dissolving 4952 mg of powdered glucose monohydrate (M = 198.17 g/mol) into 25 mL of phosphate buffered saline (PBS). The stock solution was stored at 4 °C to prevent fungal growth.

2.1.2.3 Sodium hydrogen carbonate ($NaHCO_3$) solution

A solution of 0.9 M sodium hydrogen carbonate ($NaHCO_3$) was prepared by dissolving 756,09 mg $NaHCO_3$ in 10 mL of deionized water.

2.1.2.4 Enzyme layer solution

Unless otherwise mentioned, 8 mg of the enzyme glucose oxidase (GOD) were weighed together with 50 mg bovine serum albumin (BSA) and then diluted in 250 µL PBS and 10 µL glycerine. Finally, 50 µL of glutaraldehyde (2.5 %) were added to the enzyme solution in order to start the polymerization reaction before coating.

2.1.2.5 Diffusion layer solution

The diffusion layer solution for the biosensor coating was prepared from 50 mg of a polyurethane polymer (D4, D6 or D7), 100 mg ethyl cellulose and 1.35 g of a 9:1 ethanol/water mixture.

2.1.3 Assay kits

Several enzymatic kits were applied in the course of this thesis, which are summarized in Table 2.

Table 2 Applied assay kits

Kit	Analyte	Manufacturer
Hexokinase-kit	Glucose	Sigma-Aldrich, Taufkirchen, Germany
Glucose Bio	Glucose	Roche Diagnostik GmbH, Mannheim, Germany
Glutamine V2 Bio	Glutamine	Roche Diagnostik GmbH, Mannheim, Germany
Lactate Bio	Lactate	Roche Diagnostik GmbH, Mannheim, Germany
NH3 Bio	Ammonia	Roche Diagnostik GmbH, Mannheim, Germany

2.1.4 List of chemicals and enzymes

A list with chemicals and enzymes that were applied in this thesis can be found in the Appendix.

2.1.5 List of instruments

The instruments applied for the measurement of glucose, oxygen and pH are listed in Table 3 and illustrated in Figure 17.

Table 3 List of applied instruments for pH and oxygen measurements

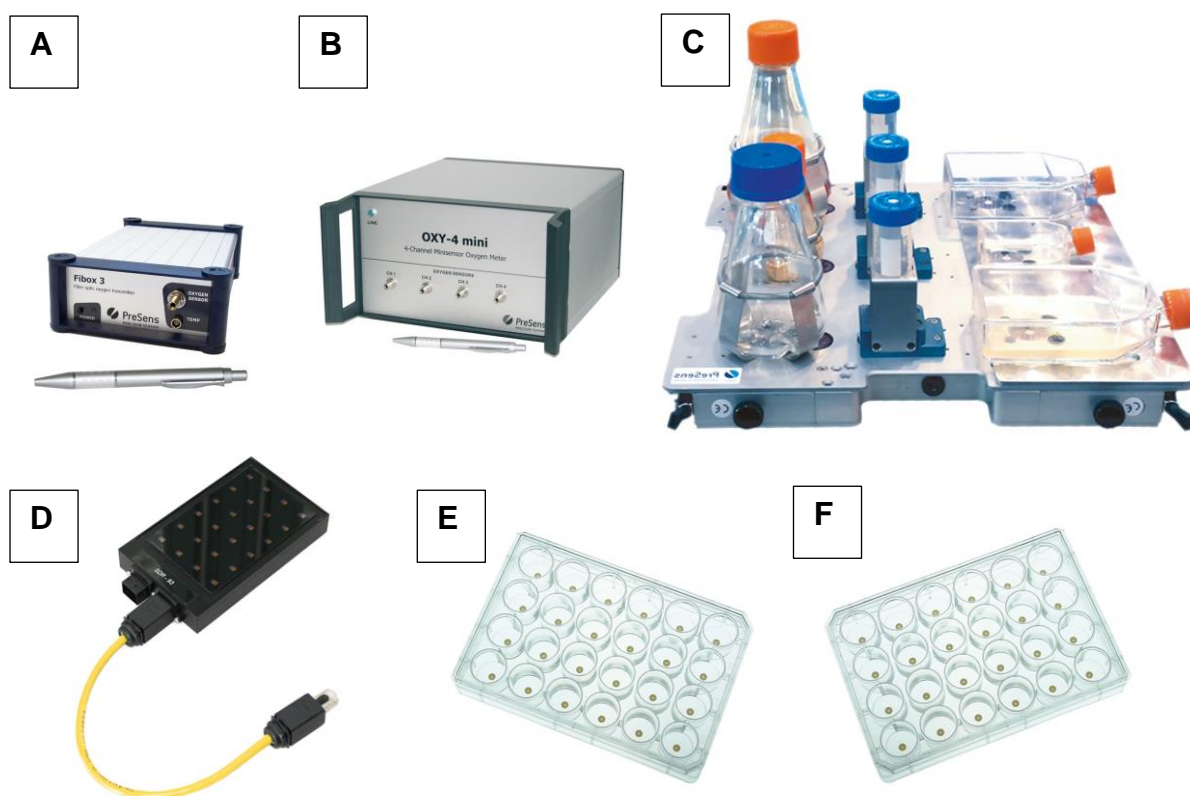| System	Probe	Software
SensorDish Reader® (SDR)	OxoDish®/HydroDish®	SDR version v28
Shake Flask Reader (SFR)	Shake Flask	SFR software
Transmitter	**Probe**	**Software**
Fibox 3	Oxygen sensors	Fibox 3 version 6.02
OXY-4 mini	Oxygen sensors	OXY-4 mini version 2.3FB

Figure 17 Applied materials for pH and oxygen measurements

(A) Fibox-3: Single channel device for oxygen measurements via an optical fibre. (B) Oxy-4 mini: Four channel device for simultaneous oxygen measurement via four optical fibres. (C) SFR: Shaker with an integrated measurement system for oxygen and pH monitoring in up to nine 125 mL shake flasks. (D) SDR: Simultaneous monitoring of HydroDish® or OxoDish® plates. (E) OxoDish®: 24-well plate with 24 integrated oxygen sensors. (F) HydroDish®: 24-well plate with 24 integrated pH sensors. All pictures were kindly provided by PreSens GmbH.

A list with additional instruments used in this thesis can be found in the Appendix.

2.2 Biosensor fabrication

In this section, the preparation of two glucose biosensor types is described. One biosensor type is based on an optical oxygen sensor, while the other one uses an optical pH-sensor as a transducer. Since the measurement of the oxygen consumption, resulting from the enzymatic reaction in the glucose biosensor, offers a much better sensitivity compared to the measurement of the pH change [11], the continuous glucose monitoring was performed solely with the help of an oxygen sensor based glucose biosensor. The pH sensor based glucose biosensor was only used to determine the gluconic acid accumulation in the enzyme layer during the glucose monitoring.

The oxygen sensor was optically isolated with a black carbon layer to avoid background fluorescence from the overlying immobilized enzyme layer.

2.2.1 Oxygen based biosensor preparation with a liquid diffusion layer solution

An oxygen sensor strip was cut from a large oxygen sensor sheet, before the enzyme solution was knife-coated by means of an applicator (see Figure 18). The enzyme solution, which composition was described in Table 4, was adapted from a previously published protocol [104] and transferred in excess onto the oxygen sensor strip using a pipette. Next, the preferred coating height was adjusted on the applicator, before it was manually pulled with a constant velocity over the enzyme solution, in order to spread it evenly over the oxygen sensor stripe. After the polymerization process of the enzyme layer was finished (5 min), the diffusion layer (which composition can be found in Table 5) was spread over the coated enzyme layer using the same method.

Table 4: Composition of the enzyme layer solution

Amount	Substance
8 mg	GOx
50 mg	BSA
250 µL	PBS
10 µL	Glycerin
50 µL	GAD

Table 5: Composition of the diffusion layer solution

Amount	Substance
50 mg	D4, D6 or D7
100 mg	Ethyl cellulose
1.35 g	9:1 Ethanol/water

Alternatively, the diffusion layer was drop-flow coated over the sensor stripe. For this purpose, the oxygen sensor strip was fixed with its shiny side to an even plastic surface using a double-faced adhesive tape. Then, the polymer solution was applied with a pipette onto the sensing side of the sensor strip. Next, the sensor strip was tilted quickly into a 90° position (see Figure 18), so that the coating solution ran over the entire sensor strip. After drying for 5 min an evenly distributed and very thin coating layer was attained. The thickness of the coating layer can be influenced by the coating angle and the viscosity of the coating solution. The drop-flow method, however, can only be applied for the diffusion layer coating, since the enzyme layer solution is hydrophilic and thus does not adhere to the hydrophobic oxygen sensor surface.

The coated stripe was dried at 4°C over night before the desired glucose biosensor size was cut with the help of a hole puncher and a hammer from the stripe (Figure 18). The resulting glucose sensor spots were then fixed with silicone glue onto a transparent surface for glucose measurement.
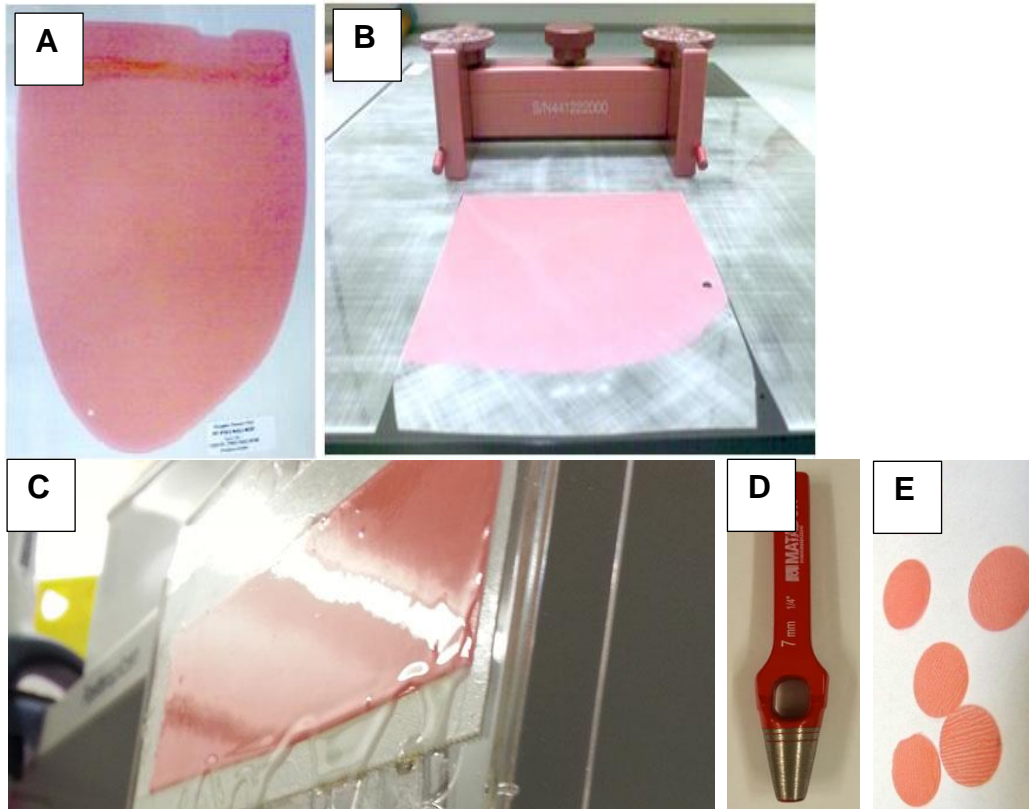

Figure 18 Glucose biosensor preparation

Oxygen sensor sheet (A). (B) Oxygen sensor stripe before knife coating of the enzyme layer with an applicator. (C) Drop-flow coating of a diffusion layer. (D) Hole puncher. (E) Glucose biosensor spots cut from a coated stripe with a hole puncher. [105]

2.2.2 Oxygen based biosensor preparation in a 24-well plate with a diffusion membrane

A standard 24-well plate was placed on top of a SensorDish® Reader (SDR) and equipped with a 5 mm oxygen sensor per well. The sensors were fixed with silicon glue in the middle of each well with the light sensitive side towards the SDR (Figure 19).
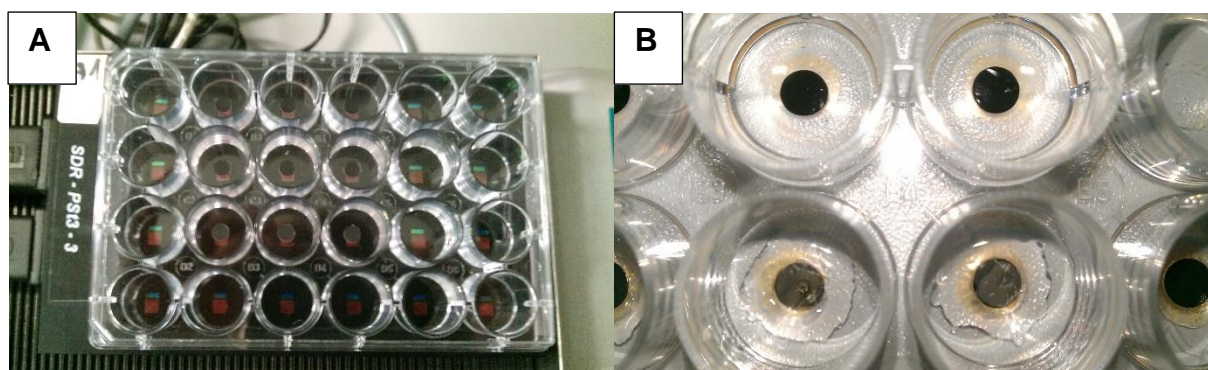
Figure 19 SDR measurement

Illustrated in (A) is a 24-well plate on a SensorDish Reader® (SDR), equipped with nine oxygen sensors. (B) shows biosensors stored in PBS after the manufacturing process.

The silicone glue was allowed to dry for 15 min while the enzyme solution was prepared in a 2 mL cup according to Table 4. After the immobilization process was initiated by adding 50 µL glutaraldehyde (2.5 % aqueous solution), the polymerising enzyme solution was thoroughly mixed and quickly spread over the oxygen sensor surface using of a micro pipette. The pipetted amount of enzyme layer solution was chosen based on the diameter of the oxygen sensor. For a 5 mm sized oxygen sensor, a volume of 2 µL was used.

Diffusion membranes with a diameter of 7 mm were previously cut with a hole puncher from a DIN A4 size diffusion membrane sheet and placed on top of the still polymerizing enzyme layer using a tweezer. This was done to utilize the capillary forces in order to achieve an evenly distributed enzyme. After the polymerization process of the enzyme layer was finished (5 min), the biosensor rim was sealed with silicone glue. The biosensors were then stored in PBS buffer at 4 °C until further usage.

The glucose measurements were performed at room temperature with a 24-channel prototype SDR from PreSens on an orbital shaker set at 230 revolutions per minute (rpm), unless mentioned otherwise. The acquired data was analyzed with the analysis freeware TReCCA Analyser [106].

2.2.3 pH based biosensor preparation for gluconic acid determination

A 24-well HydroDish® plate with optical pH sensors at the bottom of each well (see Figure 17) was used for the preparation of pH based glucose biosensors. The aim of the pH based glucose biosensors was to determine the internal gluconic acid accumulation during glucose monitoring. 2 µL of the enzyme solution (see Table 4)

were coated over each pH sensor in the HydroDish® plate using a pipette, and then covered by a diffusion membrane. In a subsequent step, the biosensor rim was sealed with silicone glue and stored in PBS at 4°C until further usage.

The gluconic acid determination was performed with a standard SDR at room temperature on an orbital shaker set to 230 rpm. The internal gluconic acid accumulation inside the enzyme layer was indirectly tracked by measuring the pH change at various glucose concentrations. Therefore, the pH based glucose biosensor was calibrated with known gluconic acid concentrations.

2.2.4 pH and oxygen sensor calibration

The oxygen and the pH sensors are already pre-calibrated by the manufacturer. Hence, the on-site calibration can be performed by entering the calibration parameters from a data sheet provided by the manufacturer, into the SDR-software.

In the case of the glucose biosensor, a two-step calibration was applied. First, the pH and the oxygen transducer of the glucose biosensor were calibrated according to the calibration data sheet provided by the manufacturer. Subsequently, a single point calibration of the glucose sensor was performed with glucose standards mixed from a glucose stock solution.

2.3 Integration of glucose biosensors into single-use bioreactors

In this section, the integration of glucose biosensors and oxygen reference sensors into 125 mL shake flasks and 6-well plates for cell culture experiments is described. To ensure sterility, the oxygen sensors and the diffusion membranes were sterilized with 70 % ethanol, and subsequently used for the biosensor fabrication and integration within a laminar flow.

2.3.1 Oxygen based glucose biosensors for shake flask bioreactors

Glucose biosensors in combination with preinstalled reference oxygen sensors were used to monitor and control the glucose level in 125 mL shake flasks during cell culture.

A transparent plastic tube and an oxygen sensor were sterilized with 70 % ethanol and then attached to each other with a transparent adhesive foil (see Figure 20). Next, 2 µL of the enzyme solution (see Table 4) was pipetted onto the optically isolated oxygen sensor surface. Subsequently, a perforated hydrophilic diffusion membrane was placed over the still polymerizing enzyme solution. Finally, the biosensor was sealed with silicone glue to prevent glucose from lateral influx before the biosensor was irradiated with UV (253.7 nm, 15 W) for one hour within the laminar flow.

The plastic tube with the biosensor (see Figure 20) was mounted on a polymer optical fibre (POF) that was pierced through the lid of the shake flask and fixed, such that the biosensor dipped into the cell culture medium (see Figure 10).
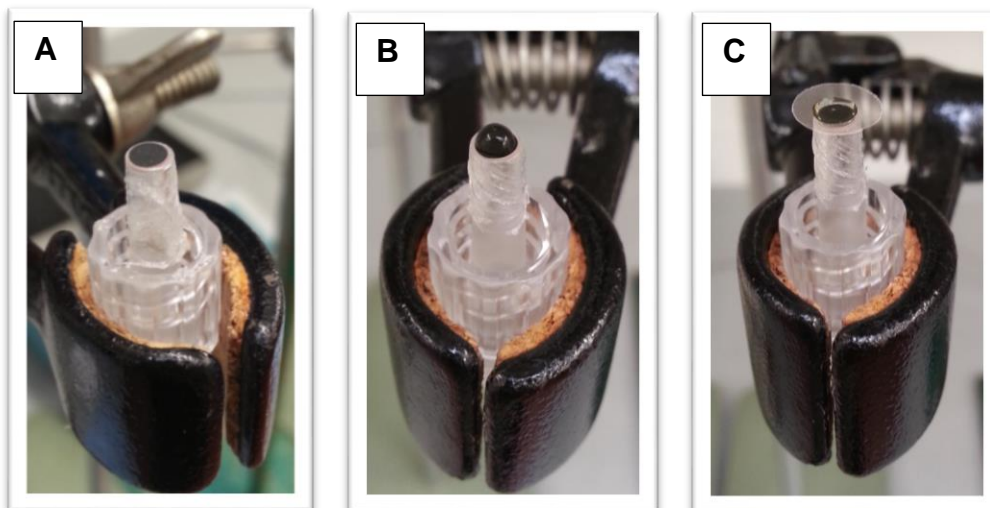
Figure 20 Biosensor fabrication for 125 mL shake flask bioreactors

Oxygen sensor placed on a plastic tube (A). (B) 2 µL enzyme solution pipetted on an oxygen sensor. (C) The enzyme solution on the oxygen sensor was covered by a hydrophilic perforated diffusion membrane.

The glucose biosensor was used in combination with a preinstalled reference oxygen sensor that was measured via the Shake Flask Reader® through the transparent bottom of the flask (see Figure 17). The glucose response was measured with the OXY-4 mini®. The measurement signal of both sensors, the glucose biosensor and the oxygen reference sensor, is expressed as oxygen partial pressure in percent air saturation. Both signals result from an oxygen concentration dependent fluorescence quenching of the excited luminophores within the oxygen sensitive layer (cf. section 1.2.2.1, Oxygen sensor principle). The glucose concentration is monitored by subtracting the oxygen partial pressure within the biosensor, from the oxygen level of

the reference sensor. In this way, oxygen fluctuations occurring during cell culture were compensated.

The shake flask lid was prepared with four tubes that were connected to the interior of each shake flask and sealed with 0.2 µM sterile filters on the exterior facing side. Three of those tubes were connected to the corresponding oxygen, nitrogen and glucose supply tubes (see Figure 21). One tube remained unconnected for pressure equalization. A syringe with a concentrated glucose solution was connected to a custom-made peristaltic pump that supplied four shake flasks with concentrated glucose through tubes. Every glucose supply tube passed a valve that was used to control which shake flask was supplied with glucose. The glucose pump operation and the time the valves remained open, determined the amount of glucose that was injected into the respective shake flasks. Hence, the glucose concentration in the 125 mL flasks was controlled through automated glucose addition via a custom-made peristaltic pump that was controlled by LabVIEW®, a system design software from National Instruments (Texas, USA).
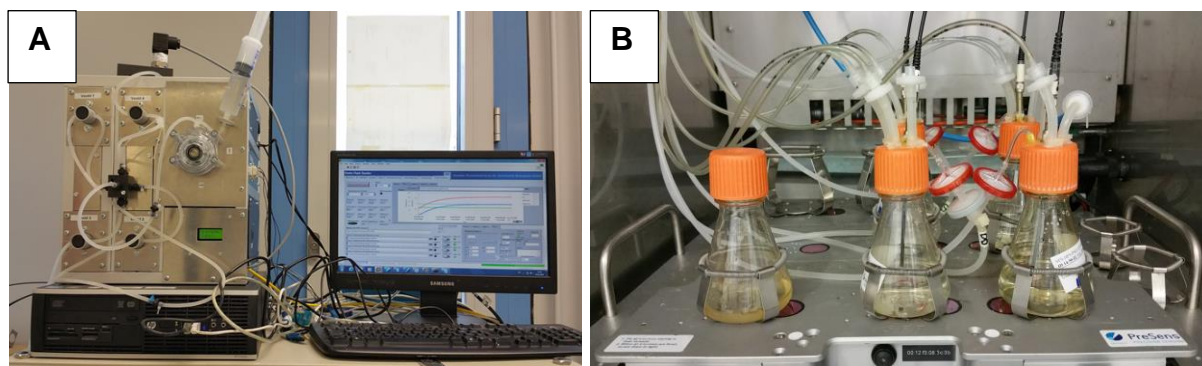
Figure 21 Instrumental setup for glucose control in shake flasks

A custom-made pump injects glucose through tubes into four shake flasks. Each glucose tube passes a valve which controls the amount of glucose solution that enters the shake flask. The peristaltic pump is connected to a computer which controls the glucose addition from a syringe filled with glucose solution. (B) Shake flasks in an incubator on a Shake Flask Reader® (SFR). The lid of the shake flasks is connected to tubes through which oxygen, nitrogen and glucose are introduced, respectively. Sterile filters are connected to the tubes to prevent a contamination of the cell culture medium.

A four-channel oxygen meter (OXY-4 mini®) and a Shake Flask Reader® (SFR) from PreSens GmbH (Regensburg, Germany) were utilized to measure the glucose concentration and the dissolved oxygen level in the cell culture medium of up to four flasks simultaneously.

2.3.2 Oxygen based glucose biosensors for 6-well cell culture plates

The preparation of the glucose biosensors in a 6-well plate is comparable to the manufacturing in a 24-well plate, which is described in chapter 2.2.2. In each well a glucose biosensor and an oxygen reference sensor was mounted with silicone glue (see Figure 22). The measurement of the glucose biosensor and the oxygen reference sensor was performed simultaneously with the SDR.
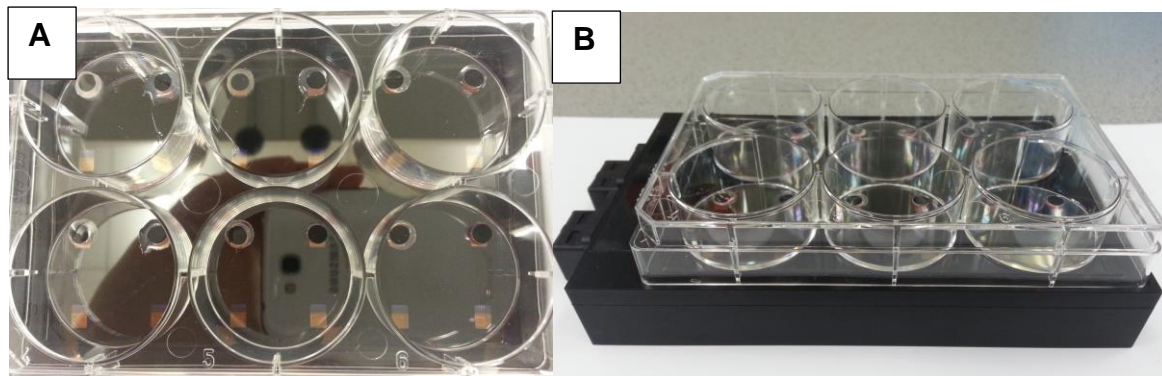

Figure 22 Biosensor integration in 6-well plate

(A) Illustrates one glucose biosensor and one oxygen reference sensor per well. (B) 6-well plate with biosensors and oxygen reference sensors on a SensorDish Reader® (SDR).

2.4 Cell culture experiments in 125 mL shake flasks

Cell culture protocols and the measurement of important cell culture parameters, such as viability and product quality are described in this section besides three cell culture experiments at different glucose levels.

2.4.1 Cell culture preparation

The cell culture preparation process begins with the revival of the cryopreserved (-196°C) CHO cells. For this purpose, CHO-5 cell culture medium was preheated to 37°C in a water bath. A 2 mL cryovial with frozen cells was put in same water bath until nearly all the ice thawed. Subsequently, the cryovial was transported quickly under the laminar flow and the vial content was transferred into a falcon tube with 10 mL warm cell culture medium. The falcon tube was then centrifuged at room temperature (150 g, 5 min) and the resulting supernatant was discarded. The agglomerated cells were then re-suspended in 20 mL warm CHO-5 cell culture medium with antibiotics (0.4 mg/mL

G418) and 4 mM glutamine and then transferred to a 75 cm² T-flask for expansion at 37°C without shaking. After several days, a cell density of over 3×10^6 cells/mL was reached. The cells were then inoculated at 2.5×10^5 cells/mL in a 125 mL shake flask with 20 mL fresh CHO-2 medium supplemented with 45 mM glucose, 4 mM glutamine and antibiotics (0.4 mg/mL G418) for further cell cultivated at 37°C, 5 % CO_2, 80 % humidity and 130 rpm. The CHO cells were kept in repeated batch mode and harvested before the stationary phase was reached. This process was repeated twice a week for up to two months, before new cells were thawed.

2.4.2 Cell culture duration

Dead cells release sialidase due to cytolysis, which can cleave the terminal sugar sialic acid [79] and compromise the quality of the recombinant protein (Darbepoetin alfa) in the medium. The cell culture experiments were therefore stopped, when the cell viability dropped below 90 %.

2.4.3 Cell culture experiments

Cell culture experiments were carried out in 125 mL shake flasks with an integrated pH and oxygen reference sensor (see Figure 10). Glucose biosensors were manufactured and mounted onto an optical fibre in every shake flask as described in section 2.3.1 (Oxygen based glucose biosensors for shake flask bioreactors). The shake flasks were then filled with a working volume of 50 mL chemically defined, serum free CHO-2 cell culture medium without glucose. The cell culture medium was supplemented in the beginning of every experiment with the desired glucose concentration and 4 mM glutamine in addition to antibiotics (0.4 mg/mL G418). All supplements were sterile filtered (0.2 µm) prior to the manual addition. The shake flasks were then placed on a Shake Flask Reader® (SFR) in a Heracell 240i incubator (Figure 21) at 37 °C, 5 % CO_2, 80 % humidity and 130 rpm.

A 48 hour pre-equilibration of the biosensors was conducted without cells to compensate an initial sensitivity increase, so that the signal remained constant during the glucose measurement over the cell culture duration. A one-point calibration was performed on the first day of each cell culture experiment. The CHO cells were

inoculation with a density of $2.5{\times}10^5$ cells/mL, unless otherwise stated. The cell culture was stopped when the viability dropped below 90 %, because dead cells release glycosidases and proteases that can negatively affect the protein glycosylation [107].

The dissolved oxygen concentration in the cell culture medium was automatically controlled by addition of nitrogen or oxygen through the oxygen and nitrogen supply tubes that were connected to the shake flask lid (Figure 21). The dissolved oxygen concentration was monitored through the Shake Flask Reader (SFR) and transmitted to LabVIEW®, that controlled the dissolved oxygen concentration at 50 % air saturation through oxygen or nitrogen addition into the flask. The pH was controlled at pH 7.0 ± 0.2 by manual addition of $NaHCO_3$ (0.9 M) with a 2 mL syringe through a 0.2 µm sterile filter connected to the shake flask lid by a clave connector. The stirring speed was maintained constant at 130 rpm, since the flow rate has an influence on the glucose biosensor signal.

2.4.4 Sampling and preparation

Periodic samples were taken from the bioreactor medium during the cell culture experiments via a 8 cm long needle. The needle was pierced through the shake flask lid and attached via a clave connector to a 2 mL syringe through which a 1 mL sample was taken. The sample was then centrifuged at 400 g for 5 min and the supernatant was utilized to determine the metabolites glucose, lactate, glutamine and ammonia offline with the Cedex-Bio. A detailed assay description is given in section 2.6.1 (Assay based automated measurement of metabolites with Cedex-bio). The remaining supernatant was frozen and stored at -80°C for later gas chromatography (GC) and capillary electrophoresis (CE) analysis. The cell pellet was re-suspended in PBS for cell density and cell viability determination with an automated counting device as described in the following section.

2.4.5 Cell density and cell viability measurement

After centrifugation of the samples, the pellet was re-dissolved in PBS buffer so that the cell density was between $0.2{\times}10^6$ cells/mL and $10{\times}10^6$ cells/mL. The re-suspended cells were subsequently transferred to a sample cup and placed into the sample wheel

of the Vi-Cell® XR (Beckmann Coulter). The viable cells were counted and distinguished from the dead cells by automatic image analysis with a CCD camera using the trypan blue exclusion method. Alternatively, 20 µL of the cell solution was mixed with 80 µL trypan blue and then 10 µL of the solution was injected into a Neubauer haemocytometer for manual counting under a microscope.

2.5 Cell culture experiments in 6-well plates with glucose and oxygen sensors

Jurkat wild type cells were cultured in preparation of the cell culture experiments in IMDM medium, supplemented with 2 mM glutamine, 10 % fetal calf serum (FCS) and 100 U/mL penicillin/streptomycin. The cells were cultured in T 75-flasks with 15 mL medium and split to $3x10^5$ cells/mL twice a week before the 6-well experiments. Glucose biosensors and oxygen reference sensors were mounted in a 6-well plate as described in section 2.3.2 (Oxygen based glucose biosensors for 6-well cell culture plates). The glucose sensors were prepared under the laminar flow (Airstream Class II, ESCO) and irradiated with UV light (15 watts, 253.7 nm) for one hour to ensure sterility.

In the following sections two experiments are described, which were designed to investigate the influence of the biosensor related hydrogen peroxide emission and the influence of cisplatin on the cell growth and glucose uptake of Jurkat cells in 6-well plates.

2.5.1 Influence of cisplatin on the glucose consumption of Jurkat cells

Jurkat cells were inoculated at $2x10^5$ cells/mL in 5 mL IMDM medium per well with 2 mM glutamine, 10 % FCS and 100 U/mL penicillin/streptomycin. In addition, the IMDM medium was supplied with 1/30 g/L catalase (127 U/mL) to prevent potential cell damage by H_2O_2 emitted from the glucose sensors. The glucose and oxygen level during cell culture was tracked with an SDR that was placed on an orbital shaker in an incubator at 150 rpm, 37°C and 5 % CO_2.

The Jurkat cell were cultured for two days before 10 µM of cisplatin was added in three wells from a freshly prepared 1 mM stock solution dissolved in 0.9 % NaCl. The cells in the remaining non-treated wells served as a control. After seven days, the experiments were ended.

Cell count and cell viability measurements were performed periodically with a Vi-Cell® cell viability analyser. For this purpose, samples of 400 µL were taken and centrifuged at 1200 rpm for two minutes. The supernatant was subsequently stored at -20°C for later glucose analysis, while the cell pellet was re-suspended in 400 µL PBS for counting. The glucose concentration in the samples was determined offline via a hexokinase assay via a photometer.

2.5.2 Influence of the emitted hydrogen peroxide on the viability of Jurkat cells

The aim of this experiment was to investigate, if the hydrogen peroxide emission from the glucose biosensors has a negative effect on the cell viability. Therefore, Jurkat wild type cells were cultured in 5 mL IMDM medium, supplemented with 2 mM glutamine, 10 % FCS and 100 U/mL penicillin/streptomycin. However, only three wells were treated with 1/30 g/L catalase (127 U/mL) on the first day to decompose the emitted hydrogen peroxide in the medium into water and oxygen (Equation 8). The medium in the remaining three wells did not contain catalase and served as a control. The inoculated cell density was 0.5×10^5 cells/mL.

2.6 Offline measurement of metabolic parameters

2.6.1 Assay based automated measurement of metabolites with Cedex-bio

2.6.1.1 Glucose measurement

Glucose is phosphorylated by ATP in presence of hexokinase (HK) to glucose-6-phosphate (Glc-6-P), which is then oxidized by NADH in presence of glucose-6-phosphate dehydrogenase (G-6-PDH). The rate of NADPH formation is directly proportional to the glucose concentration and can be measured photometrically in the UV range.

$$\text{Glucose} + \text{ATP} \xrightarrow{\text{HK}} \text{Glc6P} + \text{ADP} \qquad \text{Equation 15}$$

$$\text{Glc6P} + \text{NADP}^+ \xrightarrow{\text{G6PDH}} \text{Gluconate6P} + \text{NADPH} + \text{H}^+ \qquad \text{Equation 16}$$
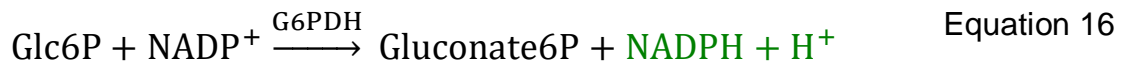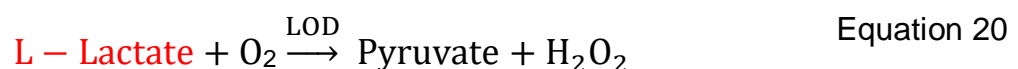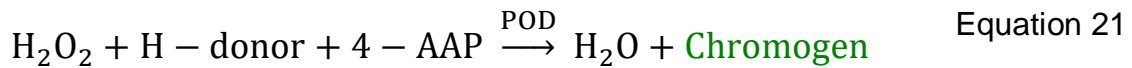
2.6.1.2 Glutamine measurement

L-glutamine is deaminated by glutaminase to L-glutamate. L-glutamate is oxidized in presence of L-glutamate oxidase (GLOD) to α-ketoglutarate, NH_4^+ and hydrogen peroxide, which generates a colored quinine dye in presence of peroxidase (POD). The formation of the dye is measured photometrically and is directly proportional to the glutamine concentration. In order to prevent any influence on the result by glutamate in the sample, glutamate oxidase and catalase are added in a prior step to degrade glutamate and hydrogen peroxide without dye formation.

$$\text{Glutamine} \xrightarrow{\text{Glutaminase}} \text{Glutamate} + \text{NH}_3 \qquad \text{Equation 17}$$

$$\text{Glutamate} \xrightarrow{\text{L−GLOD}} \alpha - \text{Ketoglutarate} + \text{NH}_4{}^+ + \text{H}_2\text{O}_2 \qquad \text{Equation 18}$$

$$\text{H}_2\text{O}_2 + 4 - \text{AAP} + \text{TOOS} \xrightarrow{\text{POD}} \text{H}_2\text{O} + \text{Chromogen} \qquad \text{Equation 19}$$
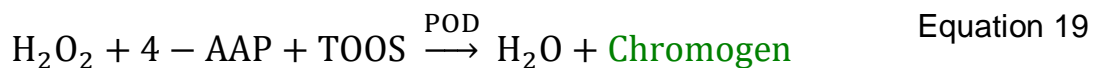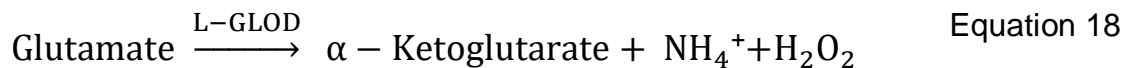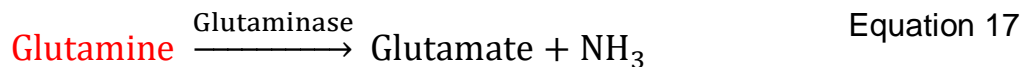
2.6.1.3 Lactate measurement

L-lactate is oxidized by lactate oxidase (LOD) to pyruvate and hydrogen peroxide, which generates a colored dye in presence of peroxidase (POD). The photometrically measured absorbance of the dye is directly proportional to the L-lactate concentration.

$$\text{L} - \text{Lactate} + \text{O}_2 \xrightarrow{\text{LOD}} \text{Pyruvate} + \text{H}_2\text{O}_2 \qquad \text{Equation 20}$$

$$H_2O_2 + H - donor + 4 - AAP \xrightarrow{POD} H_2O + Chromogen$$ Equation 21

2.6.1.4 Ammonia measurement

Ammonia (ammonia ions, NH_4^+) reacts in presence of glutamate dehydrogenase (GLDH) with 2-oxoglutarate and NADPH in a reductive amination to form L-glutamate and $NADP^+$. The decrease of NADPH is directly proportional to the ammonia concentration and measured photometrically at 340 nm.

$$NH_4^+ + 2 - oxoglutarate + NADPH \xrightarrow{GLDH} L - Glutamate + NADP^+ + H_2O$$ Equation 22
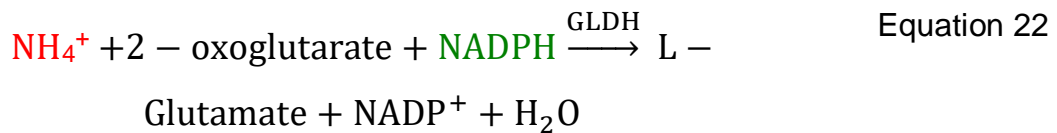
2.6.2 Amino acid determination in cell culture samples

The amino acid concentration of samples, taken at different time points during the cell culture, was analyzed with a gas chromatograph (GC) during a bachelor thesis and is described elsewhere [108]. The specific consumption or production rate (q_{spec}) of the amino acids during the cell culture experiments was determined as follows:

$$q_{spec} = \frac{\Delta\ Analyte\ concentration}{Mean\ VCD * \Delta t}$$ Equation 23

2.7 Determination of the product quality

The sialylation of the recombinant product Darbepoetin alfa is an important criterion for the determination of its quality. The supernatant of samples was therefore taken at the end of the cell culture run and send to the Hochschule Bielefeld for purification and capillary electrophoresis. The samples were purified with Toyopearl Blue by affinity chromatography and then de-salted via a centrifuge, before the isoform distribution analysis was performed by capillary electrophoresis at pH 5.5.

The retention time in capillary electrophoresis depends on the charge and the size of the molecule. Sialic acid is the terminal glycan residues of Darbepoetin alfa and negatively charged at the applied pH. Hence, the isoforms with a higher sialic acid number per protein remain the longest on the column and possess the highest retention times in the electropherogram.

2.8 Biosensor model

The geometric, kinetics and the diffusion properties of the materials applied for the biosensor fabrication are needed for the development of a one-dimensional biosensor model. Their measurement and the biosensor model is described in this section.

2.8.1 Biosensor geometry

The thickness of the biosensor materials was measured by means of a paint meter (Elcometer 345), where no specifications from the manufacturers were available.

2.8.2 Determination of diffusion coefficients

2.8.2.1 Diffusion coefficients for glucose and H_2O_2

The diffusion coefficients for glucose and hydrogen peroxide for the applied diffusion membranes and the enzyme layer was measured with a home-made device consisting of six cylindric tubes that were put in a 24-well plate. The material of interest (either the enzyme layer or a diffusion membrane) was mounted with silicone glue on one side of the tubes to separate the tube volume from the well content (Figure 23). The wells of the 24-well plate were filled with 187.5 µL reagent solution and 1312.5 µL PBS. The reagent solution contained 2,2′-Azino-bis(3-ethylbenzothiazoline-6-sulfonic acid) diammonium salt (ABTS), peroxidase from horseradish 150 U/mg (HRP, EC-Nr. 1.11.1.7) and glucose oxidase (GOD) dissolved in PBS buffer (Table 6).

Table 6: Composition of the reagent solution

Amount	Substance
3 mg/mL	ABTS
0.75 mg/mL	HRP
0.75 mg/mL	GOD
1 mL	PBS

The measurement was started by adding 200 µL of either glucose or hydrogen peroxide solution with the desired concentration into the tubes. The diffusion of either hydrogen peroxide or glucose through the material of interest into the well, lead to the formation of chromogenic ABTS radicals catalyzed by HRP (Equation 24-Equation 25) [109].

$$\text{Glucose} + O_2 \xrightarrow{\text{GOD}} \text{Gluconic acid} + H_2O_2 \qquad \text{Equation 24}$$

$$2\ \text{ABTS (colorless)} + H_2O_2 \xrightarrow{\text{HRP}} 2\ \text{ABTS* (green)} + 2\ H_2O \qquad \text{Equation 25}$$
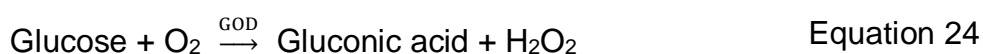
The enzymatic reaction, at which two molecules of ABTS are oxidized by one molecule of hydrogen peroxide, was tracked via a photometer at 405 nm after 5, 10, 15, 20, 25, 30, 45 and 60 minutes. The well was shaken between the measurements at 230 rpm. Figure 23 shows a schematic setup of two silicone tubes prepared with a diffusion membrane at the bottom and placed inside a well.
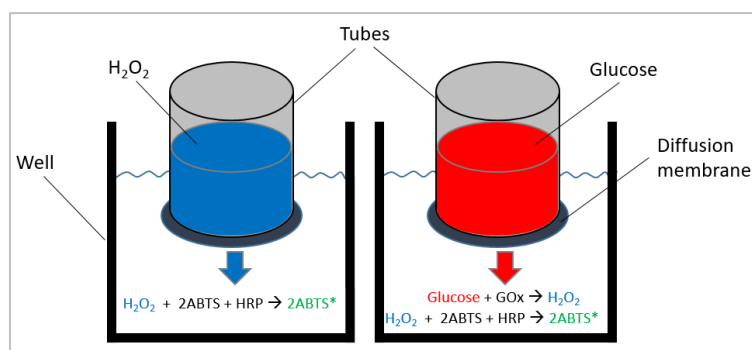
Figure 23 Schematic setup of the diffusion coefficient measurement

The measurement of the diffusion coefficient for hydrogen peroxide was performed as illustrated in the left tube, while the diffusion coefficient for glucose was measured as depicted in the right tube.

Since the diffusion rate was very small, the concentration of the diffusive in both compartments (well and tube) was assumed to be constant. Hence, the known substance concentration inside the tube was practically unchanged, while the glucose or hydrogen peroxide concentration inside the well was assumed to be virtually zero, due to the instant conversion of the diffusive. Under the assumed steady state conditions, the effective diffusion coefficient (D_i,) was calculated with Fick's first law (Equation 26) after measuring the molar flux (dni/dt/A) of the substance as increase in absorbance over time (t).

$$\frac{\mathrm{d}n_i}{\mathrm{d}t * A} = -D_i \frac{\mathrm{d}c_i}{\mathrm{d}x}$$

Equation 26

n_i denotes the amount of the substance of interest, while A and dx denote the known area and the thickness of the applied material. The concentration difference of the substance of interest between the two compartments (well and tube) is given as dc_i and is equal to the concentration of the substance in the tube. This holds true, because the concentration of the substance in the tube remains constant, while the diffused substance is instantly converted and thus its concentration in the well is virtually zero.

The calibration curves for the determination of the diffused substance were measured in wells without the tubes. For this 187.5 µL of the reagent solution (Table 6) with 0, 37.5, 75, 112.5, 150 and 187.5 µL of 0.32 mM H_2O_2 was pipetted in a 24-well plate and complemented with PBS buffer to a total volume of 1.5 mL in each well.

2.8.2.2 Determination of the diffusion coefficients for oxygen

The diffusion coefficient for oxygen was determined by mounting the material of interest in front of a 2 mm oxygen sensor, which was previously glued to a POF with silicone glue (Figure 24). The oxygen sensor was then inserted into a T-shaped flow through cell, through which water was pumped with a peristaltic pump (Minipuls 3 pump from Gilson) at 13.2 mL/min. At first, unsaturated water, which was generated by bubbling nitrogen into the water, was presented to the oxygen sensor until the oxygen partial pressure stabilized close to 0 % air saturation in the oxygen sensor (Figure 24). Then, 100 % air saturated water was pumped through the flow through cell, while

recording the change of the partial pressure within the oxygen sensor behind the material of interest (Figure 24). The measurement was performed with the Fibox 3 from PreSens at the highest frequency possible.
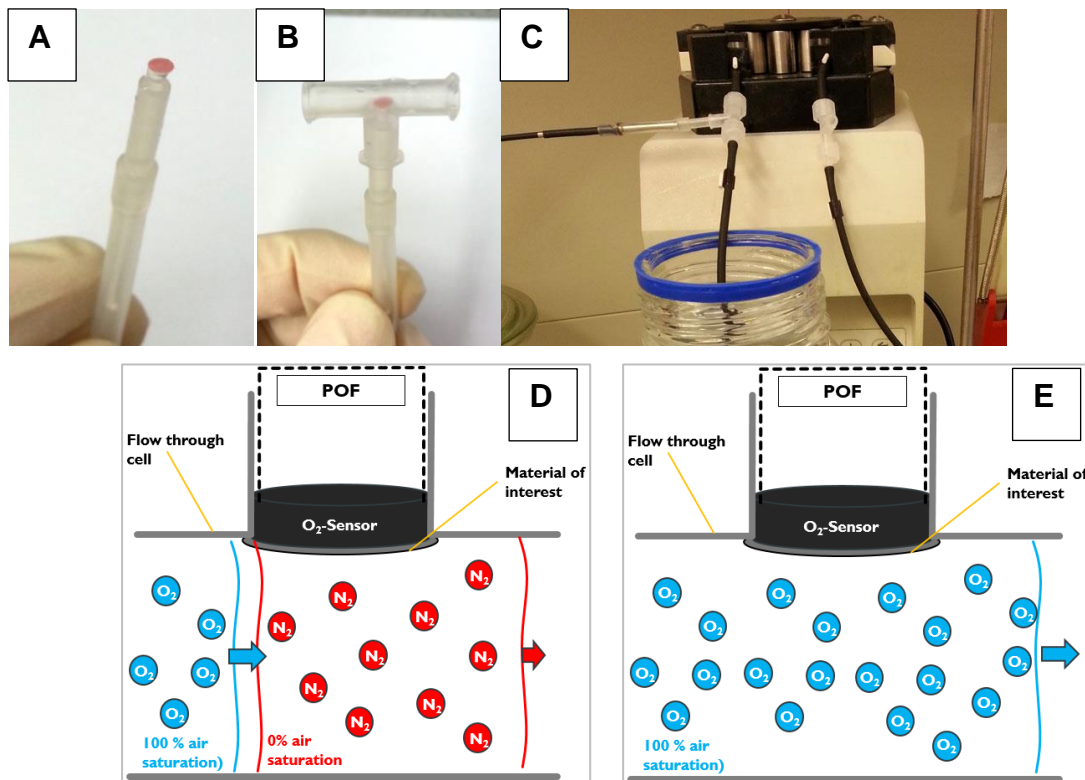
Figure 24: Determination of the diffusion coefficient for oxygen

(A) 2 mm oxygen sensor glued to a POF. (B) Oxygen sensor covered by the material of interest inserted into a T-shaped flow-through cell. (C) Flow through cell connected to a peristaltic pump. (D) Nitrogen saturated water is pumped through the flow through cell. (E) Air saturated water is pumped through the system to measure the flux of oxygen through the biosensor material in front of the oxygen sensor.

The diffusion coefficient for oxygen was likewise calculated with Fick's first law (Equation 26) after measuring the molar flux ($dn_i/dt/A$) of oxygen through the material of interest. The initial slope of the oxygen response signal represents the oxygen flux ($dn/dt/A$) at a timepoint, when the difference in the oxygen concentration (dc_i) across the material of interest was assumed to be approximately 100 % air saturation.

2.8.3 Determination of the Michaelis-Menten constant for glucose

The Michaelis-Menten constant of the enzyme glucose oxidase with respect to glucose was experimentally determined at pH 7.2 and room temperature in a 48-well plate. The enzymatic hydrogen peroxide formation for different glucose concentrations was

tracked via a HRP/ABTS assay with a photometer at 405 nm according to Equation 24 and Equation 25.

The total volume in each well was 1 mL consisting of 30 µL ABTS (c=10 mg/mL), 10 µL GOD (c=0.25 µg/mL) and 955 mL of a glucose solution with 0 mM, 5 mM, 10 mM, 15 mM, 20 mM, 30 mM, 50 mM, 100 mM, 200 mM, 300 mM, 400 mM and 600 mM. During the reaction, the plate was placed on a table shaker at 130 rpm. The absorbance was measured every 60 sec and correlated to a calibration curve that was gained simultaneously with 30 µL ABTS (c=10 mg/mL), 5 µL HRP (c=5 mg/mL) and 965 µL of a hydrogen peroxide solution with 0 mM, 0.01 mM, 0.02 mM, 0.04 mM, 0.06 mM and 0.08 mM.

The enzyme velocity for every glucose concentration was determined by means of the slope in the beginning of the reaction, when the reverse reaction was negligible. The resulting Michaelis-Menten plot was then fitted by a non-linear curve fit in Origin (Version 8.6) to yield the Michaelis-Menten constant for glucose.

2.8.4 Biosensor model

The finite element analysis software COMSOL-Multiphysics 4.4 (COMSOL Inc. Burlington, USA) was applied to create a one-dimensional model for chemical diluted species. It was used to numerically simulate the flow of the enzymatic reactants and products through the glucose biosensor for different diffusion membranes and varying glucose and oxygen levels. The time-dependent simulation of the biosensor response under various conditions was performed by coupling Fick's second law to the enzyme reaction rate Ri:

$$\frac{\mathrm{d}c_i}{\mathrm{d}t} + \nabla(-D_i \nabla c_i) = R_i \qquad \text{Equation 27}$$

where c_i denotes the concentration of the substance of interest and ∇ the nabla operator. D_i represents the diffusion coefficient for the material of interest, which was mostly obtained through measurements described previously in section 2.8.2.1 (Determination of diffusion coefficients). The material property of the oxygen sensor

layer was assumed to be silicone-like. Since water is the main component of growth medium, the diffusion coefficients for water have been applied. The reaction of glucose oxidase was simulated using the Ping-Pong mechanism [110] characterized by the following rate equation [11]:

$$R_i = \frac{V_{max}}{(1+\frac{K_G}{G}+\frac{K_O}{O})}$$

<div align="right">Equation 28</div>

where *G* and *O* are the concentration of glucose and oxygen respectively. K_G and K_O represent the Michaelis-Menten constants for glucose and oxygen. *Vmax* denotes the maximum reaction velocity. The enzymatic reaction was assumed to be described by Michaelis-Menten kinetics [111, 112] with constants derived from free enzymes [111, 113, 114]. The Michaelis-Menten constants were either measured (see section 2.8.3, Determination of the Michaelis-Menten constant for glucose) or attained from literature. The maximum enzyme velocity of the immobilized enzymes was fitted with COMSOL. It was assumed that the enzymes GOD and Cat are evenly distributed inside the enzyme layer, where the reaction occurred. The initial oxygen concentration in the medium and the biosensor was set to 0.296 mM, while all other chemical species were set to virtually zero. The hydrophobic oxygen sensor layer serves as an oxygen reservoir which is deoxygenated by the enzymatic reaction. Thus, the glucose response under the applied conditions was represented by the simulated oxygen concentration inside the oxygen sensor (see supplement Figure 80).

3 RESULTS AND DISCUSSION

For the sake of clarity, the obtained results of this thesis are divided into three main sections corresponding to the three major goals outlined in section 1.9 (Goals of this thesis). The first goal of this research was to develop and characterize an in-line glucose biosensor that is optimized for continuous glucose monitoring in single-use bioreactors. The results of this aim are presented in section 3.1 (Part I: Biosensor development and characterization). The second goal was to develop a computer model of the glucose biosensor, which provides valuable insight into the flux and accumulation of the enzymatic species within the glucose sensor and additionally supports a comprehensive understanding of the biosensor limitations. The developed glucose biosensor model is described in section 3.2 (Part II: Biosensor model). Finally, in section 3.3 (Part III: Cell culture experiments), the developed glucose biosensor was applied for cell culture experiments. The aim was to continuously control the glucose level during CHO fed-batch culture in order to improve the product quality of Darbepoetin alfa, represented by the degree of sialylation.

3.1 Part I: Biosensor development and characterization

In this part, the development and characterization of a glucose biosensor that is suitable for continuous glucose monitoring in animal cell culture, is presented. First, the influence of the auto-fluorescent property of the enzyme layer is discussed. Then biosensors with different diffusion and enzyme layers are evaluated regarding their dynamic range, response time and functional stability under continuous glucose monitoring conditions. Furthermore, the limitation of the biosensor under different environmental conditions (e.g. pH, temperature and dissolved oxygen concentration) are evaluated.

3.1.1 Background fluorescence

The emission spectra of a polymerizing enzyme solution that was excited with green light showed a time dependent fluorescence (see Figure 25). The fluorescence occurred after the immobilization process was initiated with glutaraldehyde, and intensified during the immobilization process. The finding is in agreement with Collins

et al., who have found a maximum excitation at 540 nm and a peak emission at 560 nm for glutaraldehyde crosslinked proteins [115]. Since the enzyme layer of the glucose biosensor is also crosslinked with glutaraldehyde, it disposes a similar auto-fluorescence, which interferes with the glucose biosensor measurement. The result is an increased total amplitude, due to the occurrence of background fluorescence, which translates into a higher oxygen partial pressure (see Figure 26).
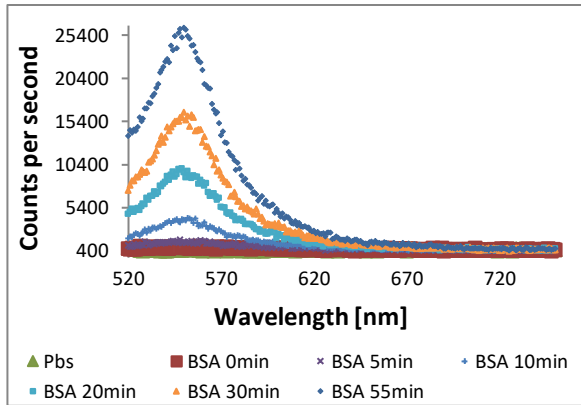
Figure 25 Background fluorescence of a polymerizing enzyme solution over time.

The emission spectra of a polymerizing enzyme solution were measured with green light after glutaraldehyde addition. The data was generated with a spectrofluorimeter from Horiba Scientific.
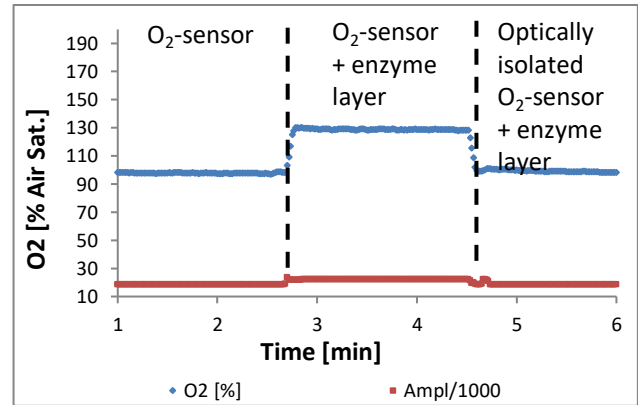
Figure 26 Oxygen sensor signal with and without background fluorescence

The signal amplitude and the apparent oxygen level is increased, by the backgrund fluorescence of a crosslinked enzyme layer, for oxygen sensors without an optical isolation.

The absorption bands of the enzyme layer and the oxygen sensor overlap, hence they are both excited at the same wavelength. However, the emission bands overlap too, which leads to an increased total amplitude (see Figure 26) and a mixed phase angle shift as described by the Dual Life-time Referencing (DLR) equation. The DLR equation is derived from the superposition of the signal amplitude of the oxygen sensor and the background fluorescence of the enzyme layer:

$$A_m \cdot \cos \theta_m = A_{Background} \cdot \cos \theta_{Background} + A_{O2} \cdot \cos \theta_{O2} \quad \text{Equation 29}$$

$$A_m \cdot \sin \theta_m = A_{Background} \cdot \sin \theta_{Background} + A_{O2} \cdot \sin \theta_{O2} \quad \text{Equation 30}$$

The emission intensity (A_{O2}) and the phase angle shift (θ_{O2}) of the luminophores inside the oxygen sensor matrix, are sensitive to the analyte oxygen, while the background fluorescence intensity ($A_{Background}$) from the crosslinked enzyme layer

is not analyte dependent and thus constant. However, the phase angle shift of the fluorophores inside the enzyme layer is negligible ($\theta_{Background} \approx 0$), since the life-time of fluorophores is very short. Therefore, the Equation 29 and Equation 30 can be simplified to:

$$A_m \cdot \cos\theta_m = A_{Background} \cdot 1 + A_{O2} \cdot \cos\theta_{O2} \qquad \text{Equation 31}$$

$$A_m \cdot \sin\theta_m = A_{O2} \cdot \sin\theta_{O2} \qquad \text{Equation 32}$$

The division of Equation 31 and Equation 32 results in the DLR equation (Equation 33), in which the mixed signal (θ_m) depends on the phase angle of the analyte sensitive luminophores (θ_{O2}) and the intensity ratio of the constant background fluorescence ($A_{Background}$) and the oxygen sensitive luminophores (A_{O2}).

$$\frac{1}{tan\theta_{Measurement}} = \frac{A_{O2} \cdot \cos\theta_{O2} + A_{Background}}{A_{O2} \cdot \sin\theta_{O2}} \qquad \text{Equation 33}$$

$$= \cot\theta_{O2} + \frac{A_{Background}}{A_{O2} \cdot \sin\theta_{O2}} = \frac{1}{tan\theta_{O2}} + \frac{A_{Background}}{A_{O2} \cdot \sin\theta_{O2}}$$

The higher the background fluorescence, the lower the resulting phase angle shift, which translates into a higher oxygen partial pressure (see Figure 26). Yet in practice, the background fluorescence intensity was not constant over a long period of time, which led to a parallel shift of the calibration curve measured between several days (see supplementary Figure 79). Collins et al. have previously described the photo induced destruction of the background fluorescence at visible light and pointed out, that the fluorescence change is also pH dependent [115]. In order to eliminate the background fluorescence, oxygen sensors with a carbon-black optical isolation were used during the course of this thesis. The carbon-black layer is located between the oxygen sensor and the enzyme layer and absorbs the background fluorescence from the crosslinked enzyme matrix and thus eliminates the influence on the biosensor signal (see Figure 26).

3.1.2 Biosensors coated with a liquid polyurethane diffusion layer

A key problem during the development and optimization of a glucose biosensor was to ensure a good mechanical and functional stability at an acceptable dynamic range and response time. Therefore, three coatable diffusion layers made from different urethane polymers (D4, D6 and D7) were studied. Two diffusion layer materials (D6 and D7), however, suffered from cracking after the storage in PBS buffer (see Figure 27) and were therefore neglected. The remaining material (D4) was applied as a diffusion layer with three different coating methods, drop-flow-coating, knife-coating and pipette-coating (see section 2.2.1, Oxygen based biosensor preparation with a liquid diffusion layer solution).

The reproducibility of the biosensor manufacturing process, which varied in the coating method, was determined by measuring the relative standard deviation (RSD) of six glucose biosensors for each method. The glucose sensors were mounted onto a 24-well plate and operated at different glucose levels. The resulting measurement deviations are compared at different signal heights (% air saturation) in Table 7.

Table 7 Reproducibility of six biosensors mannufactured with different coating methods. The reproducibility is compared at different signal levels and illustrated as relative standard deviation (RSD).

Biosensor response (pO$_2$):	~ 115 % air saturation	~ 60 % air saturation	~ 40 % air saturation	~ 20 % air saturation	~ 12 % air saturation
Drop-flow [RSD]:	0.7 %	1.1 %	1.5 %	1.6 %	1.4 %
Knife coating [RSD]:	0.2 %	3.2 %	-	14.3 %	-
Pipetting [RSD]:	1.3 %	7.6 %	19.2 %	23.7 %	19.4 %

The drop-flow coating method allowed to create biosensors with the thinnest (12 µm) diffusion layer, yielding the highest biosensor reproducibility at a very fast response time of t_{90} = 1 min (t_{90} = time until 90 % of the final sensor signal was reached) and a sufficient dynamic range of 25 mM at 100 % air saturation in the sample (see supplement Figure 78).
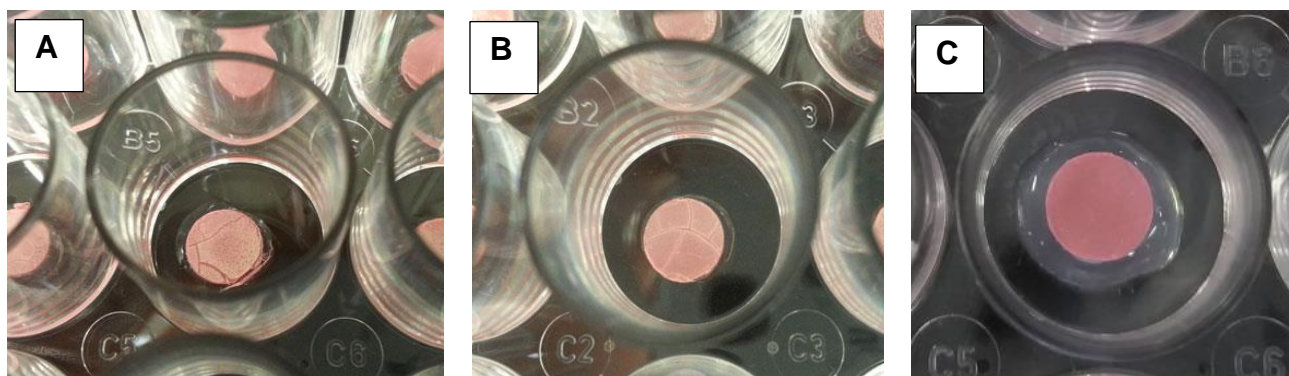
Figure 27 Biosensors with different diffusion layers after storage

The diffusion layer polymers, (A) D6 and (B) D7 cracked during storage in PBS buffer, while the D4 polymer remained intact (C).

Although biosensors with a D4 polyurethane diffusion layer showed good results, they were eventually rejected, too, because the polyurethane polymer matrix detached easily from the enzyme layer during long term measurements. This phenomenon can be explained by the weak interaction between the hydrophilic enzyme layer and the semi hydrophobic polymers. For this reason, different perforated diffusion membranes with varying permeabilities have been studied as an alternative and are discussed in the following section.

3.1.3 Biosensors coated with a solid diffusion membrane

Unlike urethane polymers, hydrophilic perforated diffusion membranes feature a good mechanical stability and allow the application of glucose biosensors for long-term measurements. Furthermore, the membranes are classified by the manufacturer as biologically inert and biocompatible with negligible toxicity (USP, Class IV) and were therefore applicable for cell culture in bioreactors. In addition, the hydrophilic surface prevents biofouling due to protein adhesion, since proteins are hydrophobic in nature [116]. Because of the superior features of biosensors with a perforated diffusion membrane, they were used henceforth during this research and are characterized in this chapter regarding the following criteria:

Table 8 Applied criteria for the characterization of biosensors with a diffusion membrane

Criterion	
Dynamic range	Glucose concentration range with a linear biosensor response
Response time (t90)	Time until 90% of the final biosensor signal is reached

Reversibility	Signal returns to the same value at the same analyte concentration
Functional stability	Biosensor stability under continuous glucose measurement
Storage stability	Biosensor stability after a certain time of storage
Reproducibility	Comparability of the measurement signal for biosensors manufactured with the same method
Selectivity	Cross sensitivity of the glucose biosensor to oxygen
Robustness	Influence of pH and temperature on the biosensor signal
Sterilizability	Biosensor stability after gamma, beta or UV irradiation

3.1.3.1 Dynamic range, response time and signal reversibility

A key problem for the biosensor development and optimization was to achieve a sufficient dynamic range with an acceptable response time for cell culture purposes. The dynamic range of the biosensor is given by the linear section of the characteristic biosensor response (see Figure 28) and depends on the permeability of the diffusion layer for glucose and oxygen. Thus, different diffusion membranes can be used in order to customize the dynamic range of the glucose biosensor. The membrane material and their porosity touches the property rights of PreSens GmbH and are therefore not disclosed in this thesis.

Table 9 illustrates the dynamic ranges and response times of biosensors with three different diffusion membranes at room temperature, 100 % air saturation and 130 rpm in a 125 mL shake flask.

Table 9 Dynamic range and response time of biosensors with different diffusion membranes
Operating conditions: room temperature, 100 % air saturation and 130 rpm in a 125 mL shake flask.

	Membrane 1	Membrane 2	Membrane 3
Dynamic range:	0-2 mM	0-20 mM	0-40 mM
Response time (t_{90})	≤ 10 min	≤ 10 min	≤ 15 min
Thickness	12 µm	6 µm	25 µm

The response time depends linearly on the diffusion coefficient of glucose, but increases with the square of the membrane thickness [117]. Due to the applied thin low permeability membranes (Membrane 2), the glucose diffusion was very low at a reasonable response time of $t_{90} < 10$ min under the given operating conditions. The high permeability membrane (Membrane 3) is thicker and had therefore a higher response time. Because of limited membrane availability, biosensors with "Membrane 2" were chosen for further characterization. The characteristic response (see Figure 28) and the calibration curve (see Figure 29) were obtained with a biosensor and a reference oxygen sensor in a 24-well plate by adding incremental amounts of glucose to 2 mL PBS buffer. Generally, the glucose response is expressed as the oxygen partial pressure (pO_2), or, if an additional oxygen reference sensor is applied, as the difference in the oxygen levels (ΔpO_2) between the biosensor and an oxygen reference sensor (see Figure 28).
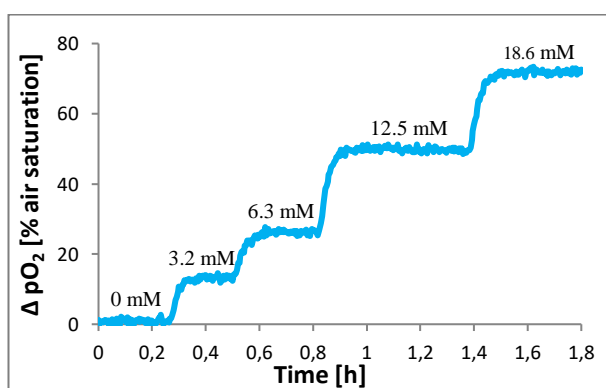
Figure 28 Characteristic biosensor response in combination with an oxygen reference sensor

Biosensor response to incremental glucose increase in 2 mL PBS in a 24-well plate at 25°C, 230 rpm and 100 % air saturation. The oxygen reference sensor was placed in a separat well under the same conditions.
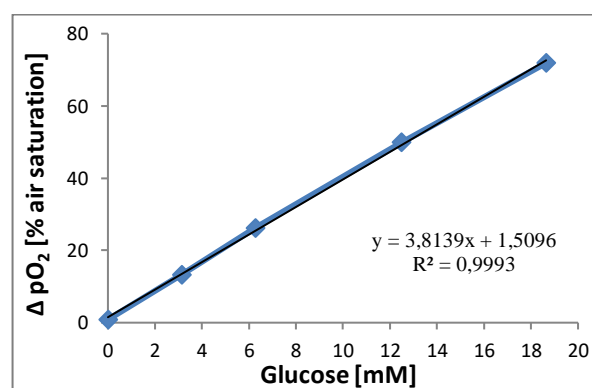
Figure 29 Resulting biosensor calibration curve after addition of glucose

The calibration curve was gained by incremental analyte increase in 2 mL PBS in a 24-well plate at 25°C, 230 rpm and 100 % air saturation. The oxygen reference sensor was placed in a separat well under the same conditions.

The sensitivity of the glucose biosensor is given by the slope of the calibration curve (see Figure 29) and depends strongly on the permeability of the diffusion layer to glucose and oxygen, but also on the ambient temperature and flow rate, as described in section 3.1.3.2 (Influence of the operating conditions on the biosensor signal).

Figure 30 illustrates the reversibility of the glucose biosensor in 125 mL shake flasks with different glucose concentrations at 25°C, 130 rpm and 100 % air saturation.

Interestingly, the response time is faster when the glucose concentration is increased. Hence, for increasing glucose concentrations the response time was $t_{90} = 6$ min compared to $t_{90} = 10$ min for decreasing glucose levels. Both, the dynamic range and the response time of the glucose biosensor depends to a great extent on the ambient operating conditions, e.g. temperature, dissolved oxygen concentration and flow rate.
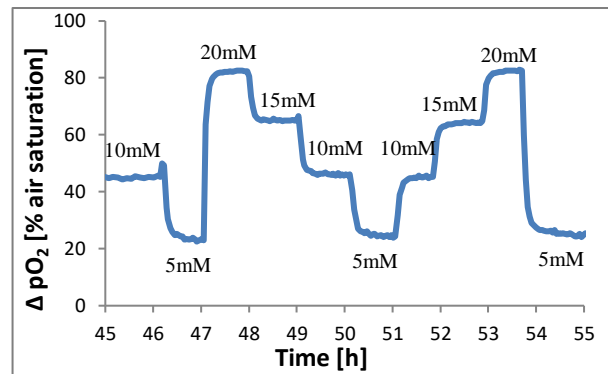
Figure 30 Reversibility of the glucose biosensor response

Reversibility of the biosensor signal for increasing and decreasing glucose concentrations in 125 mL shake flasks with different glucose solutions in 50 mL PBS buffer: 5 mM, 10 mM, 15 mM and 20 mM glucose at 25°C, 130 rpm and 100 % air saturation.

The influence of operating conditions on the glucose biosensor response are described in the following sections.

3.1.3.2 Influence of the operating conditions on the biosensor signal

The influence of different operating conditions on the biosensor signal, like temperature, flow rate, pH and ambient DO, are discussed in this section.

Temperature influence on the biosensor signal

The dynamic range and the reaction rate are limited by the diffusion of glucose and oxygen through the diffusion layer. Because diffusion is a temperature dependant process, a constant temperature must be applied to avoid a signal drift. The temperature effect on the biosensor sensitivity is illustrated in Figure 31 as a change in the slopes of the calibration curves of three glucose biosensors attained at 20°C and 37°C. Higher temperatures lead to an increase in the glucose diffusion rate and therefore to a higher biosensor sensitivity and faster response times. This comes however at the expense of a smaller dynamic range (see Figure 31).

The dynamic quenching process between oxygen and the luminophores in the oxygen sensor material, is also temperature dependent. This leads to an apparent increase in the oxygen partial pressure, when the temperature rises (data not shown). This effect can however be compensated by the SDR software [14].
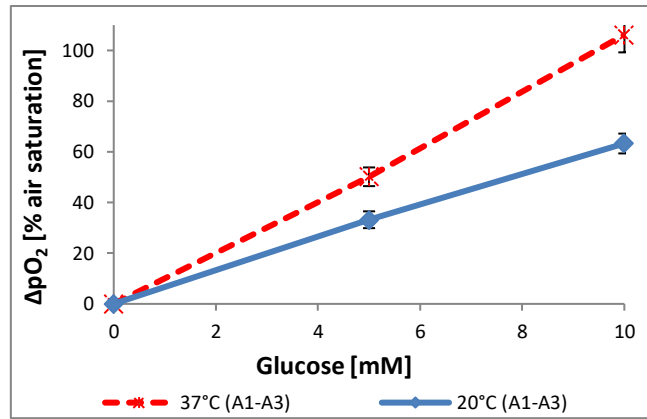
Figure 31 Temperature influence on the biosensor sensitivity

Mean calibration curves of three glucose biosensors in a 24-well plate at 20°C compared to 37°C. The error bars correspond to the standard deviation of the triplicate measured at 200 rpm.

Flow rate influence on the biosensor signal

The flow rate has an impact on the dynamic range and the response time of the glucose biosensor, because it influences the substrate gradient and thereby the diffusion rate of the substrates glucose and oxygen into the biosensor. Hence, the flow velocity must be kept stable during the measurement to prevent a signal drift (see Figure 32). The influence of convection diminishes however with increasing flow rates.
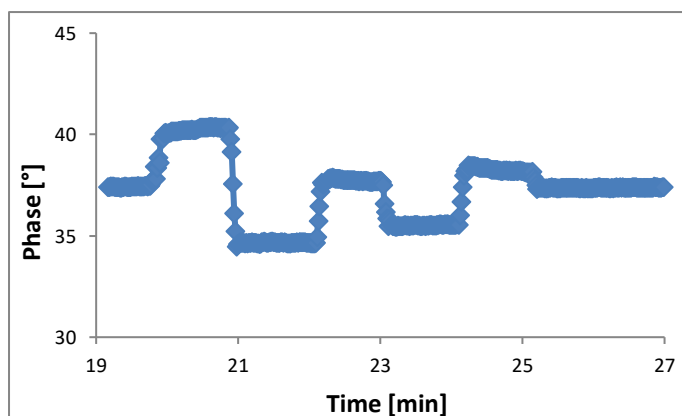
Figure 32 Flow rate influence on the biosensor signal

Biosensor signal (measured as phase shift) at different shaking velocities.

The flow rate dependency entails that the glucose biosensor can only be used for suspension cell culture, where shaking is applied.

pH influence on the biosensor signal

Gluconic acid is a weak acid (pka=3.86) that is produced during the conversion of glucose and oxygen by glucose oxidase [118]. Thereby the pH decreases within the enzyme layer of the biosensor when glucose is added. The pH decrease upon 10 mM glucose addition, was measured with four pH based glucose biosensors in a 24-well plate at room temperature and 230 rpm (see Figure 33). The biosensors consist of a pH sensor that is coated with a glucose oxidase layer and a diffusion membrane (cf. section 2.2.3, pH based biosensor preparation for gluconic acid determination).
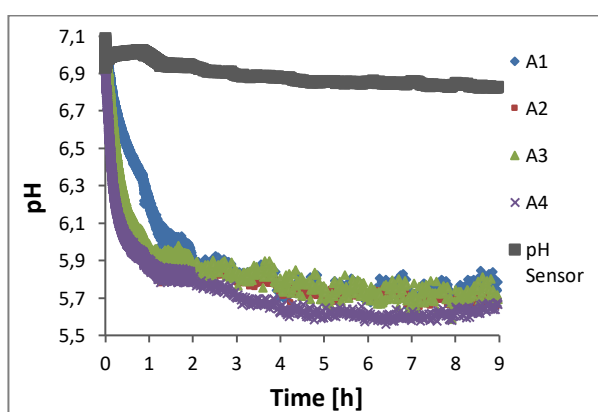
Figure 33 pH inside the biosensor during glucose measurement

pH measurement within the enzyme layer of four pH based biosensors (A1-A4) after addition of 10 mM glucose in a 24-well plate filled with PBS buffer at room temperature and 230 rpm in comparison to a pure pH sensor.
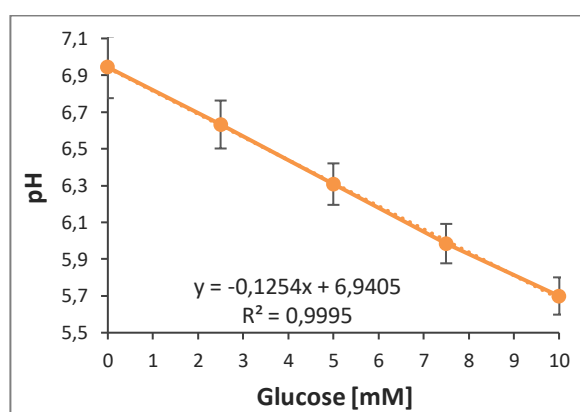
Figure 34 Calibration curve of pH based biosensors

Mean calibration curve of four pH based biosensors, attained by addition of different glucose concentrations in a 24-well plate at room temperature and 230 rpm in PBS buffer. The errorbars correspond to the standard deviation of four measurements.

The pH drop was measured in four biosensors at different glucose concentrations in PBS buffer as illustrated in Figure 33. The pH optimum for immobilized glucose oxidase lies in a range between pH 5-6 and was not surpassed at glucose levels within the dynamic range of the biosensor [119].

Despite the dependence of the enzyme kinetic on the pH, the biosensor response of oxygen based glucose biosensor, is not affected by pH ranging from 5 to 8 (data not shown), because the enzyme reaction is not the rate limited step [104]. Instead, the biosensor signal depends primarily on the diffusion rate of glucose through the diffusion layer as will be discussed in detail in section 3.2.2.1 (Diffusion coefficients for glucose, oxygen and hydrogen peroxide).

Cross sensitivity of the glucose biosensor to oxygen

Figure 35 illustrates the effect of hypoxic compared to normoxy measurement conditions on the calibration curve attained in a shake flask at 37°C, 130 rpm, 80 % humidity and 5 % CO_2. In this case, a high permeability membrane (HPM) was applied as a diffusion layer for a biosensor with a dynamic range of 30 mM at 100 % air saturation. Due to the decrease of the ambient dissolved oxygen concentration (DO) in the sample to 50 % air saturation, the dynamic range of the biosensor was almost halved (see Figure 35).
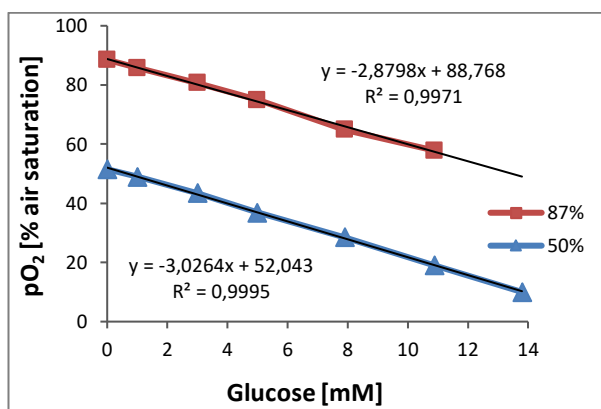
Figure 35 Influence of the dissolved oxgen concentration on the biosensor signal

A calibration curve at 87 % and 50 % air saturation, measured with the same biosensor in a 125 mL shake flask at 37°C, 80 % humidity, 5 % CO_2 and 130 rpm.
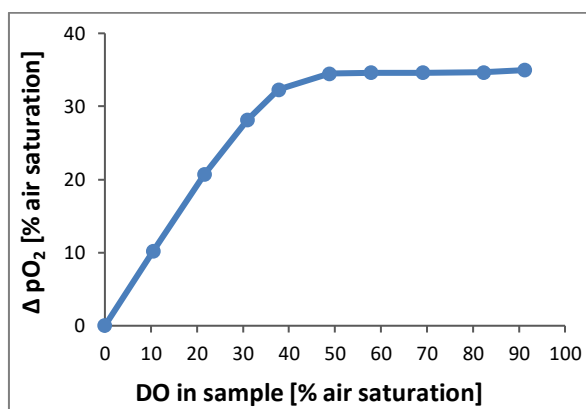
Figure 36 Cross sensitivity to oxygen

Biosensor signal at 5 mM glucose in a shake flask at decreasing of dissolved oxygen concentration (DO). Measurement conditions: 37°C, 5 % CO_2, 80 % humidity at 130 rpm.

Because of the cross sensitivity of the glucose biosensor to oxygen, an oxygen reference sensor is needed to compensate for varying oxygen levels. However, a small cross sensitivity to oxygen remains, despite the use of a reference sensor, because the biosensor signal is not only glucose diffusion limited, but also slightly oxygen diffusion dependent at glucose levels within the dynamic range. This is demonstrated in the diminishing biosensor signal (ΔpO_2) for decreasing oxygen levels at a constant glucose concentration in Figure 36. The biosensor signal decline was 1.4 %, when the dissolved oxygen concentration in the PBS sample was decreased from 90 % to 50 % air saturation. In this case, a biosensor with a low permeability membrane (LPM) was used, that featured a dynamic range of approximately 11 mM at 100 % air saturation. At an ambient DO below 50 %, the applied glucose level of 5 mM exceeded the dynamic range of the biosensor, where oxygen becomes increasingly faster diffusion limited. This lead to a sharp signal decrease (see Figure 36), because the enzymatic

reaction rate is slowed down by the slow oxygen supply at a low ambient DO levels [82, 120]. This circumstance is discussed in greater detail in section 3.2.2.1 (Biosensor response).

3.1.3.3 Functional stability

The optical glucose biosensor is dynamic in nature; hence the biosensor consumes oxygen and glucose according to Equation 5 to Equation 7. Hydrogen peroxide is a by-product of the glucose oxidase catalysed enzyme reaction, which deactivates the enzyme glucose oxidase (GOD) in a concentration dependent manner [37]. As a result, the life-time of a glucose biosensor strongly depends on the hydrogen peroxide concentration within the enzyme layer.

With respect to structural integrity and sensitivity, the glucose biosensor needs to be stable under bioreactor conditions for a typical cell culture duration around eight days. Therefore, the functional stability of glucose biosensors with different GOD loadings and two different diffusion membranes was tested under continuous glucose monitoring conditions in a 24-well plate. The experiment was performed over several weeks at a high glucose level to yield considerable hydrogen peroxide levels inside the biosensor. In one setup, the enzyme catalase was co-immobilized in the enzyme layer in order to protect the GOD by decomposing hydrogen peroxide into water and oxygen according to the following equation [121–123]:

$$H_2O_2 \xrightarrow{\text{Cat}} H_2O + \tfrac{1}{2}\, O_2 \qquad\qquad \text{Equation 34}$$

Figure 37 illustrates the emitted hydrogen peroxide concentrations within three days for several biosensor types as mean of three sensors. The emitted hydrogen peroxide concentration was determined in the beginning of the experiment (day 1-3) and after three weeks (day 21 to 23). For the catalase containing biosensors, the amount of accumulated hydrogen peroxide was significantly lower, however only in the beginning of the experiment (day 1-3). Hence, biosensors with additional catalase were found to initially emit less hydrogen peroxide, but increased to average emission rates after three weeks of continuous glucose monitoring (see Figure 37). This observation

confirms that hydrogen peroxide not only deactivates GOD, but also catalase, as previously reported in literature [37, 119, 124, 125].
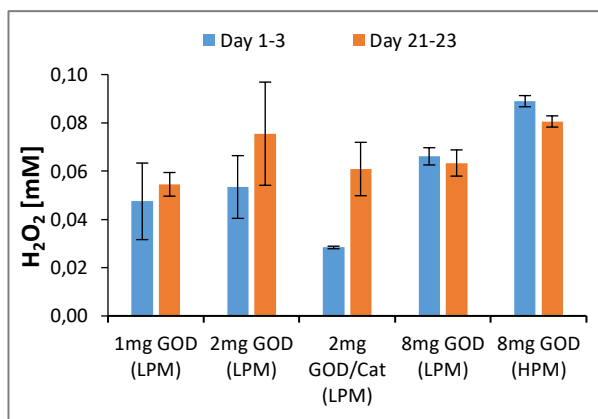
Figure 37 Hydrogen peroxide accumulation

Mean H_2O_2 accumulation of different biosensor types measured in the beginning (day 1-3) and a later phase (day 21-23) during continuous glucose monitoring in a 24-well plate at 17.5 mM glucose. Operating conditions: room temperature and 230 rpm. The error bars correspond to the standard deviation of three biosensors for each type.
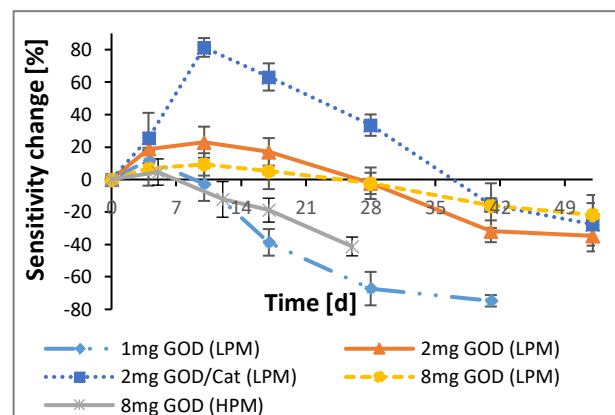
Figure 38 Sensitivity change during continuous glucose monitoring

The sensitivity change of biosensors with different enzyme layer compositions (glucose-oxidase (GOD) and catalase (Cat) concentrations) and diffusion membranes with a low permeability (LPM) and a high permeability membrane (HPM) in a 24-well plate over time at 17.5 mM glucose. Operating conditions: 25°C, 230 rpm and 100 % air saturation. The error bars correspond to the standard deviation of three biosensors for each type.

During the long-term continuous glucose monitoring experiment, the functional stability of the biosensors, expressed as sensitivity change over time (see Figure 38), was closely monitored by periodic calibrations. The slopes of the attained calibration curves were compared to the initial calibration curve on day 0 in order to track the sensitivity change over time as illustrated in Figure 38. Surprisingly, the sensitivity increased for all glucose biosensor types during the initial days of the experiment. This phenomenon is most likely caused by the inactivation of catalase in all biosensor types, because GOD is naturally contaminated with catalase (≤ 5 units/mg protein according to the manufacturer). Hence, when catalase is deactivated, the oxygen depletion after glucose addition is more pronounced. Thus, the biosensor sensitivity increases. This finding was confirmed by an increase of the oxygen partial pressure within the sensor, when 5 mM of hydrogen peroxide were added to freshly generated glucose biosensors (see supplementary Figure 81). Biosensors, whose enzyme layer was additionally supplemented with 2 mg catalase, experienced a more pronounced sensitivity increase, since more catalase was inactivated over time. Surprisingly, the biosensor sensitivity dropped much faster thereafter, which reverses the effect of catalase

completely. This can be attributed to the fact, that even though the hydrogen peroxide accumulation inside the enzyme layer was less, the enzymatic reaction rate, due to the additional oxygen generated by catalase, was increased. Hence, more GOD was in its vulnerable reduced state, which is easily deactivated by hydrogen peroxide [35]. As a consequence, no positive effect on the overall functional stability was observed, when additional catalase was added to the enzyme solution in order to protect the GOD.

Biosensors with low enzyme loadings experienced the strongest irreversible inhibition (see Figure 38), because a low amount of GOD can be deactivated faster by hydrogen peroxide. Despite a high GOD loading (8 mg), the sensitivity decrease observed for biosensors with a high permeability membrane (HPM) was much faster compared to biosensors with a low permeability membrane (LPM). As revealed by the biosensor model (see section 3.2.2.2, Enzyme inhibition), this phenomenon is caused by a higher influx of glucose and oxygen that leads to an increased enzymatic reaction rate. Thus, a higher proportion of the GOD is permanently in its reduced state, which is 100 times more vulnerable to hydrogen peroxide [35]. The functional stability can be potentially increased by using a thicker enzyme layer, as well. However, this would come at the expense of an increased response time, since the response time depends on the enzyme layer thickness [117].

3.1.3.4 Storage stability

Storage stability studies were carried out to investigate the stability of glucose biosensors at 4°C under dry and wet storage conditions. It was observed that the sensitivity of dry stored biosensors decreased dramatically during the first week of storage at 4°C. This effect was probably caused by the detachment of the diffusion membrane from the enzyme layer as depicted in the bottom row of Figure 39. The gap between the shrinking enzyme layer and the diffusion layer filled with air and compromised the glucose flux into the biosensor.

In contrast to dry storage, storing the biosensor under wet conditions in PBS buffer allowed to maintain the sensitivity of the biosensors over at least 120 days (see Figure 40).
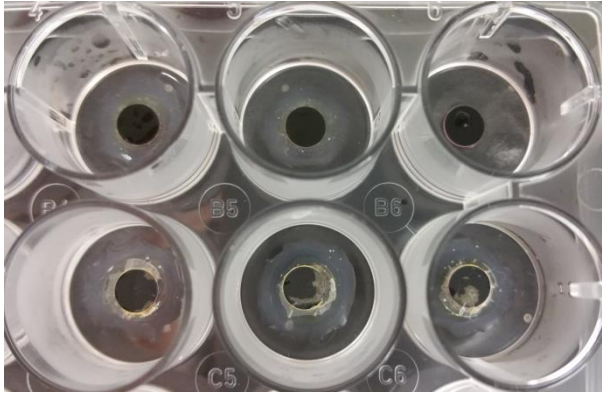
Figure 39: Biosensors after wet and dry storage in a 24-well plate

Biosensors stored in PBS (upper row) versus dry storage (bottom row). The biosensors in the bottom row suffered from an enzyme layer shrinkage, which led to a diffusion layer detachment. As a result, air accumulated between the enzyme layer and the diffusion layer. The upper row showed no signs of membrane detachment, since the biosensors were stored in PBS.
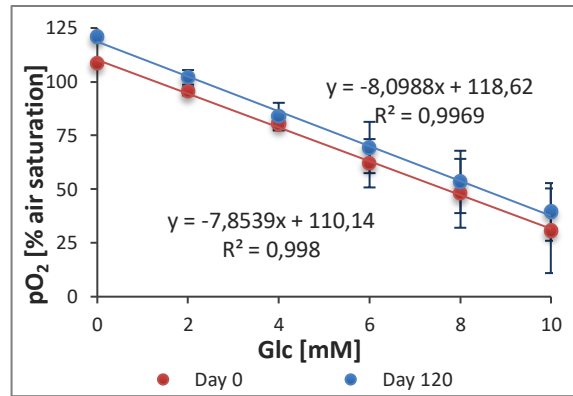
Figure 40 Biosensor sensitivity after wet storage in a 24-well plate at 130 rpm.

Mean calibration curve of three biosensors before and after storage in PBS at 4°C over 120 days. The measurement of the calibration curves was performed at room temperature without temperature control or decompensation by the software. The offset in the oxygen partial pressure between the two mean calibration curves was due to a different temperature and atmopheric pressure on day 0 and day 120. The error bars correspond to the standard deviation of the triplicate.

3.1.3.5 Biosensor reproducibility

The reproducibility of biosensors manufactured with a perforated diffusion membrane was determined by measuring the relative standard deviation (RSD) of eight glucose biosensors mounted into a 24-well plate. The signal reproducibility was determined for five signal levels within the dynamic range of the glucose biosensors with varying glucose solutions (see Table 10).

Table 10 Reproducibility of eight biosensors at different glucose levels in PBS buffer.

Biosensor response (pO2)	105 % air saturation	95 % air saturation	77 % air saturation	47 % air saturation	38 % air saturation
Relative standard deviation	0.1 %	1.5 %	4.9 %	9.3 %	11.4 %

The reproducibility of the biosensors with a diffusion membrane was below the reproducibility of biosensors with a polyurethane diffusion layer (see section 3.1.2, Biosensors coated with a liquid polyurethane diffusion layer). However, since the glucose biosensor are calibrated with a quick and simple one-point calibration before every cell culture experiment, the observed reproducibility is acceptable.

3.1.3.6 Enzyme leakage

According to the specifications of the manufacturer, the diffusion membrane is theoretically impermeable for GOD. However, an enzyme leakage in the pg range was still detected from biosensors during two hours in PBS buffer (see Figure 41).
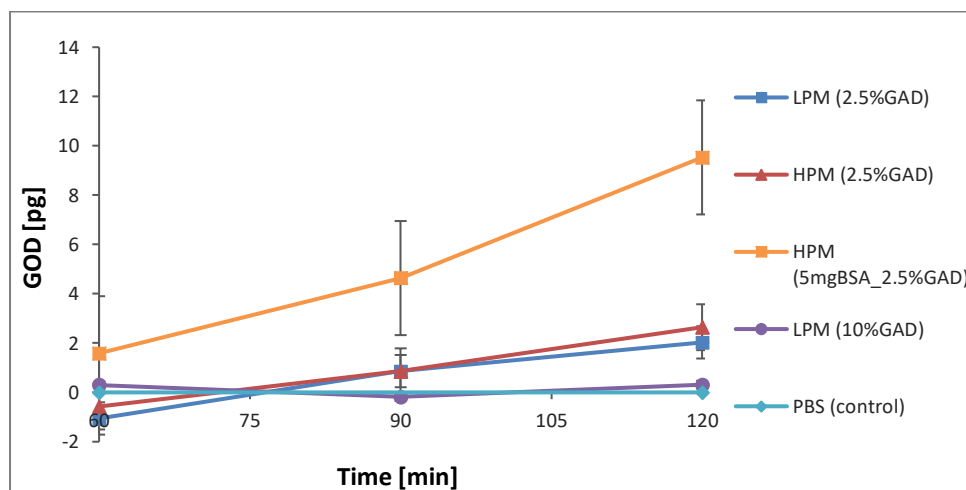
Figure 41 GOD leakage from different types of glucose biosensor

Three biosensors for each type were placed separately in a 24 well and stirred in PBS buffer at 130 rpm and room temperature. After 60, 90 and 120 min a sample was taken and analysed with a HRP/ABTS assay to measure the amount of free GOD that diffused from the biosensors into the medium. The error bars correspond to the standard deviation of each triplicate.

The leaked enzyme was photometrically quantified with ABTS and HRP from samples, in which the biosensors were shaken for 60 min, 90 min and 120 min. The leakage was less pronounced for biosensors made from enzyme solutions with a high glutaraldehyde (10 % GAD) concentration, presumably because of an increased crosslinking. This however comes most likely at the expense of a decreased enzyme activity, due to conformational changes of the enzyme, introduced by the crosslinking agent glutaraldehyde [126]. No significant difference in the GOD emission was observed for biosensors with the same enzyme layer composition (2.5 % GAD), but different diffusion membranes (LPM and HPM). Here, the low permeability membrane (LPM) was not superior to the high permeability membrane (HPM), supposedly because the HPM membrane is four times thicker.

The highest GOD leakage was encountered for biosensors with a low BSA concentration (5 mg instead of 50 mg), since BSA serves as a cross linker for GOD.

3.1.3.7 Limit of detection and limit of quantification

The limit of detection (LOD) and the limit of quantification (LOQ) were determined according to IUPAC [127], as three times and ten times the standard deviation of the biosensor response, respectively, divided by the biosensor sensitivity (slope of the calibration curve). For biosensors with a dynamic range of 20 mM the LOD was determined to be 0.45 mM, while the LOQ was 1.5 mM. Both parameters were comparable to current literature regarding optical enzymatic glucose biosensors [13, 128].

3.1.3.8 Sterilisation

In order to prevent a contamination of a bioreactor, a biosensor needs to be sterilized prior to application. Sterilization has been performed by gamma and beta irradiation at 18 kGy, which proved to be suitable with only a modest decrease in sensitivity (Figure 42 and Figure 43).
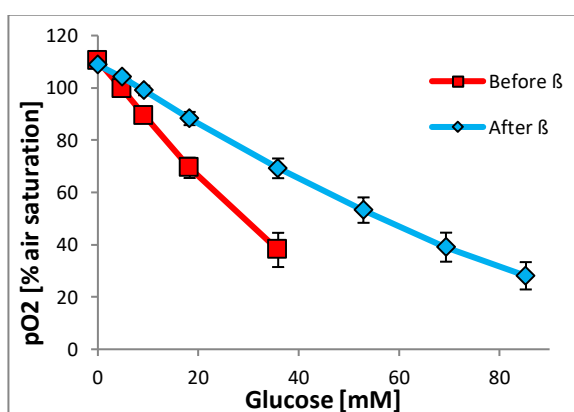
Figure 42 Influence of beta irradiation

Calibration curve as mean of ten biosensors before and after beta irradiation in a 24-well plate. Operating conditions: room temperature at 230 rpm. The error bars correspond to the standard devitation.
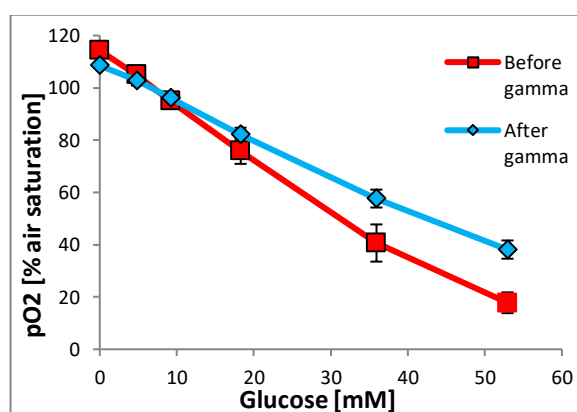
Figure 43 Influence of gamma irradiation

Calibration curve as mean of ten biosensors before and after gamma irradiation in a 24-well plate. Operating conditions: room temperature at 230 rpm. The error bars correspond to the standard devitation.

The sensitivity loss described in section 3.1.3.4 (Storage stability) after dry storage, suggests that the sensitivity decrease after the irradiation, might have been caused to some degree by the dry storage during shipment to the place of irradiation and back, which took approximately one week.

Other sterilization methods like chemical sterilization with 35 % hydrogen peroxide over 24 hours have also been conducted successfully (data not shown). It is however only advisable, if no glucose is present and thus the enzyme is not in its reduced state, which is 100-fold more sensible to hydrogen peroxide deactivation than the oxidized form [35]. Although UV exposure is described to have a negative influence on the glucose response of GOD biosensors [129], it has been applied successfully for the most cell culture experiments during this thesis. Because of the surplus of GOD in the enzyme layer, it was possible to use UV irradiation for sterilization purposes without a loss in sensitivity for the biosensors applied in the cell culture experiments outlined in section 2.4 (Cell culture experiments in 125 mL shake flasks) and section 2.5 (Cell culture experiments in 6-well plates with glucose and oxygen sensors).

3.2 Part II: Biosensor model

In this part, a one-dimensional biosensor model is presented for computational simulations of the biosensor signal at different oxygen and glucose levels in the sample. The simulations are compared to experimental results to validate the biosensor model and used for complementary characterization and optimization of the glucose biosensor life-time.

3.2.1 Development of a glucose biosensor model

The geometry and the apparent diffusion coefficients of the biosensor materials for the substrates and products involved, are crucial parameters for the development of a glucose biosensor model. The results of the parameter measurements are presented here.

3.2.1.1 Diffusion coefficients for glucose, oxygen and hydrogen peroxide

Illustrated in Figure 44 are the results of the diffusion coefficients determination for glucose, oxygen and hydrogen peroxide according to section 2.8.2 (Determination of diffusion coefficients) for a low permeability (LPM) and a high permeability membrane (HPM). Figure 45 shows the diffusion coefficients for the enzyme layer.
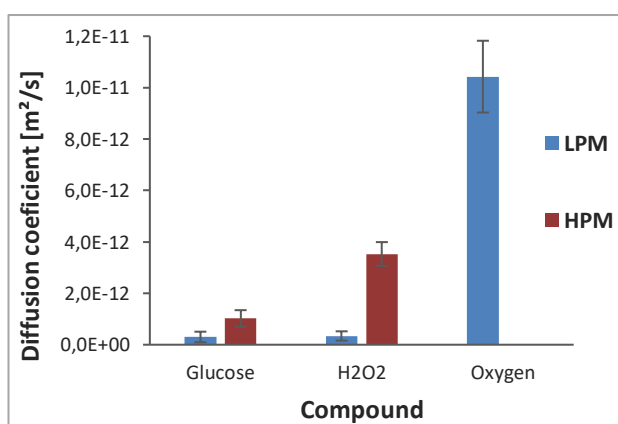
Figure 44 Diffusion coefficients of the diffusion membranes

Diffusion coefficients of a high permeability (HPM) and a low permeability membrane (LPM) for glucose, oxygen and H_2O_2. The data is presented as mean value of six measurements. The error bars correspond to the standard deviation.
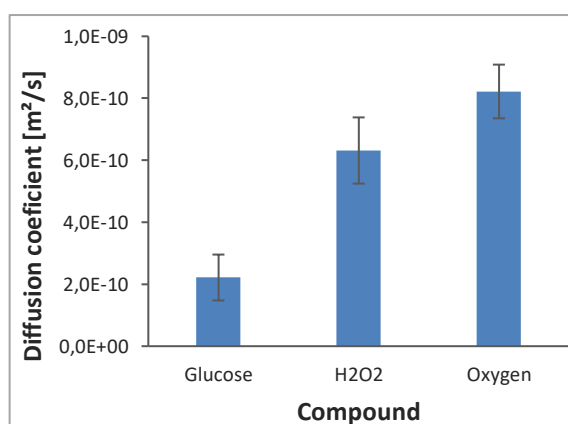
Figure 45 Diffusion coefficients for the enzyme layer

Diffusion coefficients of the enzyme layer for glucose, oxygen and H_2O_2. The data is presented as mean value of six measurements. The error bars correspond to the standard deviation.

The fluctuations in the diffusion coefficients in Figure 44 and Figure 45, show that the permeability of the biosensor materials varied strongly. As expected, the diffusion coefficients for the high permeability membrane were significantly higher. In the case of the HPM membrane, the determination of the diffusion coefficient for oxygen was not possible, because the membrane is very stiff and could therefore not be sealed such that oxygen could only pass through the HPM membrane to the oxygen sensor as described in section 2.8.2.2 (Determination of the diffusion coefficients for oxygen). The variation in the diffusion coefficients for the enzyme layer Figure 45 was mainly caused by a rather unreproducible enzyme layer thickness. The mean value for the diffusion coefficients of the hydrogel however is in good agreement with the literature [130].

3.2.1.2 Biosensor geometry

The enzyme layer thickness was calculated to be 100 µm, when an enzyme solution volume of 2 µL was applied on a 5 mm oxygen sensor. But since most of the water evaporates during the polymerization process, the final enzyme layer thickness was measured with a paint meter to be only 20 ± 1 µm, which is close to the protein mass of 13.6 % (percentage by weight) contained in the enzyme solution. The dimensions of other biosensor materials (e.g. diffusion membrane and oxygen sensor) were obtained from the specification of the manufacturer and are summarized in Table 11.

3.2.1.3 Biosensor kinetics

The developed glucose biosensor model is based on the common assumption, that the enzyme reactions can be described by Michaelis-Menten constants from free enzymes [111, 114]. The Michaelis-Menten constant for glucose was determined photometrically for free GOD at different substrate concentrations (see Figure 46).
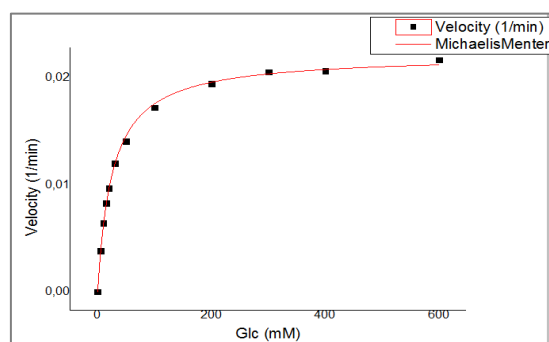
Figure 46 Michaelis Menten plot for glucose oxidase at different glucose concentrations.

The maximum velocity was determined to be Vmax=0.02215 ± 1.8E-4, while the Michaelis-Menten constant for glucose was K_G=25.9 ± 0.8 mM

The resulting constant $K_G = 25.9 \pm 0.8$ mM was found to be in good agreement with the literature [34]. The kinetic constants for oxygen and the Michaelis-Menten constant for the enzyme catalase, were attained from literature (cf. Table 11).

3.2.1.4 Biosensor model settings in COMSOL

COMSOL-Multiphysics is a finite element analysis software empowering the simulation of physical processes that can be described by partial differential equations [131]. For the sake of simplicity and limited computational power, it was decided to develop only a one-dimensional biosensor model in COMSOL. The model was time dependent and enabled the simulation of the transport of diluted species along the vertical axis. The model parameters for the simulation of a glucose biosensor with a low permeability (LPM) and a high permeability membrane (HPM) are summarized in Table 11.

Table 11 Biosensor model parameters (measured, ** assumed, *** fitted)*

Parameter	Value
Aqueous solution (boundary layer)	
Diffusion coefficients for glucose D_G [132]	6.75×10^{-10} m²/s
Diffusion coefficients for gluconic acid D_{GA}	6.75×10^{-10} m²/s **
Diffusion coefficients for oxygen D_{O2} [132]	2.3×10^{-9} m²/s
Diffusion coefficients for hydrogen peroxide D_H [133]	1.0×10^{-9} m²/s
Layer thickness	7.5 µm **
Diffusion membrane with a low permeability (LPM)	
Diffusion coefficients for glucose D_G	$3.0 \times 10^{-13} \pm 2.0 \times 10^{-13}$ m²/s *
Diffusion coefficients for gluconic acid D_{GA}	3.0×10^{-13} m²/s **
Diffusion coefficients for oxygen D_{O2}	$10.5 \times 10^{-12} \pm 0.9 \times 10^{-12}$ m²/s *
Diffusion coefficients for hydrogen peroxide D_H	$3.4 \times 10^{-13} \pm 1.8 \times 10^{-13}$ m²/s *
Layer thickness (manufacturer specification)	6 µm

Diffusion membrane with a high permeability (HPM)	
Diffusion coefficients for glucose D_G	$1.0 \times 10^{-12} \pm 3.9 \times 10^{-13}$ m²/s *
Diffusion coefficients for gluconic acid D_{GA}	1.0×10^{-12} m²/s **
Diffusion coefficients for oxygen D_{O2}	10.5×10^{-11} m²/s ***
Diffusion coefficients for hydrogen peroxide D_H	$3.5 \times 10^{-12} \pm 4.6 \times 10^{-13}$ m²/s *
Layer thickness (manufacturer specification)	25 µm
Enzyme layer	
Diffusion coefficients for glucose D_G	$2.2 \times 10^{-10} \pm 0.74 \times 10^{-10}$ m²/s *
Diffusion coefficients for gluconic acid D_{GA}	2.2×10^{-10} m²/s **
Diffusion coefficients for oxygen D_{O2}	$8.2 \times 10^{-10} \pm 0.87 \times 10^{-10}$ m²/s *
Diffusion coefficients for hydrogen peroxide D_H	$6.3 \times 10^{-10} \pm 1.07 \times 10^{-10}$ m²/s *
Layer thickness	20 ± 2.5 µm *
Oxygen sensor layer	
Diffusion coefficients for glucose D_G	1×10^{-15} m²/s **
Diffusion coefficients for gluconic acid D_{GA}	1×10^{-15} m²/s **
Diffusion coefficients for oxygen D_{O2} [134]	1.7×10^{-9} m²/s
Diffusion coefficients for hydrogen peroxide D_H	1×10^{-15} m²/s **
Layer thickness	120 ± 2.5 µm *
Reaction kinetics	
Maximum velocity V_{max}(GOD)	0.31 mM/s ***
Maximum velocity V_{max}(Cat)	0.041 mM/s ***
Michaelis-Menten constant for glucose K_G(GOD)	25.9 ± 0.8 mM *
Michaelis-Menten constant for H_2O_2 K_{H2O2}(Catalase) [135]	60 mM
Michaelis-Menten constant for oxygen K_{O2}(GOD) [136]	61.2 µM

Since the molecules glucose and gluconic acid are similar in size, the diffusion coefficients for both substances were assumed to be equal. For the diffusion property of the hydrophobic oxygen sensor, it was supposed that the diffusional features are similar to silicone.

3.2.2 Simulations

3.2.2.1 Biosensor response

The biosensor response was simulated with the parameters stated in Table 11 for varying glucose and oxygen concentrations in the sample and compared to the experimental results to validate the biosensor model. The enzyme velocity of the immobilized GOD was fitted such that the characteristic line of biosensors with a low permeability membrane (see Figure 47) and a high permeability membrane (see Figure 48) were comparable to experimental data from three biosensors in a 24-well plate. Both, the simulated and the actual characteristic line showed a transition from a linear region, where glucose diffusion is primarily rate limiting, to a non-linear region as the biosensor becomes increasingly oxygen diffusion limited [124, 137]. The linear range of the glucose biosensor signal extents from 100 % to 20 % air saturation, but decreases with time as GOD is severely inactivated and the enzyme reaction becomes eventually the rate limiting step. This hypothesis is supported by the finding, that the linear range of the characteristic line is decreased in simulations with a lower enzyme velocity as discussed in the next section 3.2.2.2 (Enzyme inhibition).
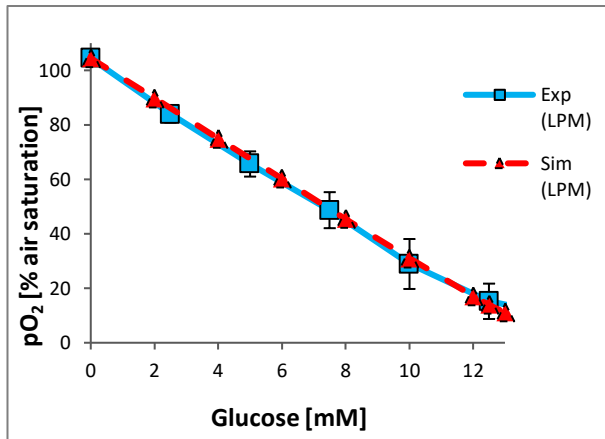
Figure 47 Simulated calibration curve compared to actual data for LPM biosensors

Experimental measurements (solid line) compared to the simulated biosensor response (dashed line) as mean of three biosensors with a low permeability membrane (LPM). The measurement was performed in a 24-well plate at 25°C, 2 mL PBS, 100 % air saturation and 130 RPM. The error bars correspond to the standard deviation calculated from the experimental data.
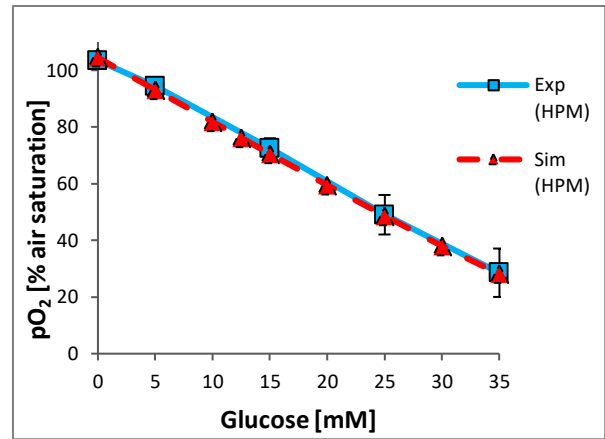
Figure 48 Simulated calibration curve compared to actual data for HPM biosensors

Experimental measurements (solid line) compared to the simulated biosensor response (dashed line) as mean of three biosensors with a high permeability membrane (HPM). The measurement was performed in a 24-well plate at 25°C, 2 mL PBS, 100 % air saturation and 130 RPM. The error bars correspond to the standard deviation calculated from the experimental data.

Because of the biosensors' cross sensitivity to oxygen, the sensor signal, as well as the dynamic range of the biosensor, is influenced by the ambient dissolved oxygen concentration in the sample. Therefore, a second oxygen sensor is applied to compensate for varying oxygen tensions. The resulting glucose response (ΔpO_2) is however still influenced to a minor degree by fluctuating oxygen levels as described in section 3.1.3.2 (Influence of the operating conditions on the biosensor signal). The cross sensitivity to oxygen was first described by Zhang et al. for amperometric sensors [120] and later by Pasic et al. for optical sensors [82]. Both found, that the influence of the dissolved oxygen level in the sample is declining, when the glucose diffusion into the enzyme layer is reduced. This finding was confirmed by simulations of the cross sensitivity to oxygen for biosensors with a low (LPM) and a high permeability membrane (HPM) at a constant glucose level of 5 mM as illustrated in Figure 49. For biosensors with a low permeability membrane (LPM), the biosensor signal decrease was less pronounced, when the DO was reduced from 90 % to 40 % air saturation. Hence, the oxygen dependence of biosensors with a LPM is rather negligible (≤ 1.4 %), if a reference oxygen sensor is applied.

The glucose biosensor model was additionally used to demonstrate the influence of co-immobilized catalase in the enzyme layer, due to catalase contamination (see

Figure 50). As discussed earlier, the sensitivity of the glucose biosensor increases during the first days of measurement, because catalase is inactivated with time (cf. section 3.1.3.3, Functional stability). As a result, the additional oxygen source in the enzyme layer dries up and thus the biosensor signal responds more sensitive to glucose.
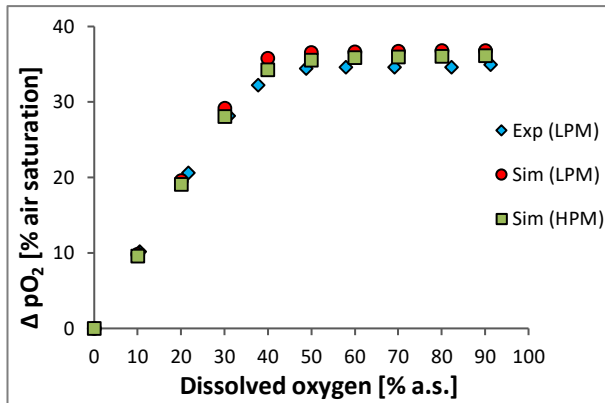
Figure 49 Cross sensitivity of the biosensor to oxygen

Simulation on the influence of varying dissolved oxygen concentrations on the glucose response (ΔpO_2), compared to an experiment with a low permeability membrane (LPM) biosensor at 5 mM glucose. The signal for the high permeability membrane biosensor was simualted at 16 mM glucose. The measurement was perfromed in a 125 mL shake flask at 37°C, 80 % humidity, 5 % CO_2 and 130 rpm.
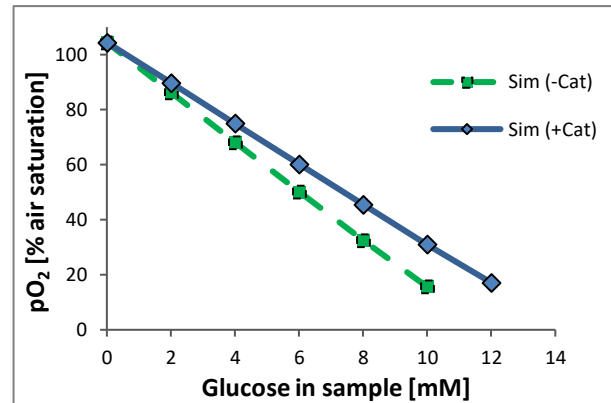
Figure 50 Simulated catalase influence on the biosensor signal

Simulated biosensor response to glucose for enzyme layers with (solid line) and without catalase (dashed line). The simulations show a sensitivity increase when catalase is inactive due to the lack of oxygen regeneration inside the enzyme layer

3.2.2.2 Enzyme inhibition

Hydrogen peroxide inhibits glucose oxidase irreversibly [138]. Therefore, the total reaction velocity is decreasing with time until the enzyme reaction rate becomes the slowest step. This leads to a lower sensitivity and thus decreasing slope of the calibration curve (see Figure 51). The enzyme inhibition was simulated with the glucose biosensor model by reducing the maximum enzyme velocity, to confirm the inhibition theory (see Figure 52). It was found, that the modelled data was consistent with empirical data and the inhibition theory.
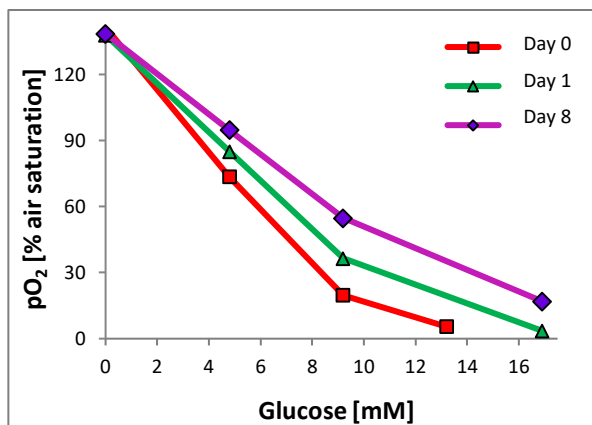
Figure 51 Sensitivity loss due to GOD inactivation

Characteristic sensitivity drop of a biosensor over time visualized by a decreasing slope of the calibration curve. The experiments were performed in a 24-well plate at 25°C, 2 mL PBS, 100 % air saturation and 130 rpm.
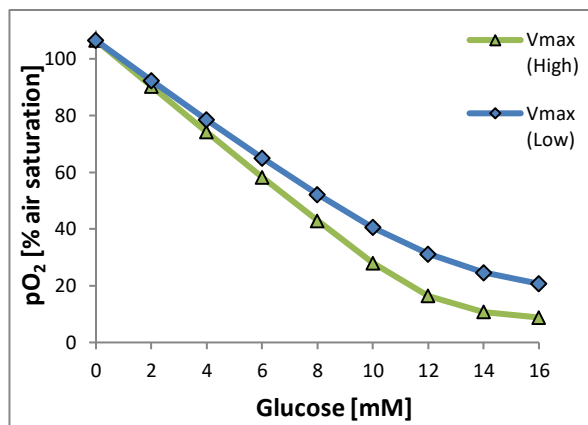
Figure 52 Simulated signal drift due to decrease in the enzyme velocity

Simulated influence of a lower reaction rate on the calibration curve.

3.2.2.3 Accumulation and emission of hydrogen peroxide and gluconic acid

Gluconic acid and hydrogen peroxide is produced during the enzymatic reaction within the enzyme layer of the glucose biosensor (see Equation 5 to Equation 7). At constant glucose concentrations in the sample, eventually a steady state equilibrium between the diffusional flux and the reaction rate inside the enzyme layer will be reached. Hence, the accumulation of the products hydrogen peroxide and gluconic acid will reach an equilibrium as well. The gluconic acid accumulation at different glucose concentrations was measured with pH based glucose biosensors, fabricated according to section 2.2.3 (pH based biosensor preparation for gluconic acid determination) with a low (LPM) and a high permeability membrane (HPM). From the simulations and the pH measurement inside the biosensor (see Figure 53), it can be deduced that at the same glucose concentration in the sample, a similar gluconic acid concentration in the enzyme layer is reached, regardless of the applied diffusion membrane. Although the enzyme reaction rate is higher in biosensors with a high permeability membrane (HPM), due to the higher influx of glucose, the amount of accumulated gluconic acid is comparable to biosensors with a low permeability membrane (LPM), because the gluconic acid emission rate is also higher.
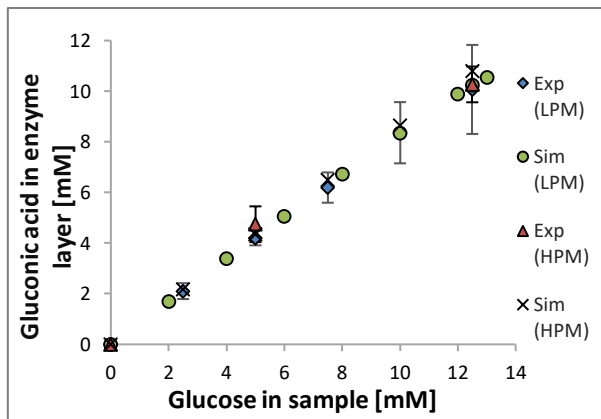
Figure 53 Gluconic acid concentration inside the biosensor

Gluconic acid accumulation inside the enzyme layer compared to computer simulations for biosensors with a high (HPM) and a low permeability (LPM) membrane. The experimental data is illustrated as mean of three measurements in a 24-well plate at 25°C, 2 mL PBS, 100 % air saturation and 130 rpm.
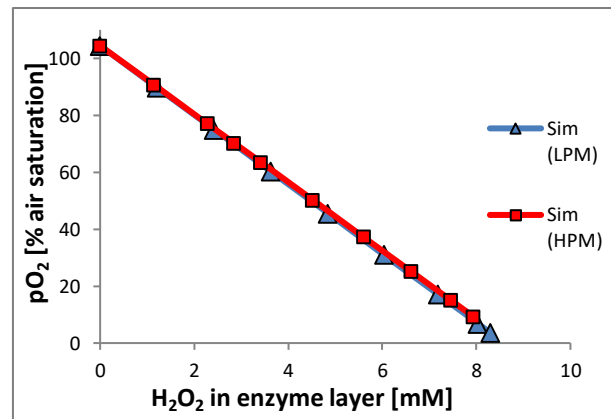
Figure 54 Simulated H_2O_2 concentration inside the biosensor

Simulated hydrogen peroxide concentration inside the enzyme layer at various glucose levels for biosensors with a low permeability membrane (LPM) and a high permeability membrane (HPM).

The accumulation of the enzyme deactivating agent hydrogen peroxide within the biosensor is comparable for both types of membranes at the same biosensor signal (see Figure 54). However, glucose biosensors with a high permeability membrane are far less stable under continuous glucose monitoring conditions (cf. section 3.1.3.3, Functional stability). Considering a higher permeability for glucose and oxygen, the enzyme reaction rate must be also higher in the HPM biosensor. Thus more GOD enzymes are in the reduced state, which is 100-fold more vulnerable for the accumulated hydrogen peroxide, compared to the oxidized form [138]. This explains why glucose biosensors with a high permeability membrane suffer earlier and more pronounced from a sensitivity drop during continuous glucose monitoring, even though the hydrogen peroxide concentration within the biosensor is comparable to LPM biosensors.

The biosensor model was also applied to predict the hydrogen peroxide emission rates for biosensors with a low permeability diffusion membrane. The simulation results are compared to experimental data gained from three biosensors in a 24-well plate in Figure 55.

The biosensors were measured in air saturated PBS buffer with different glucose concentrations at room temperature and 130 rpm with the ABTS/HRP assay. The hydrogen peroxide emission rate was experimentally determined to be between 0 – 40 nmol/h for biosensors depending on the applied glucose concentration. The simulated emission rates for biosensors with 5 mm in diameter were found to be lower than the experimental results suggest (see Figure 55).
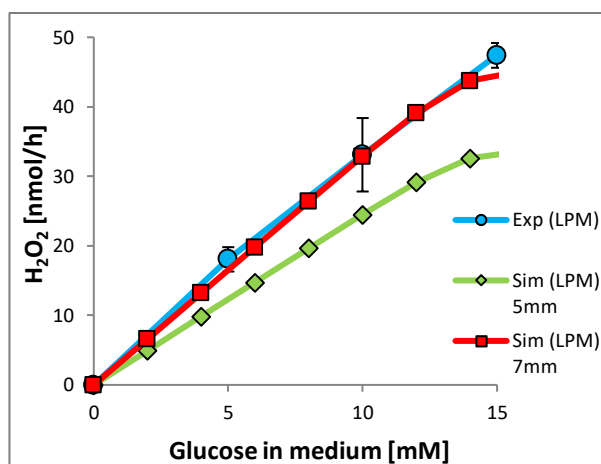
Figure 55 Simulated versus actual H₂O₂ emission rate

Mean H₂O₂ emission rate of three low permeability biosensors at different glucose levels measured in a 24-well plate at 25°C and 130 rpm versus the simulated emission rates for biosensors with different diameters.

The reason for this divergence could be, that in fact, the diameter of the biosensor was larger than the underlying 5 mm oxygen sensor. The larger biosensor diameter arises from the manufacturing process, where the enzyme solution is spread by the diffusion membrane over a larger area than the underlying 5 mm oxygen sensor. The same simulation, calculated for a 7 mm biosensor, therefore fits much better the experimental data.

3.2.2.4 Glucose consumption of LPM biosensors

The glucose consumption rate of the developed glucose biosensor is an important parameter, if the biosensor is applied in a low working volume, e.g. in cell culture plates. Under steady-state conditions, the glucose consumption rate is determined by the slowest step, the diffusion of glucose through the diffusion membrane. The emission of hydrogen peroxide is connected to the reaction rate which in turn depends on the diffusion rate of glucose. Therefore, the influx rate of glucose equals the outflux rate of H_2O_2. Hence, the glucose consumption rate, at any given glucose level, can be determined by measuring the emission rate of hydrogen peroxide. This circumstance was utilized to measure and compare the glucose consumption in a 24-well plate to a numerical calculation (see Figure 56). The calculation was performed in MatLab® with an iterative code, that applied the explicit Euler method to predict the glucose

consumption over time. The relation between the glucose level in the sample and the resulting consumption rate was gained from the hydrogen peroxide measurement (see Figure 55) in the previous section 3.2.2.2 (Enzyme inhibition). The predicted glucose consumption was compared to an empirical experiment with three LPM biosensors in a 24-well plate, filled with 2 mL glucose solution with a concentration of 7.5 mM (see Figure 56).
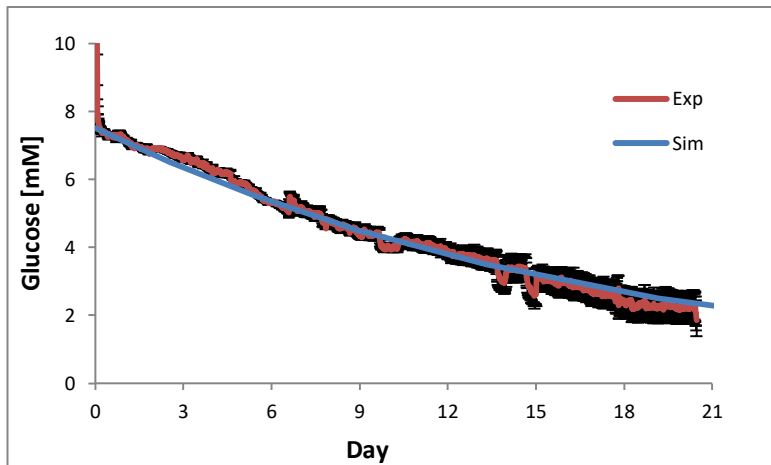
Figure 56 Glucose consumption of glucose biosensors

The mean glucose consumption of three biosensors with 7 mm in diameter (red line), is compared to a numerical calculation (blue line). Measurement conditions: 24-well plate, 25°C, 100 % air saturation, 2 mL glucose solution in PBS with 7.5 mM glucose concentration at 130 rpm. The overlapping error bars (black) correspond to the standard deviation from the experimental data.

3.3 Part III: Cell culture experiments

In this part, the applicability of the developed in-line biosensor for continuous glucose monitoring in animal cell culture is demonstrated. Therefore, the biosensor was placed in 6-well cell culture plates to investigate the effect of the hydrogen peroxide emission from the biosensor on Jurkat cells. Furthermore, the influence of cisplatin treatment on the glucose consumption of Jurkat cells is discussed.

Finally, the developed glucose biosensor was integrated into 125 mL shake flask bioreactors for continuous glucose monitoring and control in fed-batch culture. The particular aim was to improve the sialylation of the CHO product Darbepoetin alfa by ensuring a tight glucose regime at a low and a high constant glucose level in comparison to simple batch culture. The effect of different constant glucose levels on other important cell culture parameters like cell growth, viability, metabolite accumulation and amino acid consumption were additionally considered in this part to assess the cell culture efficiency under different glucose feeding strategies. Beforehand, a characterization of the Darbepoetin alfa producing CHO cell line is presented to evaluate the influence of varying pH, osmolarity and different cell culture temperature on the product quality.

3.3.1 Cell culture in 6-well plates with integrated glucose biosensors

The by-product hydrogen peroxide is emitted from the developed glucose biosensors as a consequence of the enzymatic reaction in the enzyme layer of the sensor (Equation 5 – Equation 7). Hydrogen peroxide can decay into radicals, which is not only toxic for GOD in the enzyme layer, but also for cells inoculated in a small cell culture volume. The applicability of the glucose biosensors is therefore investigated in 6-well plates in the following sections.

3.3.1.1 Jurkat cells cultured in medium with and without catalase

A 6-well plate was equipped with a glucose biosensor and an oxygen reference sensor per well, to investigate the influence of the hydrogen peroxide emission from biosensors on the cell growth of Jurkat cells inoculated at 0.5×10^5 cells/mL in 5 mL IMDM medium. The medium of three out of six wells were supplemented with catalase

to decompose hydrogen peroxide according to Equation 8. The other wells contained catalase free medium.

Cells cultured in catalase containing medium reached a peak cell density of about 2.25×10^6 cells/mL on day five (see Figure 57). Without catalase, a slightly higher peak cell density of about 2.9×10^6 cells/mL was reached at a comparable cell viability.
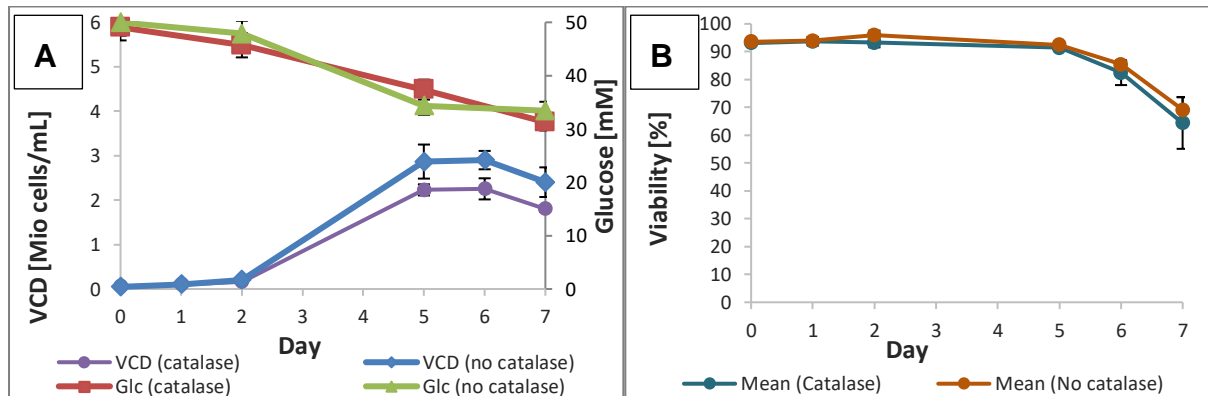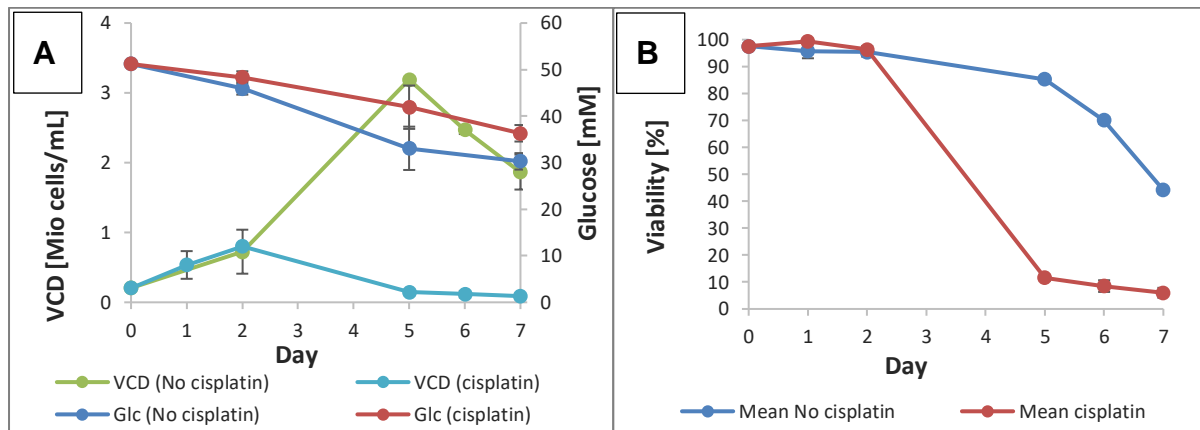

Figure 57: Influence of emitted H_2O_2 on cell growth and viability of Jurkat cells

Illustrated in (A) are the mean viable cell density (VCD) and glucose concentrations over time for three wells with and without catalase, respectively. (B) Mean cell viability for wells with and without catalase. The error bars correspond to the standard deviation. The measurement was performed in a 6-well plate with 5 mL IMDM medium at 150 rpm, 37°C and 5 % CO_2 by Igor Dolgowjasow.
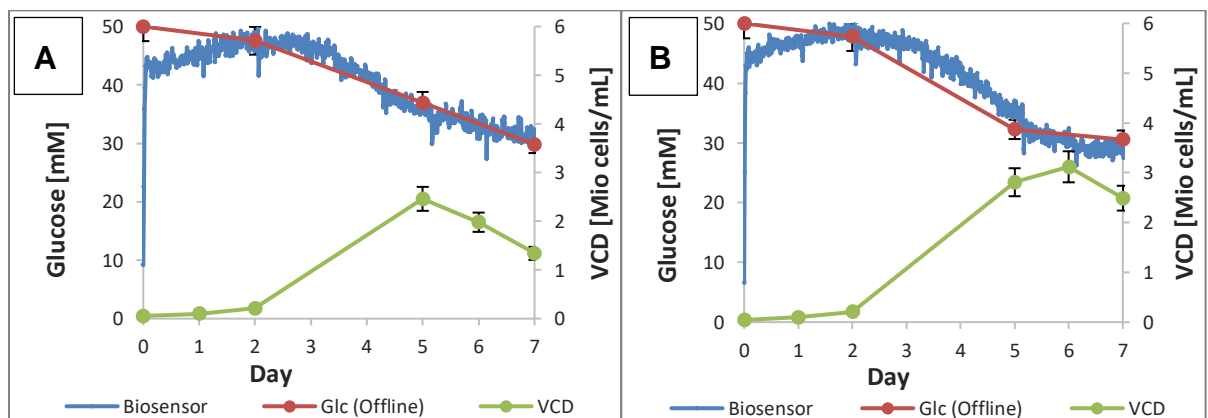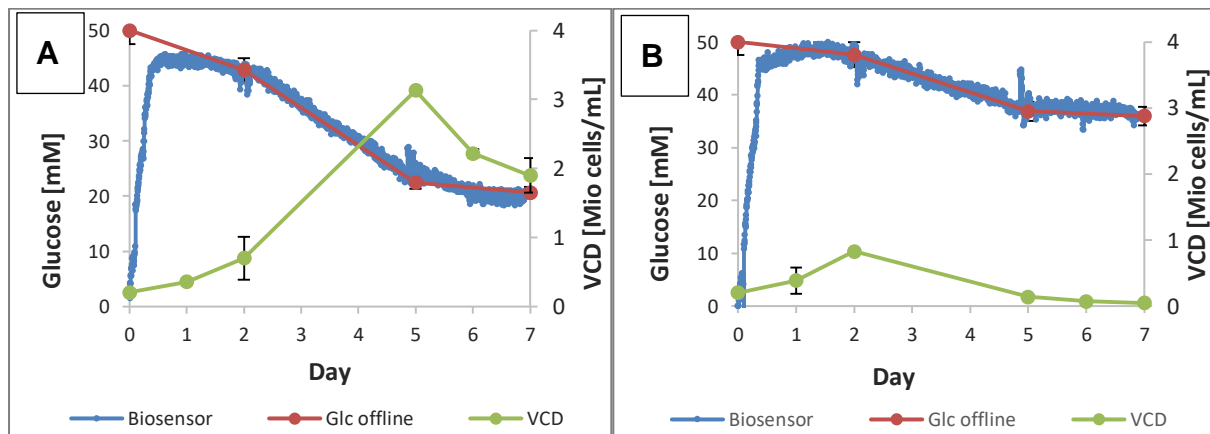

Figure 58: Glucose monitoring in a well during cell culture with and without catalase in the medium

Mean viable cell density (VCD) for wells with catalase (A) and without catalase (B). The glucose consumption is depicted as a measurement in one well for each setting (A/B). The error bars correspond to the standard deviation. The measurement was performed in a 6-well plate with 5 mL IMDM medium at 150 rpm, 37°C and 5 % CO_2 by Igor Dolgowjasow.

Although cells cultured without catalase showed higher cell counts, the glucose consumption was comparable to cells with catalase added to the medium. The glucose measurement of the glucose biosensor in a well with and without catalase is shown in Figure 58 including glucose offline measurements and cell counts. All sensors were

calibrated on day two, because the sensitivity of the biosensors increased during the first two days of the measurement.

Jurkat cells cultured without catalase reached a higher cell density in this experiment. This effect could be explained by the protective effect of hydrogen peroxide on Jurkat cells in concentrations between 5-20 µM, which is described in literature [139]. Unfortunately, no data on the actual hydrogen peroxide concentrations is available, and the amount of the accumulated hydrogen peroxide in the wells cannot be simulated, since hydrogen peroxide decays naturally with time [37].

Although the difference in cell counts were significant, the observed variance might also be due to normal variations, since the negative control in the cisplatin experiment in the following section (see section 3.3.1.2, Jurkat cells treated with cisplatin) also contained catalase and reached a similar peak density (~ 3 million cells/mL) as the wells without catalase in this experiment. However, the inoculation density in both experiments was different, which makes a direct comparison delicate.

Despite the higher viable cell density in the wells without catalase, the glucose consumption was comparable to the wells with catalase (see Figure 57). The accuracy of the glucose biosensor and the offline reference measurements was too low to distinguish any significant difference between the glucose consumption of cells in catalase containing medium, compared to cells in catalase free medium.

3.3.1.2 Jurkat cells treated with cisplatin

In this section, the applicability of glucose biosensors for chemosensitivity testing in 6-well plates was demonstrated. Therefore, one glucose biosensor was integrated into each well to monitor the glucose consumption of Jurkat cells after the addition of the cytostatic drug cisplatin on day two. Cisplatin targets DNA-dependent cellular functions and thus can lead to inhibition of replication and transcription, as well as a cell cycle arrest [140]. Furthermore, DNA damage is introduced resulting in cell death and apoptosis [140]. Hence, a reduced glucose consumption rate was expected.

The wells were seeded at 0.2×10^6 cells/mL and reached a cell density of 0.8×10^6 cells/mL until day two in each well. Three out of six wells were subsequently treated with 10 µM cisplatin, which lead to a dramatic viability drop after day two (see Figure 59). Cells that were not treated with cisplatin showed a continuous growth and reached their peak cell density of about 3×10^6 cells/mL on day five.

Figure 59 Influence of cis-platin on cell growth and viability of Jurkat cells

Illustrated in (A) are the mean viable cell density (VCD) and glucose concentration over time for treated and nontreated cells with cisplatin. (B) Mean cell viability for treated and nontreated cells with cis-platin. The measurement was performed in a 6-well plate with 5 mL IMDM medium at 150 rpm, 37°C and 5 % CO_2 by Igor Dolgowjasow.

Figure 60: Glucose monitoring a well during cell culture with and without cisplatin

Mean viable cell density (VCD) for untreated (A) and cisplatin treated (B) cells. The glucose consumption is depicted as a measurement in one well for each setting (A/B). The measurement was performed in a 6-well plate with 5 mL IMDM medium at 150 rpm, 37°C and 5 % CO_2 by Igor Dolgowjasow.

In the beginning of the experiment, the glucose concentration was raised in two steps and the shaking velocity was low (150 rpm), which resulted in a prolonged signal increase. All sensors were calibrated on day two, when the cis-platin treatment began. As excepted, the glucose consumption was more pronounced for the non-treated cells,

because the non-treated cells reached a higher viable cell density (see Figure 59). The glucose measurement and the cell count of one treated and one untreated well are illustrated in Figure 60. The evolution of the glucose level clearly reflects the viable cell density, as the glucose decrease diminishes when the cell density drops and vice versa. Hence, the glucose biosensor is able to measure the glucose consumption of cells in a 6-well format.

3.3.2 CHO cell culture experiments in 125 mL shake flasks

Cell culture conditions like temperature, osmolarity, pH, nutrient concentrations and metabolite accumulation are important parameters for the recombinant protein quality with respect to sialylation [63, 78, 79, 141]. However, a general conclusion is difficult to draw, since the reported effects are often incoherent, because the influence varies depending on the cell line [141, 142]. For this reason, the underlying CHO cell line was first characterized concerning the influence of pH, osmolarity and temperature, before the developed glucose biosensor was applied for continuous glucose control during cell culture. The final objective, was to investigate the influence of different glucose levels during fed-batch CHO culture on the sialylation of the product Darbepoetin alfa compared to a simple batch process.

3.3.2.1 Influence of pH and osmolarity on CHO cell culture

A pH value of 7 ± 0.2 is described to ensure optimal sialylation conditions for CHO cells [78]. Hence, the pH was adjusted manually by addition of sodium hydrogen carbonate ($NaHCO_3$) and carbon dioxide (CO_2) during cell culture, based on an integrated pH sensor in each shake flask bioreactor. In some cell culture experiments, base was added in excess to the medium, because of a faulty pH sensor. This led to a sudden rise in pH (+ 0.25) and osmolarity (+ 79 mOsmol/kg) as can be seen in Figure 61. The specific lactate excretion of the CHO cells subsequently increased dramatically after the addition of 3 mL $NaHCO_3$ on day three, while the ammonia excretion stagnated (see Figure 62). This metabolic shift is interpreted as a countermeasure of the CHO cells to mitigate the pH increase by an elevated lactate production [143–145].
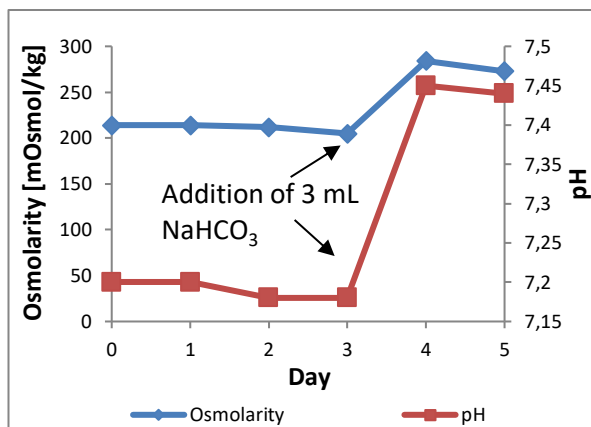
Figure 61 Influence of base addition on osmolarity and pH in the cell culture medium

3 mL NaHCO₃ was added to 50 mL cell culture medium in a 125 mL shake flask during CHO culture on day three, which led to a sudden increase in osmolarity and pH. The glucose concentrations during the cell culture is shown in the supplements (see supplement Figure 93). Operating conditions: 37°C, 80 % humidity, 5 % CO_2 and 130 rpm.
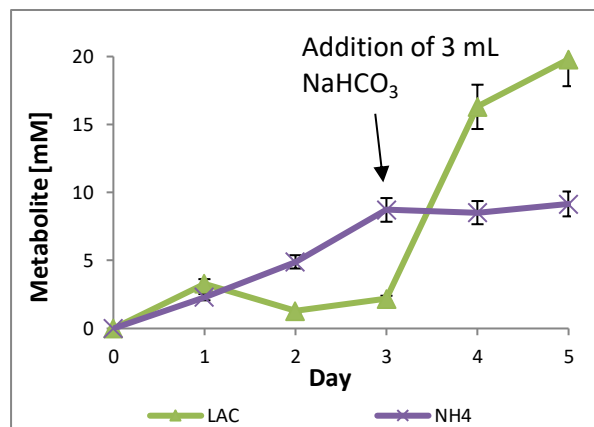

Figure 62 Influence of base addition on the accumulation of lactate and ammonia

The result of 3 mL NaHCO₃ addition on day three during CHO culture, was an increased lactate excretion, while the net excretion of ammonia was arrested. The lactate (LAC) and ammonia (NH4) concentration was measured offline with the Cedex-Bio with an accuracy of 5 % (error bars) according to the specifications of the manufacturer.

Sun and Zhang demonstrated for EPO producing CHO cells, that lactate itself had only a marginal effect on the cell growth and the product concentration [62]. It is the elevated osmolarity caused by lactate excretion, which influences the kinetics of enzyme reactions and inhibits cell growth and productivity [62]. Figure 63 illustrates that the addition of excess base led to a drop in cell viability. However, the nominal osmolarity was not particularly high. Previous reports even suggest, that for most animal cells, an osmolarity in the range between 260-320 mOsm/kg [62] at similar pH is not harmful [79]. Hence, the suddenness of the osmolarity and pH increase seems to have played a more important role for the cell growth and viability, since the CHO cells had little time to adapt.

Besides the cell growth, the sialylation of the product can also be affected by pH and osmolarity [63, 85, 86]. In Figure 64, the isoform distribution of Darbepoetin alfa from the shake flask treated with excess base, is opposed to a normal batch culture at comparable osmolarity (232-255 mOsmol/kg).
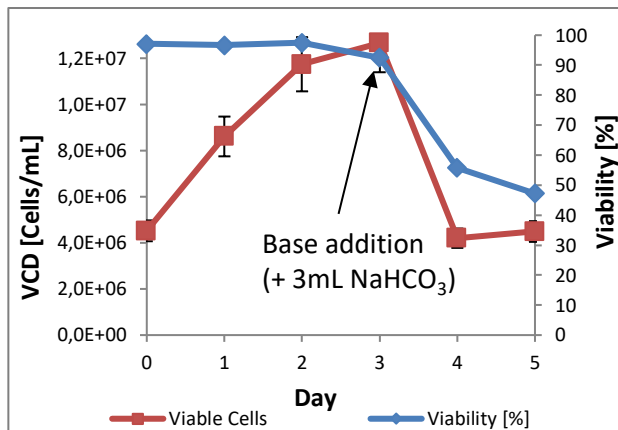
Figure 63 Influence of base addition on the cell growth and viability of CHO cells

The viable cell density (VCD) was measured offline with the ViCell. The accuracy of the measurements (error bars) was 10 % according to the specifications of the manufacturer. The glucose concentrations during the cell culture is shown in the supplements (see supplement Figure 93). Operating conditions: 37°C, 80 % humidity, 5 % CO_2 and 130 rpm.
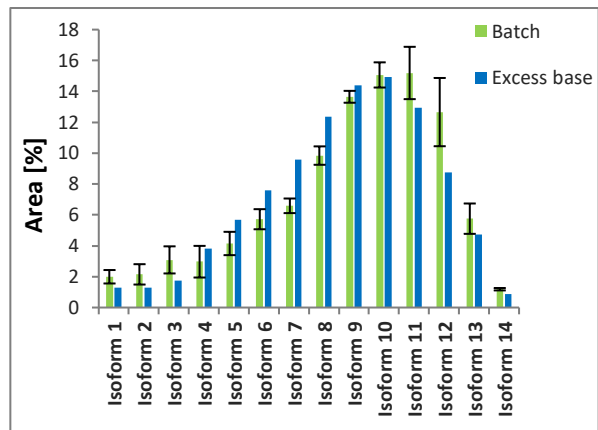
Figure 64 Isoform distribution of Darbepoetin alfa measured by capillary electrophoresis

The isoform distribution of Darbepoetin alfa from batch culture, harvested on day seven, is compared to fed-batch culture with 3 mL base addition, harvested on day five. The samples were measured offline by capillary electrophoresis. The error bars correspond to the standard deviation of three flasks. The measurement was performed by Jonas Arndt.

The product quality was measured with capillary electrophoresis and suggests that the relative isoform distribution was slightly shifted towards a lower sialylation (isoform 4-8), due to the addition of excess base (see Figure 64). Hence, the relative percentage of higher isoforms (isoform 11-14) was apparently decreased due to the sudden rise in osmolarity and pH, following the addition of excess base on day three. This is plausible, because a low cell viability (cf. Figure 63) is associated with a lower sialylation caused by the release of sialidase from dead cells, which can cleave the terminal sialic acid [79]. However, since the effect was not pronounced, the observed isoform shift can also be due to normal variations. Unfortunately, only one cell culture flask that suffered from a sudden rise in pH and osmolarity was analyzed.

3.3.2.2 Temperature influence on CHO cell culture

CHO cells were inoculated at a high viable cell density ranging from $3x10^6$ cells/mL to $5x10^6$ cells/mL in three separate fed-batch experiments at different continuously controlled glucose levels. The glucose biosensor measurements are illustrated in the supplements (see supplement Figure 90 and Figure 91). The cell culture temperature was set to 31°C to suppress the exponential growth phase and to initiate an early production phase with the aim to investigate the influence of a low temperature, while enhancing the product titer [80]. Each experiment consisted of two 125 mL shake

flasks. In one experimental setup, 4 mM of glutamine was added in the beginning, while only 1 mM glutamine was added in the other two experiments. For comparison reasons, an additional experiment at 37°C was performed, with a glucose level controlled at 1 mM and an initial glutamine concentration of 4 mM. In this experiment, the inoculated cell density was however lower (2.5×10^6 cells/mL), because the cell growth was not suppressed at a cell culture temperature of 37°C.

The maximum lactate concentration was dramatically reduced to about 2 mM (see Figure 65 to Figure 67), resulting from the suppressed cell growth at 31°C [144, 146]. As a consequence, less base was needed to keep the pH at 7 ± 0.2. Furthermore, the product concentration increased substantially (data not shown), because of the prolonged production phase at a high viable cell density (see supplement Figure 82 to Figure 85). Although glutamine is part of the recombinant protein Darbepoetin alfa, the amino acid was hardly consumed during the low temperature cell cultures (see Figure 65 to Figure 67). Nevertheless, the nominal ammonia concentration rose significantly higher at 31°C (see Figure 65 – Figure 67) compared to the experiment at 37°C (see Figure 68), regardless of the low initial glutamine concentration of 1 mM. Hence, the ammonia accumulation must result from other amino acids than glutamine, e.g. serine or asparagine [147].
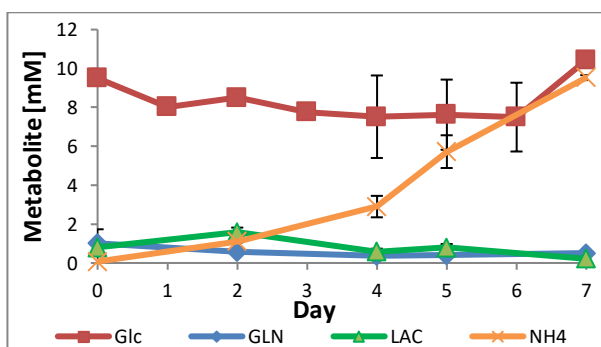
Figure 65 Metabolite accumulation during CHO culture at 31°C, ~8 mM glucose and 1 mM glutamine

The metabolite concentration was measured offline from periodic samples taken of two fed-batch cultures performed in two 125 mL shake flasks under the following experimental conditions: 50 % DO, 130 rpm, 5 % CO2 and 80 % humidity. The error bars correspond to the standard deviation. The measurement was jointly performed with Mario Lederle.
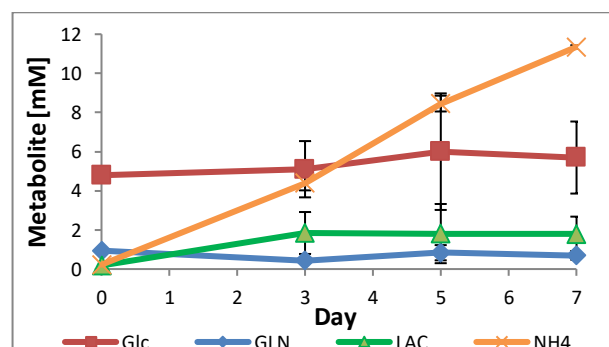
Figure 66 Metabolite accumulation during CHO culture at 31°C, ~5 mM glucose and 1 mM glutamine

The metabolite concentration was measured offline from periodic samples taken of two fed-batch cultures performed in two 125 mL shake flasks under the following experimental conditions: 50 % DO, 130 rpm, 5 % CO2 and 80 % humidity. The error bars correspond to the standard deviation. The measurement was jointly performed with Mario Lederle.
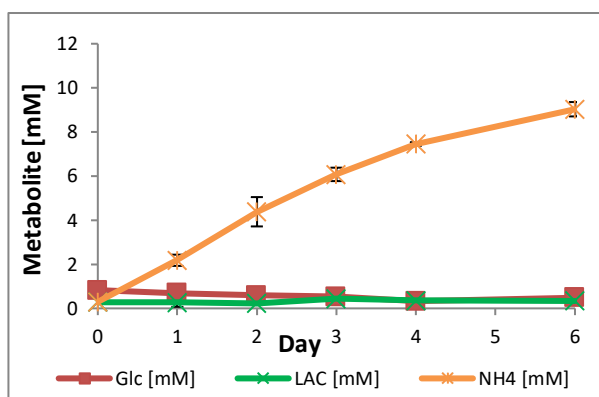
Figure 67 Metabolite accumulation during CHO culture at 31°C, ~1 mM glucose and 4 mM glutamine

The metabolite concentration was measured offline from periodic samples taken of two fed-batch cultures performed in two 125 mL shake flasks under the following experimental conditions: 50 % DO, 130 rpm, 5 % CO_2 and 80 % humidity. The error bars correspond to the standard deviation. The measurement was jointly performed with Mario Lederle.
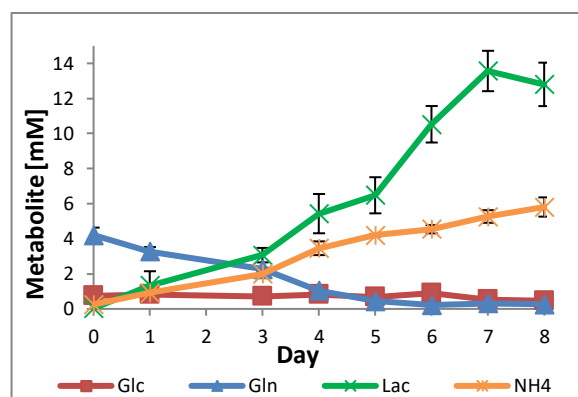
Figure 68 Metabolite accumulation during CHO culture at 37°C, ~1 mM glucose and 4 mM glutamine

The metabolite concentration was measured offline from periodic samples taken of four fed-batch cultures performed in four 125 mL shake flasks under the following experimental conditions: 50 % DO, 130 rpm, 5 % CO_2 and 80 % humidity. The error bars correspond to the standard deviation. The measurement was jointly performed with Mario Lederle.

The specific ammonia production rate is significantly higher during the exponential phase in the 37°C cell culture (see supplementary Figure 89) compared to the cell culture experiments at 31°C (see supplementary Figure 87 and Figure 88), because of the pronounced glutamine consumption during cell growth. However, the overall ammonia accumulation is lower in the 37°C cell culture compared to the experiments at 31°C (cf. Figure 65 to Figure 68), because the cell density during the first days of cell culture is significantly lower (see supplementary Figure 82 to Figure 85).

The relative amount of highly sialylated isoforms (isoform 8-17) at 31°C were found to be significantly deteriorated compared to the control culture at 37°C (see Figure 69). According to Woo et al., the optimal temperature of enzymes involved in glycosylation ranges between 32 to 37°C [146]. Hence a temperature below 32°C might have led to a lower sialylation, although the higher amount of ammonia in the experiments at 31°C cannot be ruled out as an additional cause.
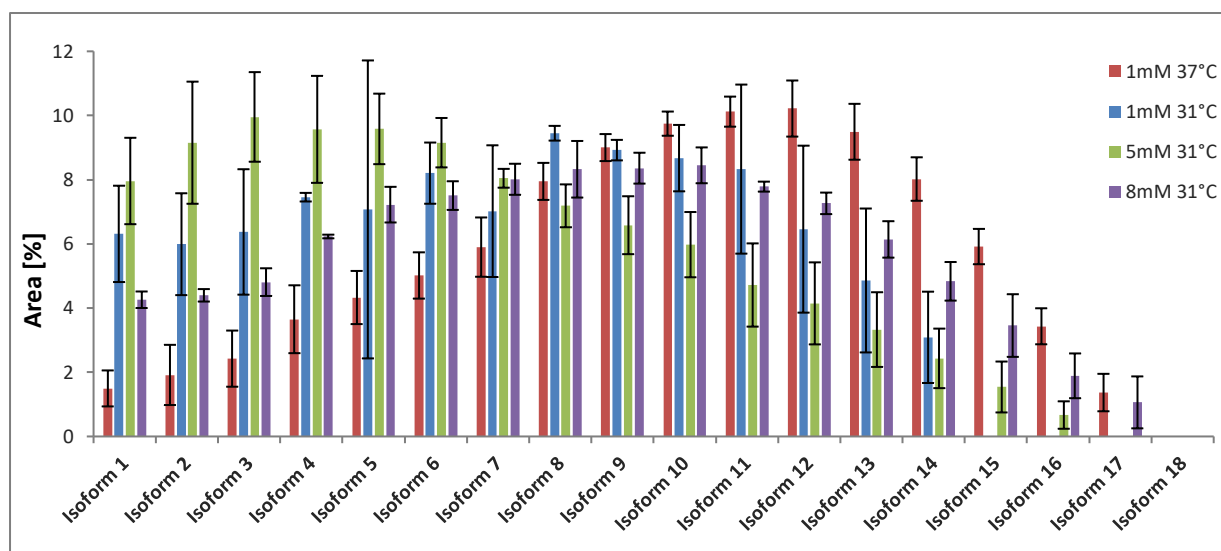
Figure 69 Temperature influence on the isoform distribution of Darbepoetin alfa at different glucose levels

The cell culture was harvested between day 6-8. Experimental conditions in a 125 mL shake flask: 50 % DO, 130 rpm, 5 % CO_2 and 80 % humidity at varying glucose levels. The error bars correspond to the standard deviation. The capillary electrophoresis measurements were performed by Dr. Anke Rattenholl.

3.3.2.3 Influence of different glucose levels in fed-batch compared to batch culture

Previous studies have shown that the glycosylation pattern of recombinant proteins is effected by the glucose concentration during cell culture by influencing the lactate production [63]. In this section, different fed batch experiments at constant glucose levels were performed and compared to batch cell culture with respect to cell growth, nutrient consumption, waste accumulation and product quality.

3.3.2.3.1 Cell growth and waste accumulation during cell culture

After a conditioning period of two days, the glucose biosensor was calibrated and applied for continuous glucose control in 125 mL shake flasks for CHO cell culture. An additional reference oxygen sensor was utilized to compensate for oxygen fluctuations and to control the dissolved oxygen level (DO) in the medium at 50 % air saturation. The pH of the cell culture was kept at pH 7 ± 0.2 with manual addition of $NaHCO_3$. A sample was taken on a periodical basis to measure offline the pH and important metabolic parameters with automated assays (Cedex-Bio, Roche) and by gas chromatography (GC).

The glucose concentration was controlled simultaneously in two CHO cell culture experiments at a low (~0.8 mM) and a high (>30 mM) glucose level (see supplement Figure 91 and Figure 92). A batch cell culture starting with 45 mM glucose served as a control. Each of the three experiments consisted of four flasks, which were inoculated with 2.5×10^6 cells/mL and supplemented with 4 mM glutamine (see Figure 70). All of the above-mentioned experiments were performed at 37°C, 5 % CO_2, 80 % humidity and 130 rpm.
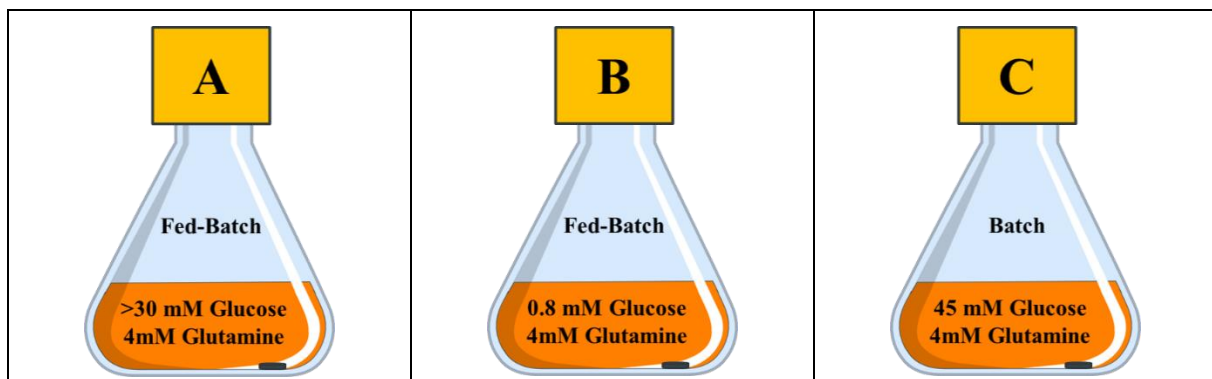
Figure 70 Three different CHO cell culture experiments in 125 mL shake flasks with biosensors

Experimental design: (A) Fed-batch at >30 mM glucose. (B) Fed-batch at 0.8 mM glucose. (C) Batch starting at 45 mM glucose. Each experiment consisted of four flasks and was operated under the following conditions: 50 % DO, 130 rpm, 5 % CO_2 and 80 % humidity. The cell culture experiments were performed jointly with Mario Lederle.

The continuously controlled fed-batch cultures at a glucose level of 0.8 mM exhibited a peak viable cell density (VCD) of 6.4×10^6 cells/mL and maintained a high cell viability (>90 %) over eight days (see Figure 71). Maximum growth rates were observed during the first six days, but continued until the end of the cell culture.

In the fed-batch mode with a high glucose level (>30 mM), the glucose control started after day two, because the dynamic range of the glucose biosensors was exceeded in the first two days. Hence, the glucose level dropped in the meantime from 45 mM to 35 mM. In the high glucose experiment, a peak VCD of 8.8×10^6 cells/mL was reached already after six days. However, because of the poor cell viability, the experiment was ended a day earlier (day 7).

Under batch conditions, the cell growth was comparable to the high glucose experiment, since the glucose level was similar during the growth phase (see Figure 72). Yet the cell viability remained a day longer above 90 %.
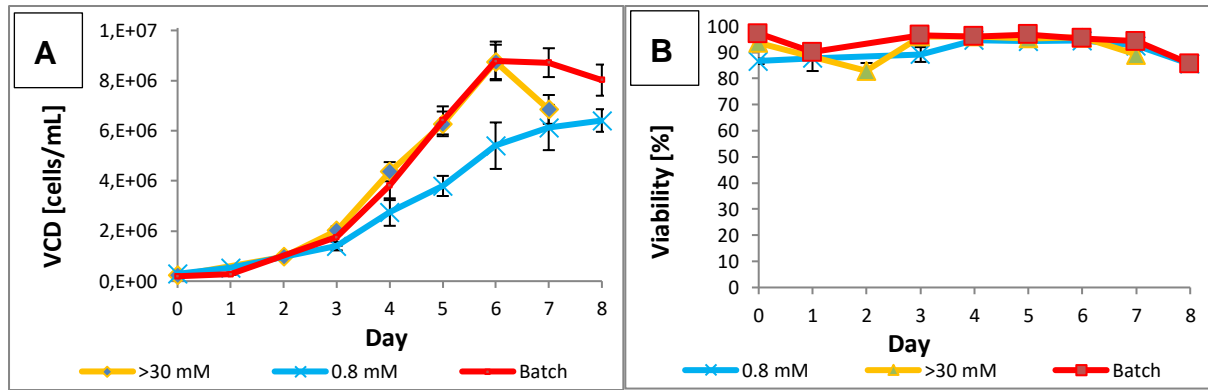
Figure 71 Comparison of cell growth and viability during three different cell culture experiments

Viable cell density (VCD) (A) and cell viability (B) as mean of four flasks during two fed-batch experiments at 0.8 mM and >30 mM glucose compared to a batch experiment. The error bars correspond to the standard deviation of four flasks. Each experiment consisted of four flasks and was operated under the following conditions: 50 % DO, 130 rpm, 5 % CO_2 and 80 % humidity.

Because of the higher cell growth rate in the high glucose fed-batch culture, the lactate concentration reached about 20 mM compared to 13.5 mM during the low glucose fed-batch culture (see Figure 72). It is widely believed, that the cell growth is affected by lactate through an increase in osmolarity, however, only for lactate levels well above 20 mM [72]. Since the growth rate was similar in the batch and the high glucose fed-batch experiment, the lactate levels were comparable. In batch mode, a lactate shift occurred on day seven, characterized by a net lactate consumption, which was not observable in any of the fed-batch cultures. The lactate shift is associated with an extended cell culture viability and a good product quality and occurs in cultures with a high cell growth rate, low glycolysis flux and high extra cellular lactate concentrations [148, 149].

Ammonia plays a more important role in cell growth inhibition and product quality than lactate [86]. Merely 1-5 mM ammonia have been reported to have a negative effect on cell growth and product quality [56, 62, 72, 86]. Yet, the underlying mechanism is not clear [87] and the threshold concentration depends on the cell line, the culture conditions and the excreted product [56]. Despite different growth rates, the nominal glutamine consumption and ammonia accumulation was comparable in all three experiments, regardless of the glucose concentration in the medium or the cell culture mode (see Figure 72). This circumstance is discussed in further detail in section 3.3.2.3.2 (Amino acid metabolism during cell culture)

The glutamine consumption rate was the highest during the exponential phase, with the cell growth rate depending on the availability of glucose in the medium (see Figure 72). The higher the glucose level during the exponential phase, the faster the cell growth rate and thus the accumulation of lactate. The inhibited growth rate under low glucose levels for CHO cells is thought to be caused by an energy shortage in form of decreased intracellular ATP below 1.22 mM glucose [83, 93]. In contrast to the literature, the cell viability was not prolonged, nor was a higher peak VCD reached at a low glucose level in continuous fed-batch mode [84, 150]. This is most likely caused by a lack of sufficient nutrient supply in the end of the cell culture, due to a higher amino acid consumption rate under a low glucose regime (cf. Figure 74). A comparable amino acid concentration in all three cultures in the end of the cell culture supports this hypothesis (see supplement Figure 86).
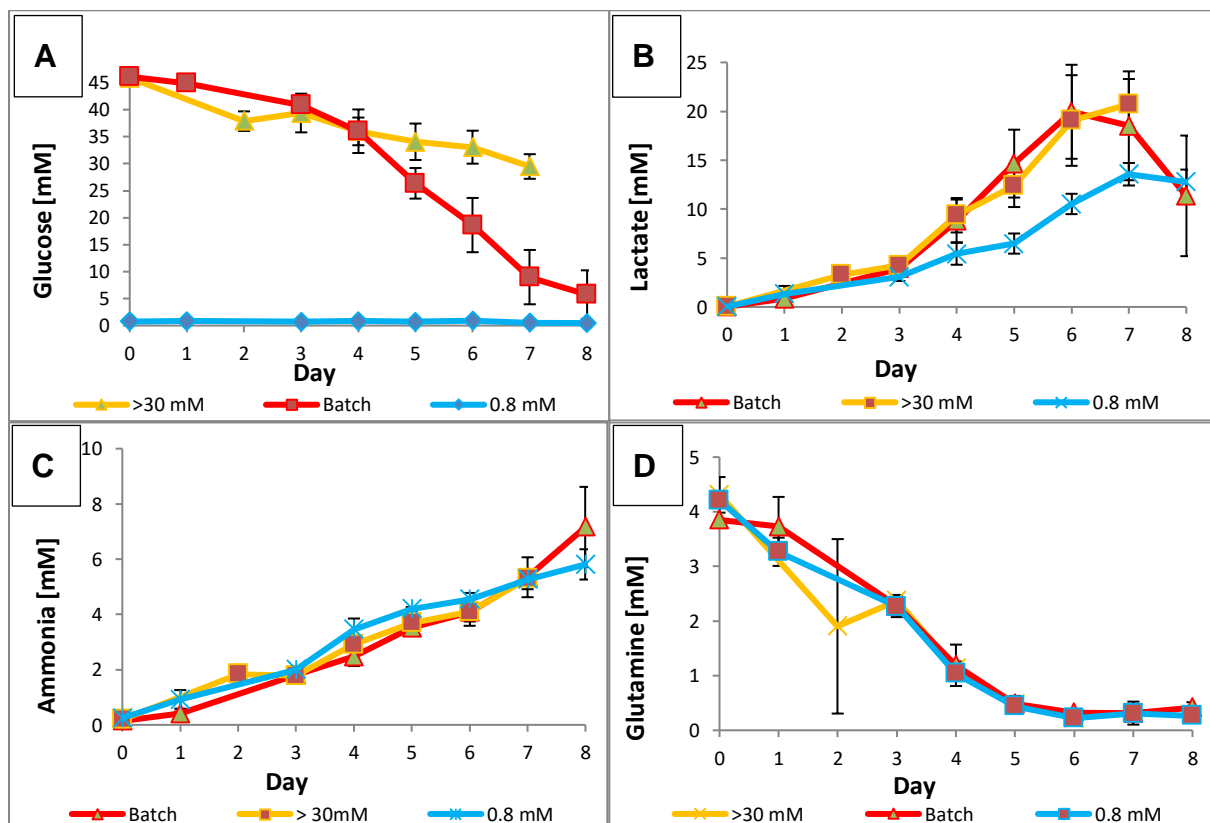
Figure 72 Comparison of metabolite concentration during three different cell culture experiments

Glucose (A), lactate (B), ammonia (C) and glutamine (D) concentration as mean of four flasks during two fed-batch experiments at 0.8 mM and >30 mM glucose compared to a batch culture. The error bars correspond to the standard deviation of four flasks. Each experiment consisted of four flasks and was operated under the following conditions: 50 % DO, 130 rpm, 5 % CO_2 and 80 % humidity.

As was reported for hybridoma cells in fed-batch cell culture [151], the limitation of only glucose did not decrease the ammonia accumulation in comparison to batch cell culture. In contrast, under a glutamine regime, 50 % less ammonia has been reported [151]. But the limitation of both nutrients, glucose and glutamine, had the greatest impact on the ammonia accumulation (80 % less ammonia) and also led to reduced alanine and lactate excretion [151].

Due to less lactate accumulation and glucose in the medium, the osmolarity was significantly lower in the fed-batch mode with a low glucose level (LG) compared to the fed-batch mode at a high glucose level (HG) (cf. Figure 73). Neither the osmolarity nor the observed pH changes were critical to the CHO cell culture [62, 79].
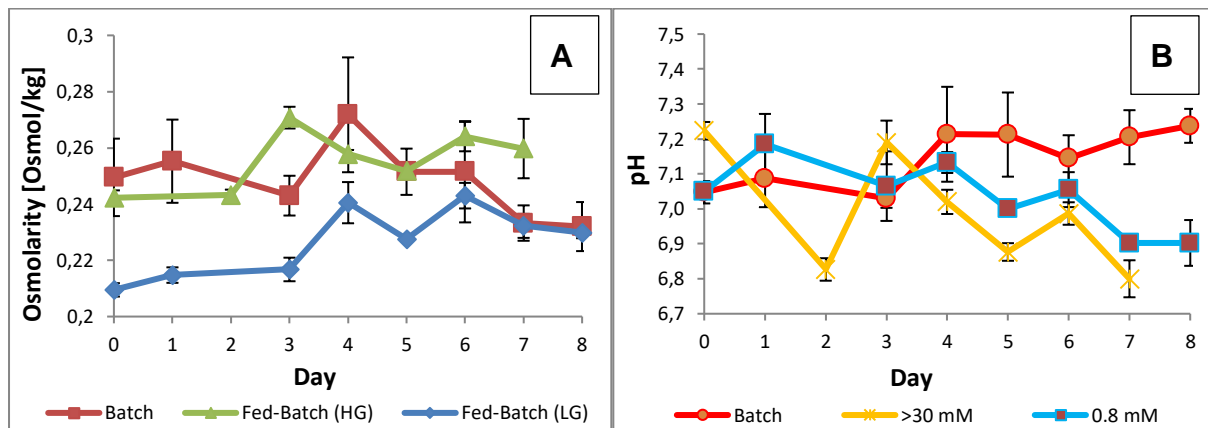
Figure 73 Comparison of osmolarity and pH level during three different cell culture experiments

Mean osmolarity (A) and pH (B) of four flasks during two fed-batch experiments at 0.8 mM and >30 mM glucose and a batch experiment. The error bars correspond to the standard deviation of four flasks. Each experiment consisted of four flasks and was operated under the following conditions: 50 % DO, 130 rpm, 5 % CO_2 and 80 % humidity.

3.3.2.3.2 Amino acid metabolism during cell culture

The accumulation of lactate and ammonia, which can be caused by nutrient imbalances (e.g. glucose and amino acid) [152], inhibits cell growth and glycosylation. The influence of different glucose concentrations and cultivation modes on the amino acid level during cell culture, was therefore investigated by gas chromatography. Table 12 presents the initial concentration of the measured amino acids in the applied chemically defined CHO-2 cell culture medium.

Table 12 Amino acid concentrations in the CHO cell culture medium, determined by gas chromatography

Essential amino acids	Concentration [nmol/mL]	Non-essential amino acids	Concentration [nmol/mL]
Histidine (HIS)	1040 ± 57.9	ALA	592 ± 32.3
PHE	936 ± 27	ASN	3856 ± 1080.6
LEU	6504 ± 154.6	SER	9344 ± 331.4
MET	1600 ± 42.3	GLN	4000
TRP	560 ± 28.6		

The consumption of amino acids depends on many cellular parameters like growth rate, metabolism, cellular stress and process parameters like pH, temperature, osmolarity and dissolved oxygen concentration [64]. Illustrated in Figure 74 is the consumption rate q of the measured amino acids per cell and day for the batch and two fed-batch experiments at a low (LG) and a high glucose level (HG) as mean of three flasks. The specific formation rate of lactate and ammonia was also included in the graphs, because they can be generated from amino acids and are important for the product quality.

As depicted in Figure 74, the amino acid consumption during the exponential phase (day 0-6) was significantly increased for the fed-batch experiment at a low glucose level compared to the other experiments. However, it is assumed that the energy shortage could not be fully compensated by the metabolism of amino acids, since the cell growth rate was significantly lower at continuous 0.8 mM glucose. CHO cell growth is reported to be affected by a glucose concentration below 6 mM, even if sufficient glutamine is available [153]. Hence, glucose is an important nutrient that cannot be fully replaced by any amino acid [153]. Because of the higher amino acid consumption during the growth phase at 0.8 mM glucose, the specific ammonia concentration was significantly increased, while the lactate level was lower in tendency. For the batch and the continuous fed-batch culture at a high glucose level (> 30 mM), there was no significant difference on the amino acid consumption, since the glucose levels and the growth rate were similar during the exponential phase.
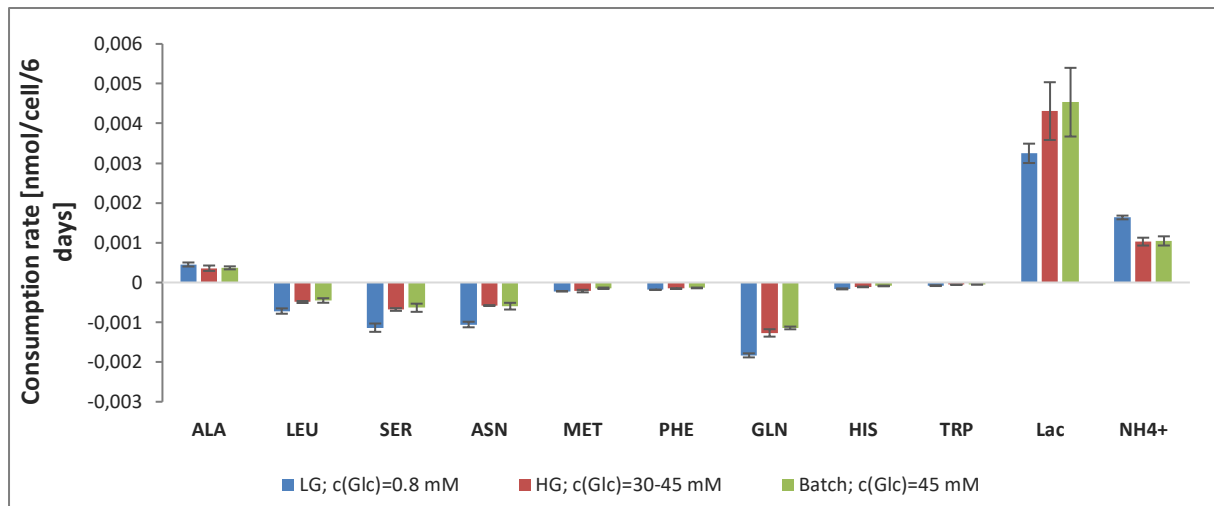
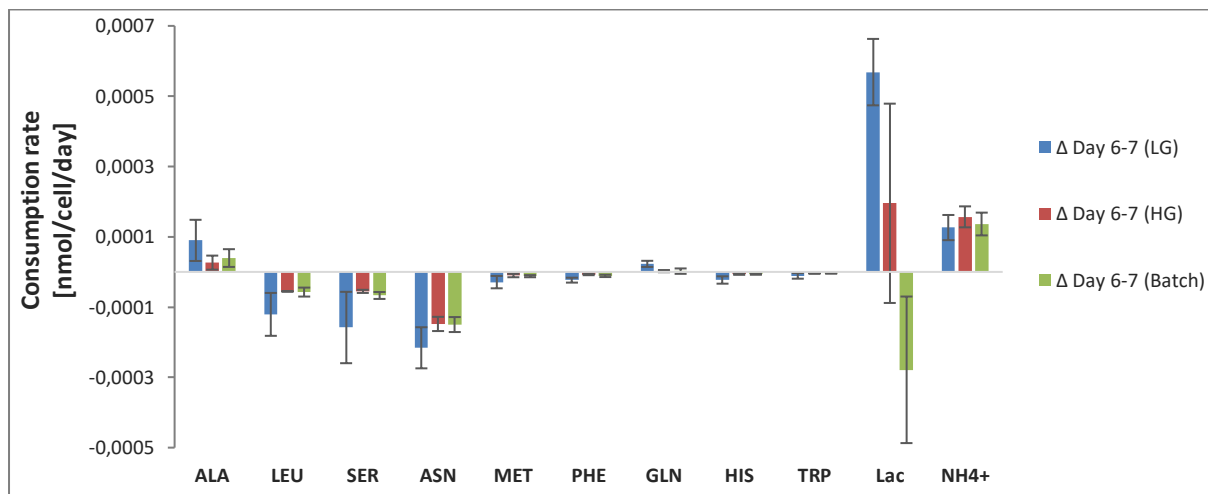*Figure 74 Consumption and production rate of amino acids during growth phase (day 0-6)*

Specific production rate (values > 0) and consumption rate (values < 0) of amino acids during fed-batch cultures at a low glucoe level (LG) and a high glucose level (HG) compared to a batch culture as mean of three flasks during the exponential phase (day 0-6). The error bars correspond to the standard deviation of the triplicates. The measurements were performed by Tatjana Roth.

Although glutamine is the prime energy source [56], other amino acids like serine (SER), histidine (HIS), methionine (MET), phenylalanine (PHE) and leucin (LEU) are reported to be metabolized in CHO cells during cell culture at low glucose levels [83]. Glutamine (GLN), asparagine (ASN), leucin (LEU) and serine (SER) were under the most consumed amino acids in all cell culture experiments. This is especially the case during the growth phase, where glucose accounts for only a small fraction of the TCA cycle metabolites in CHO cells [154]. Instead, asparagine and glutamine are responsible to a great extent for the replenishment and energy metabolism during the exponential growth phase through anaplerotic pathways of the TCA cycle, while glucose steps in when cell growth slows down [154].

In contrast to all other amino acids, alanine (ALA) was constantly produced. Alanine is a by-product of glucose and amino acid metabolism during mammalian cell culture, which accumulates as a result of the transamination reaction between pyruvate and other amino acids [56, 62]. Glutamine is preferred over asparagine as a nitrogen donor for the production of alanine [154]. Alanine has little influence on the cell growth and viability at concentrations less than 9 mM [62], which was not exceeded during the cell culture experiments (c.f. supplement Figure 86). Alanine is produced in high quantities during the growth phase, but hardly generated during the stationary phase, which

might be due to a low glutaminolysis caused by a low glutamine level in addition to the alanine consumption for the Darbepoetin alfa synthesis (see Figure 75).

Figure 75 Consumption and production rate of amino acids during the stationary phase (day 6-7)

Specific production rate (values > 0) and consumption rate (values < 0) of amino acids during fed-batch cultures at a low glucoe level (LG) and a high glucose level (HG) compared to a batch culture as mean of three flasks during the stationary phase (day 6-7). The error bars correspond to the standard deviation of the triplicates. The measurements were performed by Tatjana Roth.

Lactate, which is generated from glucose and glutamine [56], had the highest production rate during the exponential phase. The same applies for the ammonia accumulation, which is mainly generated from glutamine [56], as can be seen by the inverse correlation (see Figure 74). However, during the stationary phase, when the glutamine level is very low, ammonia is probably produced from other amino acids like serine or asparagine [147]. Glucose overfeeding is thought to cause inefficient metabolism and thus lead to the accumulation of excess lactate [84].

The amino acids GLN, LEU, SER and ASN are present in the product Darbepoetin alfa in high concentrations (LEU 14 %, SER 5%, ASN 4 %, GLN 4%) [108]. The consumption of those amino acids was about twice as high during the exponential phase, than it was during the stationary phase (see Figure 76) where most of the product is synthesized [155]. Glutamine seems to be even generated during the stationary phase.
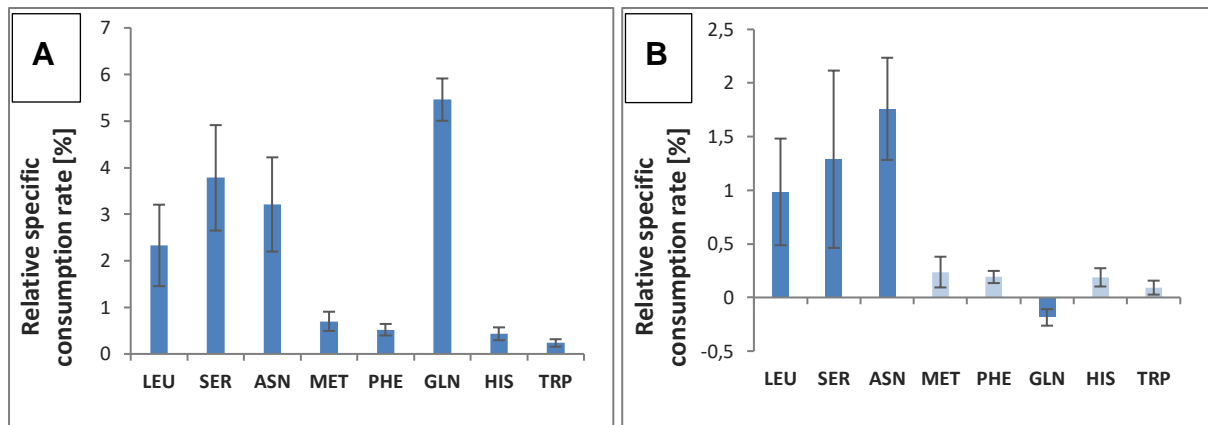
Figure 76 Relative consumption rates of relevant amino acids for Darbepoetin alfa

Relative consumption rates of important amino acids for the production of Darbepoetin alfa during (A) the growth phase (day 0-6) and (B) during the stationary phase (day 6-7). The combined amino acid consumption from day 0 to 7 equals 100 %. The error bars correspond to the standard deviation of three GC measurements performed by Tatjana Roth.

3.3.2.3.3 Product quality under batch versus fed-batch cell culture

While capillary electrophoresis (CE) does not allow an exact assignment of which peak belongs to which isoform, it is still a powerful separation technique that enables a relative comparison of the degree of protein sialylation from different cell culture modes. Generally, higher sialylated proteins (which corresponds to a higher isoform number) carry more negative charges and therefore tend to elute at higher retention times. Figure 77 shows the approximate isoform distribution for batch and two continuous fed-batch experiments at a high (HG) and a low glucose level (LG). It was found that the isoform distribution in fed-batch culture under a low glucose level (0.8 mM) was comparable to batch culture, although the overall lactate concentration was significantly higher in the batch mode (see Figure 72). The best product quality was attained under a high glucose level (> 30 mM), which showed an equivalent lactate accumulation to batch culture. Here, the relative isoform distribution was shifted towards higher sialylated isoforms (isoform 15 - 18) (see Figure 77).
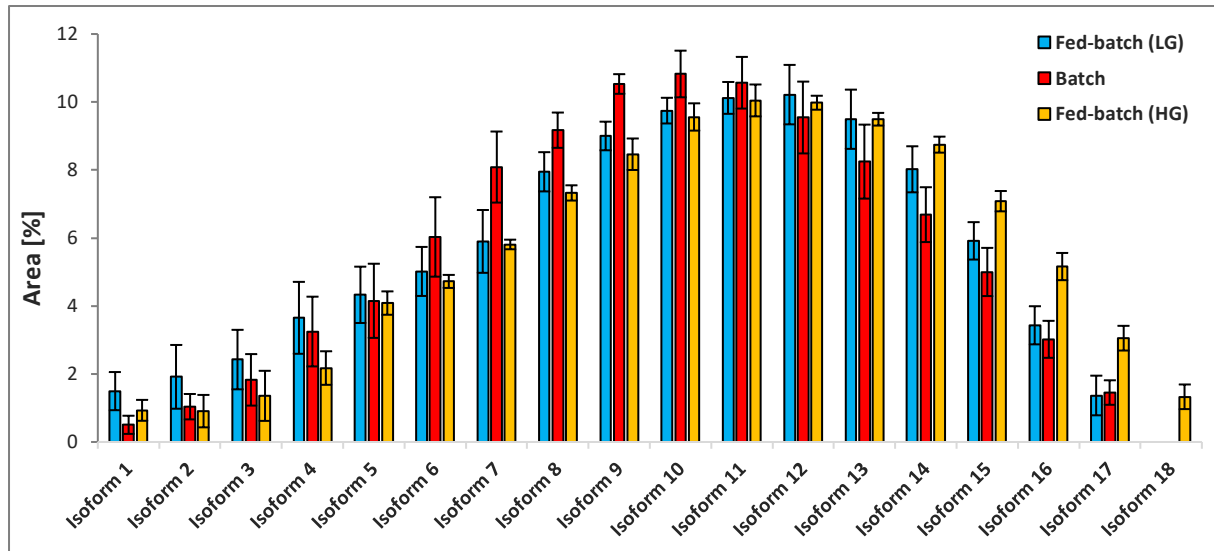
Figure 77 Comparison of the sialylation between three different cell culture experiments

The product quality of Darbepoetin alfa was compared in terms of isoform distribution between cell culture experiments performed at a low glucose (LG) and high glucose (HG) level in fed-batch mode as well as a batch culture. Each bar corresponds to the relative amount of a distinct isoform as mean of four flasks compared to the other isoforms in the same experiment. The error bars correspond to the standard deviation of four flasks. The CE measurements were performed by Dr. Anke Rattenholl.

The attained results suggest that a continuously high glucose level during the production phase is beneficial for the sialylation of Darbepoetin alfa in the applied CHO cell line, whereas the influence of the observed lactate concentrations was negligible. This outcome is plausible, since Darbepoetin alfa is highly glycosylated, and glucose starvation presumably leads to a reduced intracellular UDP-GlcNAc concentration [156], which is a precursor for sialylation (see section 1.8, Glycosylation of proteins). Yet, an orthogonal measurement is needed to underpin these results. This ongoing evaluation is, however, beyond the scope of this study, which deals primarily with the development of a glucose biosensor that is applicable for cell culture. It will be therefore the subject of another PhD and master student to confirm the sialylation results using mass spectrometry coupled with liquid chromatography (LC/MS).

4 CONCLUSION

After more than forty years of extensive research, Steiner et al. conclude that building a satisfying optical sensor for continuous long-term glucose monitoring appears to be "more challenging than flying to the moon" [13]. Even under non-healthcare and therefore less demanding conditions, such as in cell culture, offline glucose measurements are still the standard procedure for lack of a suitable in-line glucose sensor [9]. However, a consistent product quality requires a tight monitoring and control of crucial parameters during cell culture, such as glucose [1–4].

The research presented in this thesis was motivated by the need of a disposable, optical in-line biosensor for long-term continuous glucose monitoring and control in animal cell culture. This task was accomplished by utilizing a commercially available luminescent oxygen sensor that was coated with an optimized crosslinked enzyme layer and covered by a diffusion membrane that constrained the diffusion rate of glucose into the enzyme layer. The glucose concentration was measured indirectly via the oxygen consumption in the enzyme layer. The applicability of the biosensor for continuous glucose control was subsequently demonstrated under real-world conditions during CHO fed-batch culture and led to an improvement in the quality of the recombinant product Darbepoetin alfa. The developed optical in-line biosensor thereby demonstrated a unique long-term stability under practical conditions enabled by an optimized enzyme and diffusion layer.

In addition to the biosensor development, a one-dimensional sensor model was created to simulate the diffusion rates and accumulation of the involved reaction species and thus to improve the understanding of the biosensor design regarding its functional stability. The findings gained from the computer model revealed new insights into the main factors influencing biosensor stability and were utilized to improve the biosensor life-time.

In the following sections, the implications of this research for practice and theory are described. Furthermore, an outlook for the potential application of the developed glucose biosensor is given.

4.1 Biosensor benefits, limitations, and the resulting implications for practice

First, the limitations of the biosensor are described regarding the implication for practice. Subsequently, the advantageous of the sensor are outlined.

The developed biosensor type is kinetic in nature and therefore consumes glucose and oxygen in an enzymatic reaction. The reaction rate is limited by the slowest step, the diffusion of glucose through the diffusion layer. As such, the reversible biosensor signal is influenced by environmental parameters like temperature, ambient dissolved oxygen concentration and flow rate (or shaking speed, respectively). While the temperature and the flow rate should be kept as constant as possible during glucose monitoring, oxygen fluctuations can be compensated by a reference oxygen sensor. The cross sensitivity to oxygen is thereby reduced to 1.4 % or less. A moderate flow rate and an ambient oxygen concentration above 50 % air saturation is recommended during measurement, because the dynamic range of the biosensor is strongly affected by both factors. Hence, the presented glucose biosensor is only suitable for application in suspension cell culture. Since the biosensor signal is primarily limited by the diffusion rate of glucose rather than the enzyme reaction rate, pH values between pH 5 to 8, which are rarely exceeded during cell culture, do not affect the biosensor signal.

The biosensor can be stored in PBS buffer at 4°C over at least four months without a noticeable loss in sensitivity. However, an initial signal drift over approximately two days is observed during the very first utilization, which results from the deactivation of catalase impurities in the enzyme layer. Hence, a previous exposure to glucose over a period of 48 hours is required to avoid such a signal drift. For long-term continuous glucose monitoring over more than seven days, the glucose biosensor can be re-calibrated by a simple one-point calibration to compensate for signal drifts resulting from a GOD deactivation.

Any device or material that is integrated into a bioreactor or comes into contact with cell culture medium, must be sterilized. The developed glucose biosensor was found to be sterilisable with UV, beta and gamma irradiation, due to a surplus of the exceptionally stable enzyme GOD. Biofouling, which results from the adhesion of cells

or protein material onto the diffusion membrane, was not observed due to the hydrophilic property of the diffusion membrane. Furthermore, no cytotoxic effects on Jurkat or CHO cells were observed in 6-well plates and 125 mL shake flasks, respectively, which renders the glucose biosensor suitable for cell culture applications in bioreactor formats with a working volume of 5 mL or more.

The diffusion layer thickness and its permeability for glucose and oxygen determine the dynamic range and the response time of the glucose biosensor. Three diffusion membranes with different permeabilities that provide the glucose biosensor with a good mechanical stability and a tuneable dynamic range have been identified. An enzyme layer with a high GOD loading in combination with a low permeability membrane delivers the best functional stability at a dynamic range of 0 – 20 mM. This allowed the in-line biosensor to be used for continuous glucose monitoring and control in three subsequent cell culture experiments (≥ 21 days). The demonstrated long-term applicability under real-world conditions is a key requirement in the biotechnological industry and represents a major improvement over the previously published optical glucose biosensors, which demonstrated only 86 hours of operational capability [44, 82, 104, 157]. Although amperometric biosensors with life-times around 14-21 days are described in literature [158, 159], the developed optical biosensor offers the additional advantage of a non-invasive optical read-out, which is not prone to contaminations or signal drifts caused by electrochemical interferences [44, 82, 104]. Furthermore, the in-line biosensor does not require daily calibrations or a time delayed and inconvenient on-line measurement in a bypass [159].

In summary, the developed optical in-line biosensor offers a reversible glucose response and a unique long-term stability, which is of utmost importance for the application in animal cell culture. The dynamic range depends on many environmental factors (e.g. temperature, flow rate, DO), but can be tuned by an appropriate diffusion layer. Furthermore, the disposable biosensor is sterilisable with UV, gamma and beta irradiation and does not suffer from biofouling, which renders the developed glucose biosensor suitable for suspension cell culture processes.

4.2 Biosensor application for optimizing cell culture

The lack of essential nutrients and the accumulation of waste products can lead to lower cell densities, premature cell death [149] and impaired product quality in mammalian cell culture [63]. In order to avoid the accumulation of high amounts of catabolic waste products, continuous low level nutrient feeding has been proposed in literature [74, 95]. Glucose poses one of the most important nutrients to be controlled in mammalian cell culture [149], because its availability is crucial for cell growth and glycosylation of recombinant proteins [83, 84]. However, glucose can also promote inefficient metabolism and thus the accumulation of lactate, if provided in abundance [63]. Hence, a continuous glucose control that prevents depletion on the one hand and inefficient cell metabolism on the other hand is beneficial for the cultivation process.

The glucose biosensor described in this thesis was developed and optimized to enable such a continuous glucose control with the aim to improve the sialylation quality of the recombinant protein Darbepoetin alfa. Therefore, the glucose sensor was applied in two separate CHO fed-batch cultures to maintain a glucose level around 0.8 mM and above 30 mM. Using capillary electrophoresis, the influence of the continuously controlled fed-batch culture on the sialylation of the product Darbepoetin alfa under a low and a high glucose level was evaluated and compared to a simple batch culture. Although the nominal lactate concentration under a low glucose level was diminished, no relevant improvement in the sialylation of the product was observed. Yet, the cell growth rate was reduced, while the cell viability was not prolonged in contrast to previous literature [95, 156]. Under a high glucose level, a significant improvement of the terminal sialylation abundancy over batch and low glucose fed-batch culture was observed. In addition, the cell growth rate was not compromised as compared to a low glucose fed-batch culture. Clearly, a high glucose level during the production phase of the cell culture was beneficial for the sialylation of the highly-glycosylated product Darbepoetin alfa.

In summary, the developed glucose biosensor enabled a continuous glucose control during CHO fed-batch culture, which improved the sialylation of Darbepoetin alfa under a high glucose level.

4.3 The biosensor model and its implications for theory

In this section, the reason behind the limited biosensor life-time and signal drifts are outlined.

A fast removal of hydrogen peroxide is described in literature to prevent the deactivation of GOD [37], e.g. through decomposition by catalase [121–123]. However, the enzymatic decomposition of H_2O_2 proved to be ineffective during this research, due to the fast deactivation of catalase.

In order to gain more insight into the internal diffusion profiles of the involved reaction species and to pinpoint the main factor for the limited biosensor life-time, a customized computer model was developed based on Michaelis-Menten kinetics. In particular, the accumulation of the enzyme deactivating by-product hydrogen peroxide was simulated, because it compromises the biosensor stability [37, 44]. The computer model relied on previously determined geometry and diffusion properties of the applied materials and revealed that the accumulation of hydrogen peroxide is not the main factor that impacts the functional stability of the biosensor. Instead, the biosensor life-time is more strongly influenced by the reaction rate, which depends on the influx of glucose and oxygen through the diffusion membrane. An enhanced substrate influx leads to an increased proportion of the enzyme GOD being in its reduced state (GOD_{red}), which is 100-fold more vulnerable to hydrogen peroxide than the oxidized state (GOD_{ox}) [35]. For this reason, the biosensor life-time is drastically reduced if a diffusion membrane with a high permeability is applied, although the accumulation of hydrogen peroxide is comparable to biosensors with a low permeability membrane.

The computer model was additionally utilized to investigate the opposing biosensor drifts, which were observed during long-term glucose monitoring. Therefore, the enzyme velocities for GOD and catalase were reduced to simulate the influence of the enzyme deactivation on the biosensor signal. It was found that the fast deactivation of the co-immobilized enzyme catalase is responsible for the initial sensitivity increase, since less oxygen is produced by the enzymatic decomposition of H_2O_2. In contrast, the slow deactivation of the robust enzyme GOD leads to a decreasing biosensor sensitivity in the long term, because less oxygen is consumed.

In summary, the findings attained in the experimental part of this research and the improved understanding enabled by the biosensor model suggest, that the biosensor

life-time can be significantly prolonged by lowering the permeability of the diffusion layer for glucose.

4.4 Potential future development and applications

Bioprocesses are maintained preferably close to optimal parameters and rely at best on real-time sensors for temperature, oxygen, pH and nutrients like glucose. With respect to current demands for process analytical technology and for quality by design concepts, the developed glucose biosensor has the potential to improve process operation and process understanding [141]. Especially in combination with other in-line optical sensing probes, such as oxygen and pH sensors, the developed glucose biosensor is a valuable tool for optimizing animal cell culture conditions in both, industrial biotechnological applications and research. Such a troika could for example be combined in a multi sensing platform to improve the understanding of cell metabolism under drug treatment over time. Other optical based biosensors that rely on oxidoreductases, such as lactate oxidase and glutaminase/glutamate oxidase, could extend such a multi-sensing platform with further important analytes (e.g. lactate and glutamine).

With regard to a potential commercialization of the presented glucose biosensor, the reproducibility of the manufacturing process and the long-term stability of the glucose biosensors could be further improved. Therefore, a more reproducible coating method (e.g. spray-coating) could be applied for the oxygen transducer coating with a (preferably catalase-free) enzyme solution. Moreover, the applied diffusion membrane could be replaced by a thinner diffusion layer with an even lower permeability for glucose. As a consequence, the biosensor would benefit from a higher dynamic range along with a decreased enzyme reaction rate, which was discovered in this research to extend the biosensor life-time.

In this thesis, it was shown that the limitation of only glucose does not decrease the accumulation of ammonia for the applied cell line. However, it has been reported that the co-limitation of both, glucose and glutamine, leads to an even higher ammonia suppression than glutamine regime alone [151]. In the short term, the simultaneous

co-feeding of glucose and glutamine could easily be performed to minimize the lactate and ammonia formation during cell culture, while potentially improving the product quality. Furthermore, additional nutrients could be fed in combination with glucose in order to increase the product titer through a prolonged cell culture duration, and to prevent possible nutrient imbalances that are assumed to jeopardize the product glycosylation [152]. Additionally, the developed biosensor offers the opportunity of a biphasic fed-batch strategy. Thus, a low glucose level could be applied during the exponential phase and a high glucose level during the production phase. This strategy would combine two advantages, namely a low lactate accumulation during cell growth and a high glucose availability for glycosylation during the production phase.

In conclusion, the continuous glucose monitoring capabilities of the developed glucose biosensor opens the door for numerous applications in order to improve biotechnological processes and address glucose related research questions.

5 BIBLIOGRAPHY

1. Read E k., Shah R b., Riley B s., Park J t., Brorson K a., Rathore A s. (2010) Process analytical technology (PAT) for biopharmaceutical products: Part II. Concepts and applications. Biotechnol Bioeng 105:285–295. doi: 10.1002/bit.22529

2. Lourenço ND, Lopes JA, Almeida CF, Sarraguça MC, Pinheiro HM (2012) Bioreactor monitoring with spectroscopy and chemometrics: a review. Anal Bioanal Chem 404:1211–1237. doi: 10.1007/s00216-012-6073-9

3. Landgrebe D, Haake C, Höpfner T, Beutel S, Hitzmann B, Scheper T, Rhiel M, Reardon KF (2010) On-line infrared spectroscopy for bioprocess monitoring. Appl Microbiol Biotechnol 88:11–22. doi: 10.1007/s00253-010-2743-8

4. FDA (2004) Guidance for Industry PAT - A Framework for Innovative Pharmaceutical Development, Manufacturing, and Quality Assurance.

5. Tric M, Lederle M, Neuner L, Dolgowjasow I, Wiedemann P, Wölfl S, Werner T (2017) Optical biosensor optimized for continuous in-line glucose monitoring in animal cell culture. Anal Bioanal Chem 1–11. doi: 10.1007/s00216-017-0511-7

6. Goal: online glucose sensor for bioreactors. https://www.biooekonomie-bw.de/en/articles/news/goal-online-glucose-sensor-for-bioreactors/. Accessed 13 Mar 2017

7. Wilkins J (2011) Disposable Bioreactor Sensors Play Catch-Up. BioProcess Int.

8. Krishnan R, Chen H (2012) A Comprehensive Strategy to Evaluate Single-use Bioreactors for Pilot-scale Cell Culture Production. http://www.americanpharmaceuticalreview.com/Featured-Articles/111768-A-Comprehensive-Strategy-to-Evaluate-Single-use-Bioreactors-for-Pilot-scale-Cell-Culture-Production/. Accessed 9 Mar 2017

9. Moser I, Jobst G (2013) Pre-Calibrated Biosensors for Single-Use Applications. Chem Ing Tech 85:172–178. doi: 10.1002/cite.201200129

10. Saucedo B, Diehl H, Mark A, LaPack T, Wang Y, Robert E, Kottmeier S A Biopharmaceutical Industry Perspective on Single-Use Sensors for Biological Process Applications. http://www.biopharminternational.com/biopharmaceutical-industry-perspective-single-use-sensors-biological-process-applications. Accessed 2 Aug 2017

11. Banica F-G (2012) Chemical Sensors and Biosensors: Fundamentals and Applications. John Wiley & Sons

12. Quaranta M, Borisov SM, Klimant I (2012) Indicators for optical oxygen sensors. Bioanal Rev 4:115–157. doi: 10.1007/s12566-012-0032-y

13. Steiner M-S, Duerkop A, S. Wolfbeis O (2011) Optical methods for sensing glucose. Chem Soc Rev 40:4805–4839. doi: 10.1039/C1CS15063D

14. PreSens Precision Sensing GmbH (2012) OxoPlates Instruction Manual.

15. Instrumentelle Analytische Chemie - Verfahren, Anwendungen, | Karl Cammann | Springer.

16. Gupta A, Rao G (2003) A study of oxygen transfer in shake flasks using a non-invasive oxygen sensor. Biotechnol Bioeng 84:351–358. doi: 10.1002/bit.10740

17. Lakowicz JR (2013) Principles of Fluorescence Spectroscopy. Springer Science & Business Media

18. Liebsch G, Klimant I, Frank B, Holst G, Wolfbeis OS (2000) Luminescence Lifetime Imaging of Oxygen, pH, and Carbon Dioxide Distribution Using Optical Sensors. Appl Spectrosc 54:548–559. doi: 10.1366/0003702001949726

19. Huber C, Klimant I, Krause C, Wolfbeis OS (2001) Dual Lifetime Referencing as Applied to a Chloride Optical Sensor. Anal Chem 73:2097–2103. doi: 10.1021/ac9914364

20. Demuth C (2014) Chemische Sensoren in der Bioprozessanalytik. Chem Unserer Zeit 48:60–67. doi: 10.1002/ciuz.201300609

21. Peterson JI, Goldstein SR, Fitzgerald RV, Buckhold DK (1980) Fiber optic pH probe for physiological use. Anal Chem 52:864–869.

22. Kosch U, Klimant I, Werner T, Wolfbeis OS (1998) Strategies To Design pH Optodes with Luminescence Decay Times in the Microsecond Time Regime. Anal Chem 70:3892–3897. doi: 10.1021/ac971282x

23. F. Kirkbright G, Narayanaswamy R, A. Welti N (1984) Fibre-optic pH probe based on the use of an immobilised colorimetric indicator. Analyst 109:1025–1028. doi: 10.1039/AN9840901025

24. Korostynska O, Arshak K, Gill E, Arshak A (2007) Review on State-of-the-art in Polymer Based pH Sensors. Sensors 7:3027–3042.

25. F. Turner AP (2013) Biosensors: sense and sensibility. Chem Soc Rev 42:3184–3196. doi: 10.1039/C3CS35528D

26. WHO | *Global report on diabetes*. In: WHO. http://www.who.int/diabetes/publications/grd-2016/en/. Accessed 11 Jul 2017

27. Aggidis AGA, Newman JD, Aggidis GA (2015) Investigating pipeline and state of the art blood glucose biosensors to formulate next steps. Biosens Bioelectron 74:243–262. doi: 10.1016/j.bios.2015.05.071

28. Vigneshvar S, Sudhakumari CC, Senthilkumaran B, Prakash H (2016) Recent Advances in Biosensor Technology for Potential Applications – An Overview. Front Bioeng Biotechnol. doi: 10.3389/fbioe.2016.00011

29. Sassolas A, Blum LJ, Leca-Bouvier BD (2012) Immobilization strategies to develop enzymatic biosensors. Biotechnol Adv 30:489–511. doi: 10.1016/j.biotechadv.2011.09.003

30. Zhao W-W, Xu J-J, Chen H-Y (2017) Photoelectrochemical enzymatic biosensors. Biosens Bioelectron 92:294–304. doi: 10.1016/j.bios.2016.11.009

31. Ferri S, Kojima K, Sode K (2011) Review of Glucose Oxidases and Glucose Dehydrogenases: A Bird's Eye View of Glucose Sensing Enzymes. J Diabetes Sci Technol 5:1068–1076. doi: 10.1177/193229681100500507

32. Wong CM, Wong KH, Chen XD (2008) Glucose oxidase: natural occurrence, function, properties and industrial applications. Appl Microbiol Biotechnol 78:927–938. doi: 10.1007/s00253-008-1407-4

33. Sari N, Antepli E, Nartop D, Yetim NK (2012) Polystyrene Attached Pt(IV)–Azomethine, Synthesis and Immobilization of Glucose Oxidase Enzyme. Int J Mol Sci 13:11870–11880. doi: 10.3390/ijms130911870

34. Wilson R, Turner APF (1992) Glucose oxidase: an ideal enzyme. Biosens Bioelectron 7:165–185. doi: 10.1016/0956-5663(92)87013-F

35. Kleppe K (1966) The Effect of Hydrogen Peroxide on Glucose Oxidase from Aspergillus niger*. Biochemistry (Mosc) 5:139–143. doi: 10.1021/bi00865a018

36. Greenfield PF, Kittrell JR, Laurence RL (1975) Inactivation of immobilized glucose oxidase by hydrogen peroxide. Anal Biochem 65:109–124. doi: 10.1016/0003-2697(75)90497-2

37. Hernandez, Karel, Berenguer-Murcia, Angel, C. Rodrigues, Rafael, Fernandez-Lafuente, Roberto (2012) Hydrogen Peroxide in Biocatalysis. A Dangerous Liaison. Curr Org Chem Volume 16:2652–2672(21).

38. Schomburg D, Salzmann M, Stephan D (1994) Enzyme Handbook 7: Class 1.5–1.12: Oxidoreductases, 1st ed. Springer Science & Business Media, Berlin Heidelberg

39. Krishnaswamy S, Kittrell JR (1978) Deactivation studies of immobilized glucose oxidase. Biotechnol Bioeng 20:821–835. doi: 10.1002/bit.260200605

40. Wang H-C, Lee A-R (2015) Recent developments in blood glucose sensors. J Food Drug Anal 23:191–200. doi: 10.1016/j.jfda.2014.12.001

41. Wang J (2008) Electrochemical Glucose Biosensors. Chem Rev 108:814–825. doi: 10.1021/cr068123a

42. Weltin A, Kieninger J, Urban GA (2016) Microfabricated, amperometric, enzyme-based biosensors for in vivo applications. Anal Bioanal Chem 408:4503–4521. doi: 10.1007/s00216-016-9420-4

43. Senthamizhan A, Balusamy B, Uyar T (2016) Glucose sensors based on electrospun nanofibers: a review. Anal Bioanal Chem 408:1285–1306. doi: 10.1007/s00216-015-9152-x

44. Nacht B, Larndorfer C, Sax S, Borisov SM, Hajnsek M, Sinner F, List-Kratochvil EJW, Klimant I (2015) Integrated catheter system for continuous glucose measurement and simultaneous insulin infusion. Biosens Bioelectron 64:102–110. doi: 10.1016/j.bios.2014.08.012

45. Optische Messung der Sauerstoff- Konzentration im Wasser - PDF. http://docplayer.org/20555143-Optische-messung-der-sauerstoff-konzentration-im-wasser.html. Accessed 4 Mar 2017

46. Li L, Walt DR (1995) Dual-analyte fiber-optic sensor for the simultaneous and continuous measurement of glucose and oxygen. Anal Chem 67:3746–3752.

47. Harris JM, Reyes C, Lopez GP (2013) Common causes of glucose oxidase instability in in vivo biosensing: a brief review. J Diabetes Sci Technol 7:1030–1038. doi: 10.1177/193229681300700428

48. Wang B, Takahashi S, Du X, Anzai J (2014) Electrochemical Biosensors Based on Ferroceneboronic Acid and Its Derivatives: A Review. Biosensors 4:243–256. doi: 10.3390/bios4030243

49. Pickup JC, Khan F, Zhi Z-L, Coulter J, Birch DJS (2013) Fluorescence Intensity- and Lifetime-Based Glucose Sensing Using Glucose/Galactose-Binding Protein. J Diabetes Sci Technol 7:62–71.

50. Khan F, Saxl TE, Pickup JC (2010) Fluorescence intensity- and lifetime-based glucose sensing using an engineered high-Kd mutant of glucose/galactose-binding protein. Anal Biochem 399:39–43. doi: 10.1016/j.ab.2009.11.035

51. Cummins BM, Garza JT, Coté GL (2013) Optimization of a Concanavalin A-based glucose sensor using fluorescence anisotropy. Anal Chem 85:5397–5404. doi: 10.1021/ac303689j

52. Nolan RP, Lee K (2011) Dynamic model of CHO cell metabolism. Metab Eng 13:108–124. doi: 10.1016/j.ymben.2010.09.003

53. Luo J, Vijayasankaran N, Autsen J, Santuray R, Hudson T, Amanullah A, Li F (2012) Comparative metabolite analysis to understand lactate metabolism shift in Chinese hamster ovary cell culture process. Biotechnol Bioeng 109:146–156. doi: 10.1002/bit.23291

54. Xing Z, Kenty B, Koyrakh I, Borys M, Pan S-H, Li ZJ (2011) Optimizing amino acid composition of CHO cell culture media for a fusion protein production. Process Biochem 46:1423–1429. doi: 10.1016/j.procbio.2011.03.014

55. Berg J, Stryer L, Tymoczko J (2013) Stryer Biochemie, 7th ed. Springer Spektrum, Berlin Heidelberg

56. Schneider M, Marison IW, von Stockar U (1996) The importance of ammonia in mammalian cell culture. J Biotechnol 46:161–185. doi: 10.1016/0168-1656(95)00196-4

57. Kaadige MR, Looper RE, Kamalanaadhan S, Ayer DE (2009) Glutamine-dependent anapleurosis dictates glucose uptake and cell growth by regulating MondoA transcriptional activity. Proc Natl Acad Sci U S A 106:14878–14883. doi: 10.1073/pnas.0901221106

58. Altman BJ, Stine ZE, Dang CV (2016) From Krebs to clinic: glutamine metabolism to cancer therapy. Nat Rev Cancer 16:619–634. doi: 10.1038/nrc.2016.71

59. Warburg O (1956) On the origin of cancer cells. Science 123:309–314.

60. Vander Heiden MG, Cantley LC, Thompson CB (2009) Understanding the Warburg effect: the metabolic requirements of cell proliferation. Science 324:1029–1033. doi: 10.1126/science.1160809

61. Abu-Absi S, Xu S, Graham H, Dalal N, Boyer M, Dave K (2013) Cell Culture Process Operations for Recombinant Protein Production. In: Zhou W, Kantardjieff A (eds) Mamm. Cell Cult. Biol. Manuf. Springer Berlin Heidelberg, pp 35–68

62. Zhong J-J, Bai F-W, Zhang W (2009) Biotechnology in China I: From Bioreaction to Bioseparation and Bioremediation. Springer

63. Butler M (2006) Optimisation of the Cellular Metabolism of Glycosylation for Recombinant Proteins Produced by Mammalian Cell Systems. Cytotechnology 50:57. doi: 10.1007/s10616-005-4537-x

64. Salazar A, Keusgen M, von Hagen J (2016) Amino acids in the cultivation of mammalian cells. Amino Acids 48:1161–1171. doi: 10.1007/s00726-016-2181-8

65. Bhutia YD, Babu E, Ramachandran S, Ganapathy V (2015) Amino Acid Transporters in Cancer and Their Relevance to "Glutamine Addiction": Novel Targets for the Design of a New Class of Anticancer Drugs. Cancer Res 75:1782–1788. doi: 10.1158/0008-5472.CAN-14-3745

66. Street JC, Delort AM, Braddock PSH, Brindle KM (1993) A 1H/15N n.m.r. study of nitrogen metabolism in cultured mammalian cells. Biochem J 291:485–492. doi: 10.1042/bj2910485

67. Owen OE, Kalhan SC, Hanson RW (2002) The Key Role of Anaplerosis and Cataplerosis for Citric Acid Cycle Function. J Biol Chem 277:30409–30412. doi: 10.1074/jbc.R200006200

68. Wise DR, Thompson CB (2010) Glutamine addiction: a new therapeutic target in cancer. Trends Biochem Sci 35:427–433. doi: 10.1016/j.tibs.2010.05.003

69. De Jesus M, Wurm FM (2011) Manufacturing recombinant proteins in kg-ton quantities using animal cells in bioreactors. Eur J Pharm Biopharm Off J

Arbeitsgemeinschaft Pharm Verfahrenstechnik EV 78:184–188. doi: 10.1016/j.ejpb.2011.01.005

70. Al-Rubeai M (2015) Animal Cell Culture. Springer Berlin Heidelberg, Switzerland

71. Xu X, Nagarajan H, Lewis NE, Pan S, Cai Z, Liu X, Chen W, Xie M, Wang W, Hammond S, Andersen MR, Neff N, Passarelli B, Koh W, Fan HC, Wang J, Gui Y, Lee KH, Betenbaugh MJ, Quake SR, Famili I, Palsson BO, Wang J (2011) The genomic sequence of the Chinese hamster ovary (CHO)-K1 cell line. Nat Biotechnol 29:735–741. doi: 10.1038/nbt.1932

72. Altamirano C, Berrios J, Vergara M, Becerra S (2013) Advances in improving mammalian cells metabolism for recombinant protein production. Electron J Biotechnol 16:10–10. doi: 10.2225/vol16-issue3-fulltext-2

73. Lao MS, Toth D (1997) Effects of ammonium and lactate on growth and metabolism of a recombinant Chinese hamster ovary cell culture. Biotechnol Prog 13:688–691. doi: 10.1021/bp9602360

74. Gagnon M, Hiller G, Luan Y-T, Kittredge A, DeFelice J, Drapeau D (2011) High-end pH-controlled delivery of glucose effectively suppresses lactate accumulation in CHO fed-batch cultures. Biotechnol Bioeng 108:1328–1337. doi: 10.1002/bit.23072

75. Rothman R, Warren L, Vliegenthart J, Härd K (1989) Clonal analysis of the glycosylation of immunoglobulin G secreted by murine hybridomas. Biochemistry (Mosc) 28:1377–1384. doi: 10.1021/bi00429a065

76. Borys MC, Linzer DI, Papoutsakis ET (1993) Culture pH affects expression rates and glycosylation of recombinant mouse placental lactogen proteins by Chinese hamster ovary (CHO) cells. Biotechnol Nat Publ Co 11:720–724.

77. Gawlitzek M, Estacio M, Fürch T, Kiss R (2009) Identification of cell culture conditions to control N-glycosylation site-occupancy of recombinant glycoproteins expressed in CHO cells. Biotechnol Bioeng 103:1164–1175. doi: 10.1002/bit.22348

78. Trummer E, Fauland K, Seidinger S, Schriebl K, Lattenmayer C, Kunert R, Vorauer-Uhl K, Weik R, Borth N, Katinger H, Müller D (2006) Process parameter shifting: Part I. Effect of DOT, pH, and temperature on the performance of Epo-Fc expressing CHO cells cultivated in controlled batch bioreactors. Biotechnol Bioeng 94:1033–1044. doi: 10.1002/bit.21013

79. Ivarsson M, Villiger TK, Morbidelli M, Soos M (2014) Evaluating the impact of cell culture process parameters on monoclonal antibody N-glycosylation. J Biotechnol 188:88–96. doi: 10.1016/j.jbiotec.2014.08.026

80. Yoon SK, Hong JK, Choo SH, Song JY, Park HW, Lee GM (2006) Adaptation of Chinese hamster ovary cells to low culture temperature: cell growth and recombinant protein production. J Biotechnol 122:463–472. doi: 10.1016/j.jbiotec.2005.09.010

81. Yoon SK, Kim SH, Song JY, Lee GM (2006) Biphasic culture strategy for enhancing volumetric erythropoietin productivity of Chinese hamster ovary cells. Enzyme Microb Technol 39:362–365. doi: 10.1016/j.enzmictec.2005.11.029

82. Pasic A, Koehler H, Klimant I, Schaupp L (2007) Miniaturized fiber-optic hybrid sensor for continuous glucose monitoring in subcutaneous tissue. Sens Actuators B Chem 122:60–68. doi: 10.1016/j.snb.2006.05.010

83. Lu S, Sun X, Zhang Y (2005) Insight into metabolism of CHO cells at low glucose concentration on the basis of the determination of intracellular metabolites. Process Biochem 40:1917–1921. doi: 10.1016/j.procbio.2004.07.004

84. Chee Furng Wong D, Tin Kam Wong K, Tang Goh L, Kiat Heng C, Gek Sim Yap M (2005) Impact of dynamic online fed-batch strategies on metabolism, productivity and N-glycosylation quality in CHO cell cultures. Biotechnol Bioeng 89:164–177. doi: 10.1002/bit.20317

85. Andersen DC, Goochee CF (1995) The effect of ammonia on the O-linked glycosylation of granulocyte colony-stimulating factor produced by chinese hamster ovary cells. Biotechnol Bioeng 47:96–105. doi: 10.1002/bit.260470112

86. Yang M, Butler M (2002) Effects of ammonia and glucosamine on the heterogeneity of erythropoietin glycoforms. Biotechnol Prog 18:129–138. doi: 10.1021/bp0101334

87. Grammatikos SI, Valley U, Nimtz M, Conradt HS, Wagner R (1998) Intracellular UDP-N-acetylhexosamine pool affects N-glycan complexity: a mechanism of ammonium action on protein glycosylation. Biotechnol Prog 14:410–419. doi: 10.1021/bp980005o

88. Leong DSZ, Tan JGL, Chin CL, Mak SY, Ho YS, Ng SK (2017) Evaluation and use of disaccharides as energy source in protein-free mammalian cell cultures. Sci Rep. doi: 10.1038/srep45216

89. McAtee AG, Templeton N, Young JD (2014) Role of Chinese hamster ovary central carbon metabolism in controlling the quality of secreted biotherapeutic proteins. Pharm. Bioprocess. 2:

90. Hu W-S (2012) Cell Culture Bioprocess Engineering. Wei-Shou Hu, USA

91. Gorfien S, Paul W, Judd D, Tescione L, Jayme D (2003) Optimized Nutrient Additives for Fed-Batch Cultures. In: BioPharm Int. http://connection.ebscohost.com/c/articles/9491338/optimized-nutrient-additives-fed-batch-cultures. Accessed 18 Mar 2017

92. Darling RJ, Kuchibhotla U, Glaesner W, Micanovic R, Witcher DR, Beals JM (2002) Glycosylation of Erythropoietin Affects Receptor Binding Kinetics: Role of Electrostatic Interactions. Biochemistry (Mosc) 41:14524–14531. doi: 10.1021/bi0265022

93. Sinclair AM, Elliott S (2005) Glycoengineering: the effect of glycosylation on the properties of therapeutic proteins. J Pharm Sci 94:1626–1635. doi: 10.1002/jps.20319

94. Hayter PM, Curling EMA, Baines AJ, Jenkins N, Salmon I, Strange PG, Tong JM, Bull AT (1992) Glucose-limited chemostat culture of chinese hamster ovary cells producing recombinant human interferon-γ. Biotechnol Bioeng 39:327–335. doi: 10.1002/bit.260390311

95. Liu B, Spearman M, Doering J, Lattová E, Perreault H, Butler M (2014) The availability of glucose to CHO cells affects the intracellular lipid-linked oligosaccharide distribution, site occupancy and the N-glycosylation profile of a monoclonal antibody. J Biotechnol 170:17–27. doi: 10.1016/j.jbiotec.2013.11.007

96. Nyberg GB, Balcarcel RR, Follstad BD, Stephanopoulos G, Wang DI (1999) Metabolic effects on recombinant interferon-gamma glycosylation in continuous culture of Chinese hamster ovary cells. Biotechnol Bioeng 62:336–347.

97. Rijcken WRP, Overdijk B, Eijnden DHV den, Ferwerda W (1995) The effect of increasing nucleotide-sugar concentrations on the incorporation of sugars into glycoconjugates in rat hepatocytes. Biochem J 305:865–870. doi: 10.1042/bj3050865

98. Moremen KW, Tiemeyer M, Nairn AV (2012) Vertebrate protein glycosylation: diversity, synthesis and function. Nat Rev Mol Cell Biol 13:448–462. doi: 10.1038/nrm3383

99. Stanley P (2011) Golgi Glycosylation. Cold Spring Harb Perspect Biol 3:a005199. doi: 10.1101/cshperspect.a005199

100. Tian E, Hagen KGT (2009) Recent insights into the biological roles of mucin-type O-glycosylation. Glycoconj J 26:325–334. doi: 10.1007/s10719-008-9162-4

101. Elliott S, Lorenzini T, Asher S, Aoki K, Brankow D, Buck L, Busse L, Chang D, Fuller J, Grant J, Hernday N, Hokum M, Hu S, Knudten A, Levin N, Komorowski R, Martin F, Navarro R, Osslund T, Rogers G, Rogers N, Trail G, Egrie J (2003) Enhancement of therapeutic protein in vivo activities through glycoengineering. Nat Biotechnol 21:414–421. doi: 10.1038/nbt799

102. Egrie JC, Browne JK (2001) Development and characterization of novel erythropoiesis stimulating protein (NESP). Nephrol Dial Transplant 16:3–13. doi: 10.1093/ndt/16.suppl_3.3

103. Shukurov RR, Lobanova NV, Savinova IN, Vorobyova IG, Nurbakov AA, Ermolina LV, Orlova NV, Mosina AG, Antonova LP, Khamitov RA, Seryogin YA (2014) Design of a stable cell line producing recombinant darbepoetin alpha based on CHO cells. Appl Biochem Microbiol 50:812–818. doi: 10.1134/S0003683814090063

104. Pasic A, Koehler H, Schaupp L, Pieber TR, Klimant I (2006) Fiber-optic flow-through sensor for online monitoring of glucose. Anal Bioanal Chem 386:1293–1302. doi: 10.1007/s00216-006-0782-x

105. Tric M (2013) Entwicklung eines neuen Verfahrens zur Herstellung von reproduzierbaren Biosensoren. Master's thesis, Hochschule Mannheim

106. Lochead J, Schessner J, Werner T, Wölfl S (2015) Time-Resolved Cell Culture Assay Analyser (TReCCA Analyser) for the Analysis of On-Line Data: Data Integration—Sensor Correction—Time-Resolved IC 50 Determination. PLOS ONE 10:e0131233. doi: 10.1371/journal.pone.0131233

107. Gramer MJ, Goochee CF (1993) Glycosidase activities in Chinese hamster ovary cell lysate and cell culture supernatant. Biotechnol Prog 9:366–373. doi: 10.1021/bp00022a003

108. Roth T (2017) Änderung der Aminosäurekonzentration im CHO-Medium bei Zugabe unterschiedlicher Glucosekonzentrationen. Bachelor's thesis, Hochschule Mannheim

109. Bergmeyer HU, Bernt E (1974) Colorimetric Assay with 6-Benzamido-4-methoxy-m-toluidine Diazonium Chloride. In: Methods Enzym. Anal. Second Ed. Academic Press, pp 742–745

110. Gibson QH, Swoboda BE, Massey V (1964) KINETICS AND MECHANISM OF ACTION OF GLUCOSE OXIDASE. J Biol Chem 239:3927–3934.

111. Parker JW, Schwartz CS (1987) Modeling the kinetics of immobilized glucose oxidase. Biotechnol Bioeng 30:724–735. doi: 10.1002/bit.260300605

112. Jones P, Suggett A (1968) The catalase–hydrogen peroxide system. Kinetics of catalatic action at high substrate concentrations. Biochem J 110:617–620.

113. Tse PHS, Leypoldt JK, Gough DA (1987) Determination of the intrinsic kinetic constants of immobilized glucose oxidase and catalase. Biotechnol Bioeng 29:696–704. doi: 10.1002/bit.260290606

114. Bao J, Furumoto K, Yoshimoto M, Fukunaga K, Nakao K (2003) Competitive inhibition by hydrogen peroxide produced in glucose oxidation catalyzed by glucose oxidase. Biochem Eng J 13:69–72. doi: 10.1016/S1369-703X(02)00120-1

115. Collins JS, Goldsmith TH (1981) Spectral properties of fluorescence induced by glutaraldehyde fixation. J Histochem Cytochem 29:411–414. doi: 10.1177/29.3.6787116

116. Kumar R, Ismail AF (2015) Fouling control on microfiltration/ultrafiltration membranes: Effects of morphology, hydrophilicity, and charge. J Appl Polym Sci 132:n/a-n/a. doi: 10.1002/app.42042

117. Jobst G, Moser I, Urban G (1996) Numerical simulation of multi-layered enzymatic sensors. Biosens Bioelectron 11:111–117. doi: 10.1016/0956-5663(96)83718-3

118. Ramachandran S, Nair S, Larroche C, Pandey A (2017) 26 - Gluconic Acid. In: Curr. Dev. Biotechnol. Bioeng. Elsevier, pp 577–599

119. Bankar SB, Bule MV, Singhal RS, Ananthanarayan LA (2011) Co-Immobilization of Glucose Oxidase-Catalase: Optimization of Immobilization Parameters to Improve the Immobilization Yield. Int J Food Eng. doi: 10.2202/1556-3758.1919

120. Zhang Y, Wilson GS (1993) In vitro and in vivo evaluation of oxygen effects on a glucose oxidase based implantable glucose sensor. Anal Chim Acta 281:513–520. doi: 10.1016/0003-2670(93)85009-9

121. Yoshimoto M, Sato M, Wang S, Fukunaga K, Nakao K (2006) Structural stability of glucose oxidase encapsulated in liposomes to inhibition by hydrogen peroxide produced during glucose oxidation. Biochem Eng J 30:158–163. doi: 10.1016/j.bej.2006.03.004

122. Mirón J, González MP, Vázquez JA, Pastrana L, Murado MA (2004) A mathematical model for glucose oxidase kinetics, including inhibitory, deactivant and diffusional effects, and their interactions. Enzyme Microb Technol 34:513–522. doi: 10.1016/j.enzmictec.2003.12.003

123. Blandino A, Macías M, Cantero D (2002) Modelling and simulation of a bienzymatic reaction system co-immobilised within hydrogel-membrane liquid-core capsules. Enzyme Microb Technol 31:556–565. doi: 10.1016/S0141-0229(02)00154-0

124. Buchholz K, Gödelmann B (1978) Macrokinetics and operational stability of immobilized glucose oxidase and catalase. Biotechnol Bioeng 20:1201–1220. doi: 10.1002/bit.260200807

125. Blandino A, Macías M, Cantero D (2003) Calcium alginate gel as encapsulation matrix for coimmobilized enzyme systems. Appl Biochem Biotechnol 110:53–60. doi: 10.1385/ABAB:110:1:53

126. Mateo C, Palomo JM, Fernandez-Lorente G, Guisan JM, Fernandez-Lafuente R (2007) Improvement of enzyme activity, stability and selectivity via immobilization techniques. Enzyme Microb Technol 40:1451–1463. doi: 10.1016/j.enzmictec.2007.01.018

127. Shrivastava A, Gupta VB (2011) Methods for the determination of limit of detection and limit of quantitation of the analytical methods. Chron Young Sci 2:21. doi: 10.4103/2229-5186.79345

128. del Barrio M, Cases R, Cebolla V, Hirsch T, de Marcos S, Wilhelm S, Galbán J (2016) A reagentless enzymatic fluorescent biosensor for glucose based on upconverting glasses, as excitation source, and chemically modified glucose oxidase. Talanta 160:586–591. doi: 10.1016/j.talanta.2016.07.062

129. House JL, Anderson EM, Ward WK (2007) Immobilization techniques to avoid enzyme loss from oxidase-based biosensors: a one-year study. J Diabetes Sci Technol 1:18–27. doi: 10.1177/193229680700100104

130. van Stroe-Biezen SAM, Everaerts FM, Janssen LJJ, Tacken RA (1993) Diffusion coefficients of oxygen, hydrogen peroxide and glucose in a hydrogel. Anal Chim Acta 273:553–560. doi: 10.1016/0003-2670(93)80202-V

131. IntroductionToCOMSOLMultiphysics.pdf.

132. Albin G, Horbett TA, Ratner BD (1985) Glucose sensitive membranes for controlled delivery of insulin: Insulin transport studies. J Controlled Release 2:153–164. doi: 10.1016/0168-3659(85)90041-0

133. Dayal R, Godjevargova T (2006) Pore diffusion studies with immobilized glucose oxidase plus catalase membranes. Enzyme Microb Technol 39:1313–1318. doi: 10.1016/j.enzmictec.2006.03.018

134. Brandrup J, Edmund H (1999) Polymer Handbook, 4th edition. Wiley, New York

135. Mafra ACO, Kopp W, Ramos MD, Beltrame MB, Ribeiro MPA, Badino AC, Tardioli PW (2015) CROSS-LINKED ENZYME AGGREGATES OF CATALASE FROM BOVINE LIVER. In: Blucher Chem. Eng. Proc. pp 1714–1721

136. Hsieh DPH, Silver RS, Mateles RI (1969) Use of the glucose oxidase system to measure oxygen transfer rates. Biotechnol Bioeng 11:1–18. doi: 10.1002/bit.260110102

137. Bolivar JM, Consolati T, Mayr T, Nidetzky B (2013) Quantitating intraparticle O2 gradients in solid supported enzyme immobilizates: experimental determination of their role in limiting the catalytic effectiveness of immobilized glucose oxidase. Biotechnol Bioeng 110:2086–2095. doi: 10.1002/bit.24873

138. Kleppe K (1966) The effect of hydrogen peroxide on glucose oxidase from Aspergillus niger. Biochemistry (Mosc) 5:139–143.

139. Barbouti A, Doulias P-T, Nousis L, Tenopoulou M, Galaris D (2002) DNA damage and apoptosis in hydrogen peroxide-exposed Jurkat cells: bolus addition versus continuous generation of H2O2. Free Radic Biol Med 33:691–702. doi: 10.1016/S0891-5849(02)00967-X

140. Alborzinia H, Can S, Holenya P, Scholl C, Lederer E, Kitanovic I, Wölfl S (2011) Real-Time Monitoring of Cisplatin-Induced Cell Death. PLOS ONE 6:e19714. doi: 10.1371/journal.pone.0019714

141. Pais DAM, Carrondo MJ, Alves PM, Teixeira AP (2014) Towards real-time monitoring of therapeutic protein quality in mammalian cell processes. Curr Opin Biotechnol 30:161–167. doi: 10.1016/j.copbio.2014.06.019

142. Zhang P, Chan KF, Haryadi R, Bardor M, Song Z (2012) CHO Glycosylation Mutants as Potential Host Cells to Produce Therapeutic Proteins with Enhanced

Efficacy. In: Zhong J-J (ed) Future Trends Biotechnol. Springer Berlin Heidelberg, pp 63–87

143. Yoon SK, Choi SL, Song JY, Lee GM (2005) Effect of culture pH on erythropoietin production by Chinese hamster ovary cells grown in suspension at 32.5 and 37.0°C. Biotechnol Bioeng 89:345–356. doi: 10.1002/bit.20353

144. Tsao Y-S, Cardoso AG, Condon RGG, Voloch M, Lio P, Lagos JC, Kearns BG, Liu Z (2005) Monitoring Chinese hamster ovary cell culture by the analysis of glucose and lactate metabolism. J Biotechnol 118:316–327. doi: 10.1016/j.jbiotec.2005.05.016

145. Kuwae S, Ohda T, Tamashima H, Miki H, Kobayashi K (2005) Development of a fed-batch culture process for enhanced production of recombinant human antithrombin by Chinese hamster ovary cells. J Biosci Bioeng 100:502–510. doi: 10.1263/jbb.100.502

146. Ahn WS, Jeon J-J, Jeong Y-R, Lee SJ, Yoon SK (2008) Effect of culture temperature on erythropoietin production and glycosylation in a perfusion culture of recombinant CHO cells. Biotechnol Bioeng 101:1234–1244. doi: 10.1002/bit.22006

147. Duarte TM, Carinhas N, Barreiro LC, Carrondo MJT, Alves PM, Teixeira AP (2014) Metabolic responses of CHO cells to limitation of key amino acids. Biotechnol Bioeng 111:2095–2106. doi: 10.1002/bit.25266

148. Mulukutla BC, Gramer M, Hu W-S (2012) On metabolic shift to lactate consumption in fed-batch culture of mammalian cells. Metab Eng 14:138–149. doi: 10.1016/j.ymben.2011.12.006

149. Xie L, Wang DIC (2006) Fed-batch cultivation of animal cells using different medium design concepts and feeding strategies. Biotechnol Bioeng 95:270–284. doi: 10.1002/bit.21160

150. Wingens M, Gätgens J, Schmidt A, Albaum SP, Büntemeyer H, Noll T, Hoffrogge R (2015) 2D-DIGE screening of high-productive CHO cells under glucose limitation—Basic changes in the proteome equipment and hints for epigenetic effects. J Biotechnol 201:86–97. doi: 10.1016/j.jbiotec.2015.01.005

151. Ljunggren J, Häggström L (1994) Catabolic control of hybridoma cells by glucose and glutamine limited fed batch cultures. Biotechnol Bioeng 44:808–818. doi: 10.1002/bit.260440706

152. Fan Y, Jimenez Del Val I, Müller C, Wagtberg Sen J, Rasmussen SK, Kontoravdi C, Weilguny D, Andersen MR (2015) Amino acid and glucose metabolism in fed-batch CHO cell culture affects antibody production and glycosylation. Biotechnol Bioeng 112:521–535. doi: 10.1002/bit.25450

153. Sun X, Zhang Y (2004) Glutamine cannot support recombinant CHO cell growth and maintenance in the absence of glucose. Process Biochem 39:719–722. doi: 10.1016/S0032-9592(03)00182-1

154. Dean J, Reddy P (2013) Metabolic analysis of antibody producing CHO cells in fed-batch production. Biotechnol Bioeng 110:1735–1747. doi: 10.1002/bit.24826

155. Carrillo-Cocom LM, Genel-Rey T, Araíz-Hernández D, López-Pacheco F, López-Meza J, Rocha-Pizaña MR, Ramírez-Medrano A, Alvarez MM (2015) Amino acid consumption in naïve and recombinant CHO cell cultures: producers of a monoclonal antibody. Cytotechnology 67:809–820. doi: 10.1007/s10616-014-9720-5

156. Fan Y, Jimenez Del Val I, Müller C, Lund AM, Sen JW, Rasmussen SK, Kontoravdi C, Baycin-Hizal D, Betenbaugh MJ, Weilguny D, Andersen MR (2015) A multi-pronged investigation into the effect of glucose starvation and culture duration on fed-batch CHO cell culture. Biotechnol Bioeng 112:2172–2184. doi: 10.1002/bit.25620

157. Rumpler M, Mader JK, Fischer JP, Thar R, Granger JM, Deliane F, Klimant I, Aberer F, Sinner F, Pieber TR, Hajnsek M (2017) First application of a transcutaneous optical single-port glucose monitoring device in patients with type 1 diabetes mellitus. Biosens Bioelectron 88:240–248. doi: 10.1016/j.bios.2016.08.039

158. Spichiger S, Spichiger-Keller UE (2010) Process monitoring with disposable chemical sensors fit in the framework of process analysis technology (PAT) for innovative pharmaceutical development and quality assurance. Chimia 64:803–807.

159. Weichert H, Becker M (2013) Online glucose-lactate monitoring and control in cell culture and microbial fermentation bioprocesses. BMC Proc 7:P18. doi: 10.1186/1753-6561-7-S6-P18

6 LIST OF FIGURES

7 LIST OF TABLES

8 ABBREVIATIONS

ABTS	2,2'-azino-bis(3-ethylbenzothiazoline-6-sulphonic acid)
ATP	Adenosine triphosphate
BSA	Bovine serum albumin
Cat	Catalase
CE	Capillary electrophoresis
CHO	Chinese hamster ovary cells
Cisplatin	(SP-4-2)-diamminedichloroplatinum(II)
DO	Dissolved oxygen
EtOH	Ethanol
FAD	Flavine adenine dinucucleotide
FCS	Foetal Calf Serum
GAD	Glutaraldehyde
Glycerol	Propane-1,2,3-triol
GOD	Glucose oxidase
H_2O_2	Hydrogen peroxide
HG	High glucose level
HPM	High permeability membrane
HRP	Horseradish peroxidase
IC	Internal conversion
ISC	Inter system crossing
IMDM	Iscove's Modified Dulbecco's Medium
LED	Light-emitting diode
LG	Low glucose level
LPM	Low permeability membrane
NAD	Nicotinamide adenine dinucleotide, oxidised form
NADH	Nicotinamide adenine dinucleotide, reduced form
NADP	Nicotinamide adenine dinucleotide phosphate, oxidised form
NADPH	Nicotinamide adenine dinucleotide phosphate, reduced form
$NaHCO_3$	Sodium bicarbonate
NaOH	Sodium hydroxide
O_2	Oxygen
PAT	Process analytical technology

PBS	Phosphate-buffered saline
pO_2	Oxygen partial pressure
POF	Polymer optical fibre
rpm	Rotation per minute
RSD	Relative standard deviation
RT	Room temperature
SDR	Sensor-Dish Reader
t_{90}	Time until 90 % of the final signal is reached
UV	Ultra violet light

9 ACKNOWLEDGEMENTS

The group of **Prof. Dr. Dirk Lütkemeyer** at the Fachhochschule Bielefeld for the fruitful cooperation regarding the determination of the product quality of Darbepoetin alfa.

The students I worked with for their contributions to this thesis, their fresh perspectives, as well as the nice times spent together. In particular:

Igor Dolgowjasow for his contribution to the biosensor model, and arousing my interest for history.

Tatjana Roth for her work on the GC measurements.

Julian Mochayedi for his relaxed attitude and correcting my thesis.

My colleagues from the Heidelberg University and the Hochschule Mannheim for the relaxed and friendly atmosphere. In particular:

Mario Lederle for taking over the cell culture experiments and the fun times spent in or outside of the lab.

Lisa Neuner for the glucose offline measurements and the interesting talks about things that matter in life.

Julia Lochead for her support and previous work on the glucose sensor.

Ali Ghanem for our interesting talks on astronomy.

Suzan Can for storing my letters and our interesting talks during lunch.

All the friends who supported me during the years of my PhD and especially:

Rebekka Rauschopf for taking care of me and giving me endless support and love.

10 APPENDIX

10.1 List of chemicals and enzymes used in this thesis

Tabelle 3: Applied chemicals and reagents

Name	Information	Manufacturer
ABTS	2,2′-Azino-bis(3-ethylbenzothiazoline-6-sulfonic acid) diammonium salt	Sigma Aldrich, Taufkirchen, Germany
Activator	1 mL	Roche Diagnostik GmbH, Mannheim, Germany
Bovine serum albumin	BSA, powder	Sigma Aldrich, Taufkirchen, Germany
Catalase	Cat from bovine liver, powder	Sigma Aldrich, Taufkirchen, Germany
Cis-diaminoplatinum (II) dichloride	From Heidelberg	Sigma Aldrich, Taufkirchen, Germany
Ethanol	denatured; 70%	Carl Roth GmbH & CO. KG, Karlsruhe, Germany
Ethanol	undenatured; 100%	Carl Roth GmbH & CO. KG, Karlsruhe, Germany
Ethyl cellulose	powder	Merck KgaA, Darmstadt, Germany
Geneticin (G418)	50 mg/mL	Sigma Aldrich, Taufkirchen, Germany
Glucose oxidase	From Aspergillus Niger, powder	Sigma Aldrich, Taufkirchen, Germany
Glutaraldehyde	250 mL	Sigma Aldrich, Taufkirchen, Germany
Glycerine	250 mL	Merck KgaA, Darmstadt, Germany
Horseradish peroxidase	HRP, powder	Sigma Aldrich, Taufkirchen, Germany
Hydrochloric acid (HCl)	37% (10,15 M)	Carl Roth GmbH & CO. KG, Karlsruhe, Germany
Hydromed D4, D6, D7	ether-based hydrophilic urethanes	AdvanSource Biomaterials, Willington, USA
IMDM medium	Without glutamine	Sigma Aldrich, Taufkirchen, Germany
ISE Deproteinizer Bio	1 mL	Roche Diagnostik GmbH, Mannheim, Germany
Isopropanol	100%	Carl Roth GmbH & CO. KG, Karlsruhe, Germany

Name	Information	Manufacturer
L-Glutamine	200 mM	Sigma Aldrich, Taufkirchen, Germany
pH calibrator standards	pH 4.01; 7.00 and 9.21	Mettler Toledo, Gießen, Germany
Phosphate buffer saline	Dulbecco's PBS	Sigma Aldrich, Taufkirchen, Germany
Polyurethane polymer	D4, D6, D7	Hydromed, Hannover, Germany
Potassium chloride	3 M Solution	Mettler Toledo, Gießen, Germany
ProCHO-2 CD	Serum-free, without L-Glutamin and Glucose, 0,1% pluronic-F68®	Lonza, Basel, Swiss
Silicone glue	RS 232	PresSens GmbH, Regensburg, Germany
Sodium chloride	NaCl, powder	AppliChem, Darmstadt, Germany
Sodium hydroxide	NaOH	AppliChem, Darmstadt, Germany
Trypanblau	10 g	Carl Roth GmbH & CO. KG, Karlsruhe, Germany

10.2 List of other materials

10.2.1 Devices

Tabelle 1: List of other devices

Device	Name	Manufacturer
Applicator	ZUA 2000 universal applicator	Zehntner, Sissach, Swiss
Autoclave	VX-150 und 2540 EL	Systec GmbH, Wettenberg, Germany
Balance	Kern 770	Kern & Sohn GmbH, Balingen, Germany
CO_2-Incubator	HeraCell® 240i	Thermo Scientific, Waltham, USA
Floor-standing centrifuge	ZK 380	Hermle Labortechnik, Wehingen, Germany
Freezer (-80°C)	VIP Series	Sanyo, Osaka, Japan
Haemocytometer	Neubauer Zählkammer	Carl Roth GmbH & CO. KG, Karlsruhe, Germany
Incubator	Lab-Therm LT-X	Kühner, Basel, Swiss
Incubator	Function Line	Heraeus, Hanau, Germany

Device	Name	Manufacturer
Laminar flow (class II)	HeraSafe	Thermo Scientific, Waltham, USA
Magnetic stirrer	IKA MAGRH	IKA Labortechnik, Staufen, Germany
Metabolic analyzer	Cedex-Bio	Roche Diagnostic GmbH, Mannheim, Germany
Micro pipettes	Pipetman® 0,5-1000 µl	Gilson Inc., Middleton, USA
Microscope	Axiovert 25C	Carl Zeiss, Jena, Germany
Osmometer	Osmomat 030	Gonotec, Berlin, Germany
Paint meter	Elcometer 345	Elcometer GmbH, Aalen, Germany
Peristaltic pump	Minipuls 3	Gilson, Villiers-le-Bel, France
pH-meter	Semi-Micro pH	VWR, Bruchsal, Germany
Plate reader	HT3 photometer	Anthos, Friesoythe, Germnay
Refrigerator (+4°C, -20°C)	Comfort NoFrost	Liebherr, Nürnberg, Germany
Shaker	WAVE Bioreactor system 20/50	GE Healthcare Munich, Germany
Shake Flask Reader	For PreSens shake flasks	PreSens GmbH, Regensburg, Germany
Spectrofluorimeter	FluoroLog	Horiba Scientific Ltd., München, Germany
Table centrifuge	Fresco 21	Thermo Scientific, Waltham, USA
Table shaker	Edmund Bühler	Edmund Bühler GmbH, Tübingen, Germany
Ultrapure water system	Milli-Q® Reference	Merck Millipore, Darmstadt, Germany
Viability Analyzer	ViCell® XR	Beckman Coulter Inc., Brea, USA
Vortexer	Yellow Line TTS 2	IKA Labortechnik, Staufen, Germany
Water bath	SW22	Julabo, Seelbach, Germany

10.2.2 List of other materials

Tabelle 2: Applied materials

Name	Information	Manufacturer
6-well plates	Nunclon Vita Multidish Polystyrene	Thermo Scientific, Waltham, USA
96-well plates	Polystyrene	Greiner-Bio-One, Frickenhausen, Germany
Cell culture flask	75 cm^2	Greiner-Bio-One, Frickenhausen, Germany
Clave Connector	CLAVE® Needlefree Connector	Neo Care GmbH, Lüdenscheid, Germany
Cryovial	CryoPure vial 1,6 mL	Sarstedt, Nürnbrecht, Germany
Diffusion membranes	Hydrophilic perforrated membrane	PreSens GmbH, Regensburg, Germany
Disposable cell bag bioreactor	2 L volume with screw cap	GE Healthcare, Munich, Germany
Disposable cuvettes (CedexBio)	MicroCuvette Segments Bio	Roche Diagnostik GmbH, Mannheim, Germany
Disposable Sterican needles	2,1x80 mm	B. Braun, Melsungen, Germany
Disposable gloves	Safetec	Unigloves, Rochester, UK
Erlenmeyer flask	125 mL polycarbonate	Corning, Tewksbury, USA
Erlenmeyer flask with O_2 and pH sensors	125 mL polycarbonate	PreSens GmbH, Regensburg, Germany
HydroDish	24-well plate with integrated pH-sensors	PreSens GmbH, Regensburg, Germany
Luer Lock adapter	„female" and „male"	Applied Critical Fluids, Mannheim, Germany
Luer Lock syringe	Omnitix® 2 mL, 5 mL, 50 mL	B. Braun, Melsungen, Germany
Silicone tubes	Oxygen permeable	Applied Critical Fluids, Mannheim, Germany
Syringe sterile filter	0.22 µm (cellulose acetate)	VWR, Bruchsal, Germany
Vial for cell counting	4 mL sample cup	Beckman Coulter Inc., Brea, USA

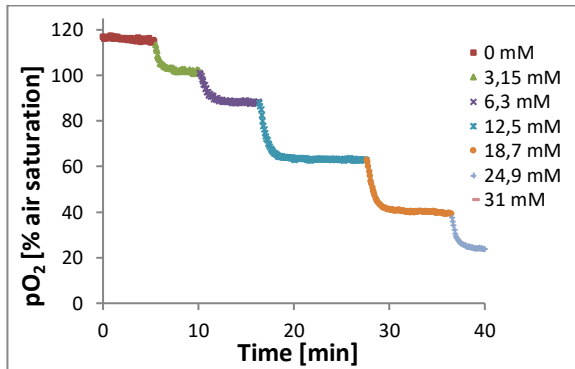## 10.3 Supplementary data

Figure 78 Biosensor response to glucose addition

Addition of glucose to a glucose biosensor with a D4 polyurethane diffusion layer in PBS buffer leads to a signal drop.
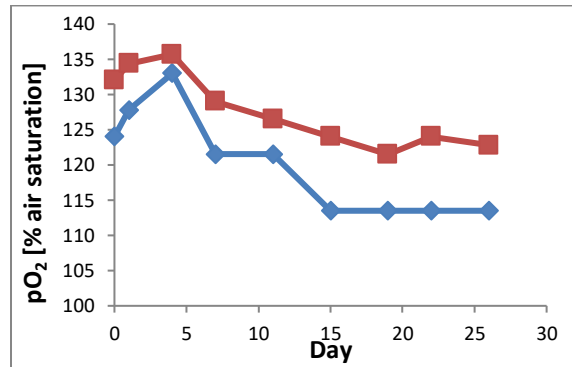

Figure 79 Change in background fluorescence over time of two glucose biosensors at 0 mM glucose

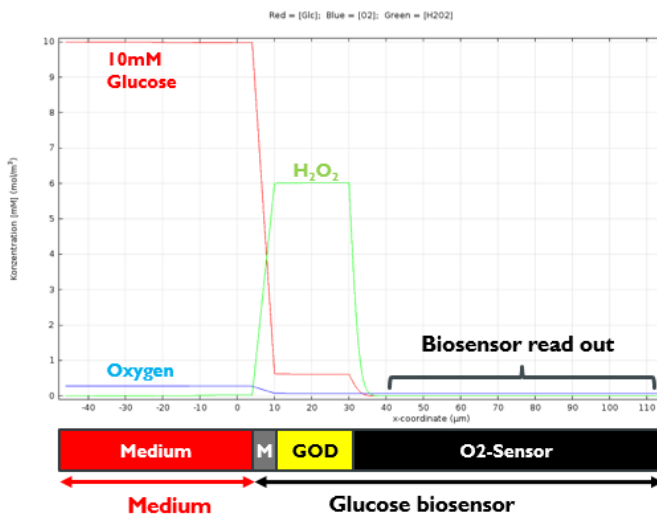The signal evolution represents the change in the background fluorescence over time.

Figure 80 Graph of a glucose biosensor simulation with COMSOL

The simulation of glucose biosensor response at the applied oxygen and glucose level in the medium, can be read out as the oxygen level in the oxygen sensor.
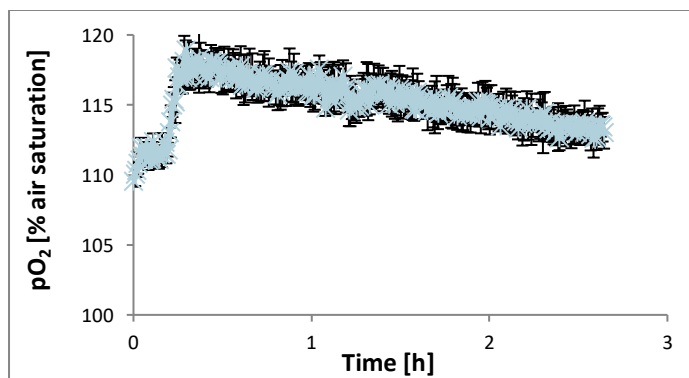
Figure 81 Influence of 5 mM hydrogen peroxide addition on the biosensor signal

The error bars correspond to the standard deviation of three measurements in a 24-well plate.
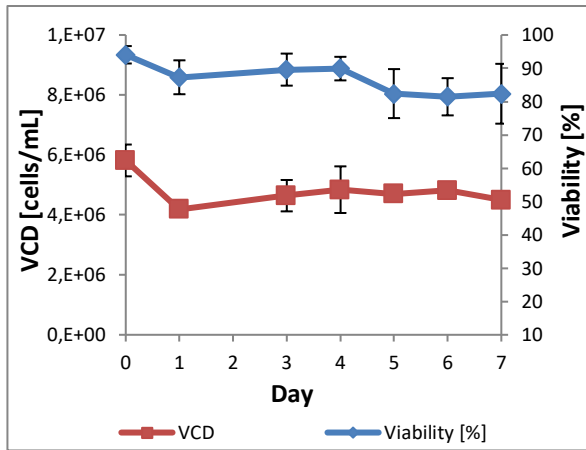
Figure 82 Viable cell density (VCD) and cell viability as mean of two flasks from a CHO fed-batch culture at 31°C, ~5 mM glucose and 1 mM glutamine

Experimental conditions in a 125 mL shake flask: 50 % DO, 130 rpm, 5 % CO2 and 80 % humidity. The error bars correspond to the standard deviation of two flasks.
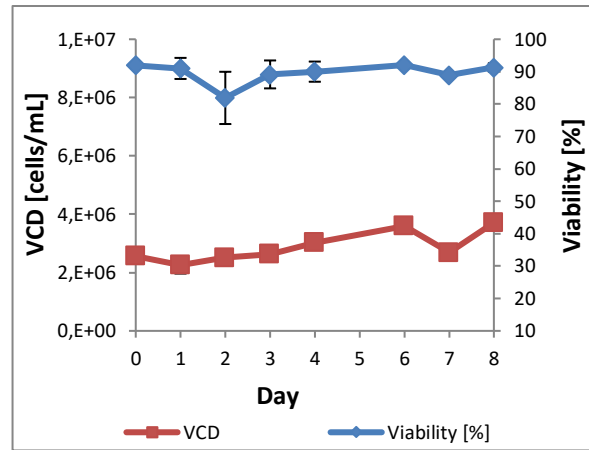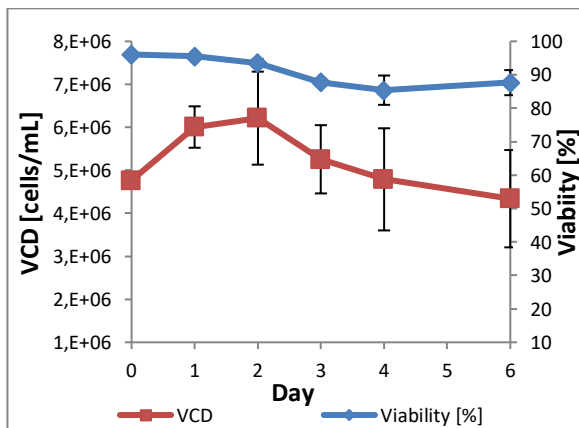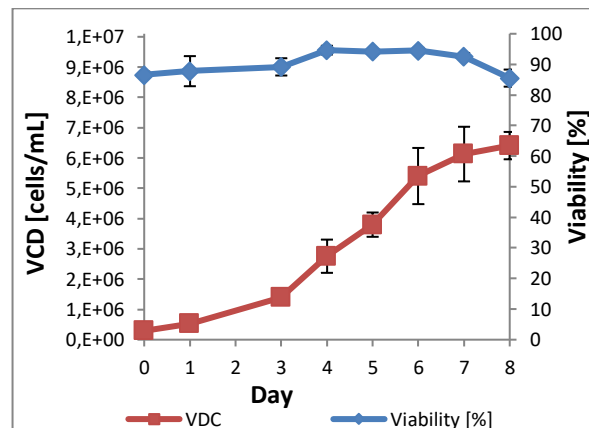

Figure 83 Viable cell density (VCD) and cell viability as mean of two flasks from a CHO fed-batch culture at 31°C, ~8 mM glucose and 1 mM glutamine

Experimental conditions in a 125 mL shake flask: 50 % DO, 130 rpm, 5 % CO2 and 80 % humidity. The error bars correspond to the standard deviation of two flasks.

Figure 84 Viable cell density (VCD) and cell viability as mean of two flasks from a CHO fed-batch culture at 31°C, ~1 mM glucose and 4 mM glutamine

Experimental conditions in a 125 mL shake flask: 50 % DO, 130 rpm, 5 % CO2 and 80 % humidity. The error bars correspond to the standard deviation of two flasks.

Figure 85 Viable cell density (VCD) and cell viability as mean of four flasks from a CHO batch culture at 37°C, ~1 mM glucose and 4 mM glutamine

Experimental conditions in a 125 mL shake flask: 50 % DO, 130 rpm, 5 % CO2 and 80 % humidity. The error bars correspond to the standard deviation of four flasks.
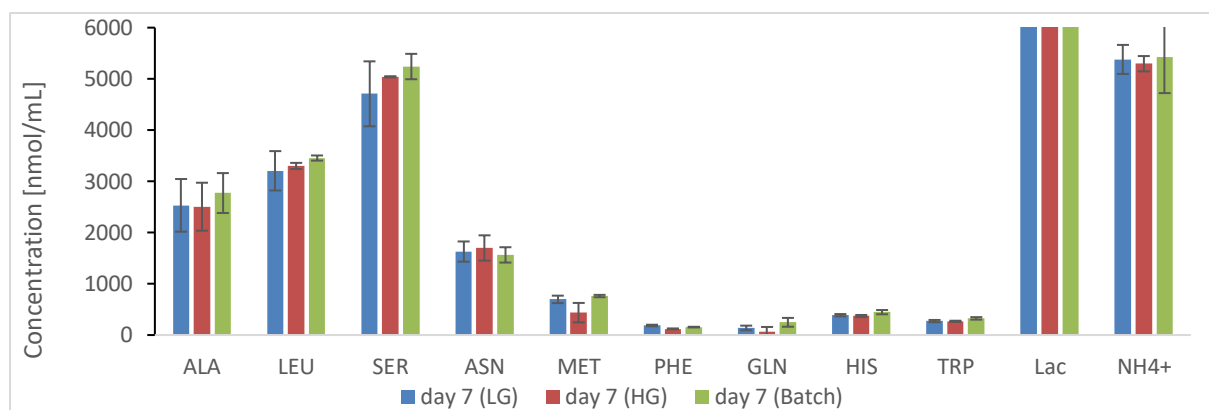
Figure 86 Nominal amino acid concentrations on day seven for three different cell culture experiments

The amino acid concentration on day seven is compared for two fed-batch cultures at a low (LG) and a high (HG) glucose regime and a batch culture. The data is presented as mean of three flasks for each cell culture type. The GC measurement was performed by Tatjana Roth.
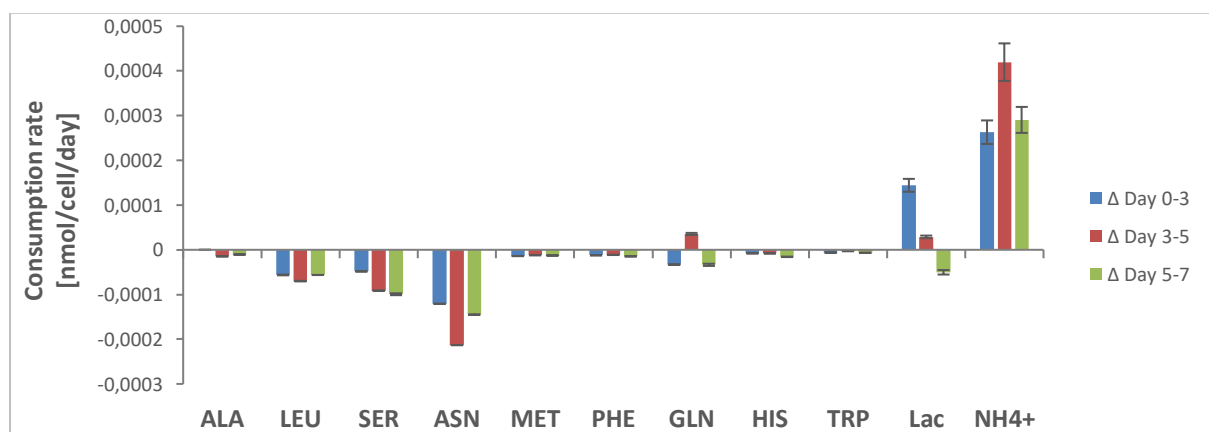

Figure 87 Amino acid consumption rate during CHO culture at 31°C, ~5 mM glucose and 1 mM glutamine

Amino acid consumption rate determined by GC and accumulation rate of metabolites measured by the Cedex-Bio. Experimental conditions: 50 % DO, 130 rpm, 5 % CO2 and 80 % humidity. The error bars correspond to the standard deviation of three measurements performed by Tatjana Roth.
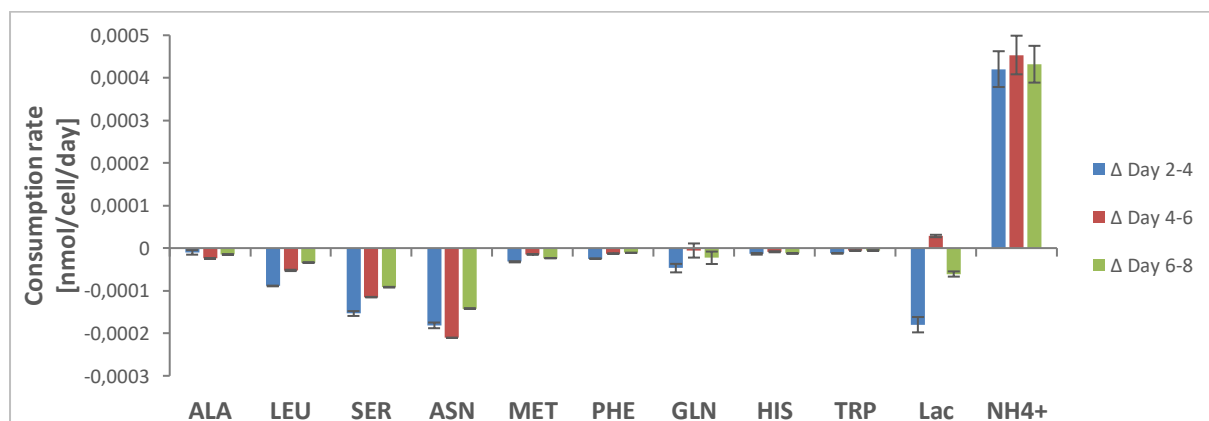

Figure 88 Amino acid consumption rate during CHO culture at 31°C, ~8 mM glucose and 1 mM glutamine

Amino acid consumption and accumulation rate of metabolites measured with GC and Cedex-Bio. Experimental conditions: 50 % DO, 130 rpm, 5 % CO2 and 80 % humidity. The error bars correspond to the standard deviation of three measurements. The GC measurement was performed by Tatjana Roth.
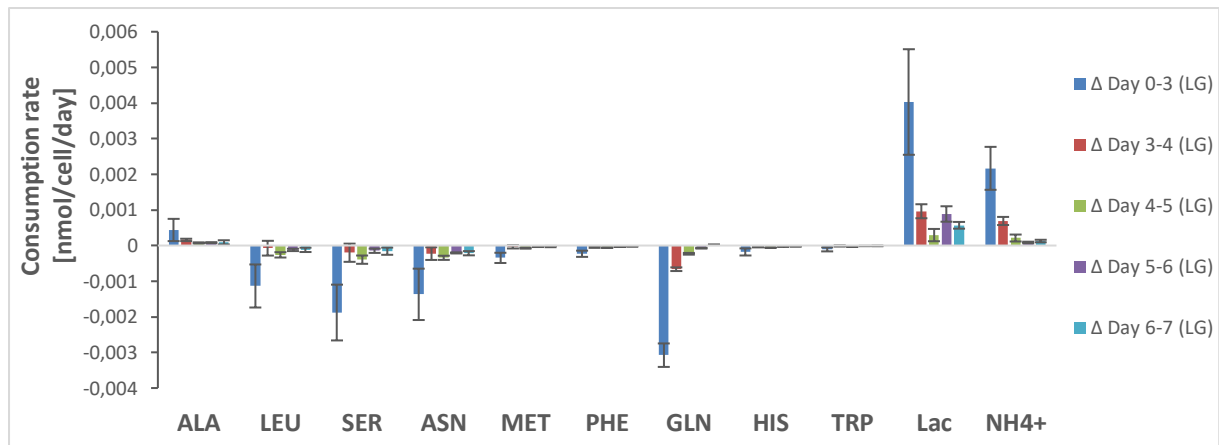
Figure 89 Consumption rate of amino acids during a fed-batch CHO culture at 37°C, ~1 mM glucose and 4 mM glutamine

Amino acid consumption rate determined by gas chromatography and accumulation rate of metabolites measured with the Cedex-Bio. Experimental conditions: 50 % DO, 130 rpm, 5 % CO2 and 80 % humidity in a 125 mL shake flask. The error bars correspond to standard deviation of three shake flasks. The GC measurement was performed by Tatjana Roth.
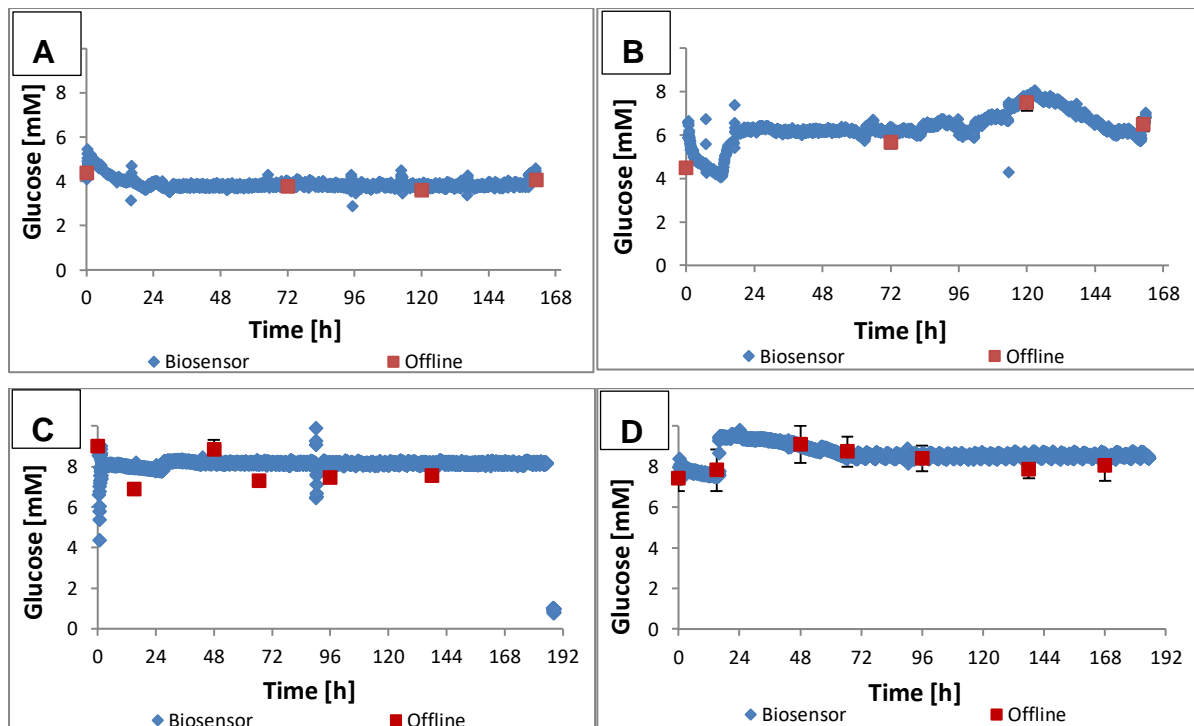

Figure 90 Biosensor and offline measurements of glucose during cell culture at 31°C and 1 mM glutamine

CHO culture experiment carried out in 50 mL at 37 °C, 130 RPM, 5 % CO$_2$ and 50 % DO. The medium in (B) and (D) exhibited a minimal glucose overshoot after 20 hours, due to a pressure build up caused by the 0.2 µm sterile filter resistance in the tubing of the glucose feed. The offline measurements in (A) and (B) were performed with the Cedex-Bio at an accuracy of 5 % (error bars) according to the manufacturer. The offline measurements in (C) and (D) were performed as a triplicate with a hexokinase assay. The measurements were jointly performed with Mario Lederle and Lisa Neuner.
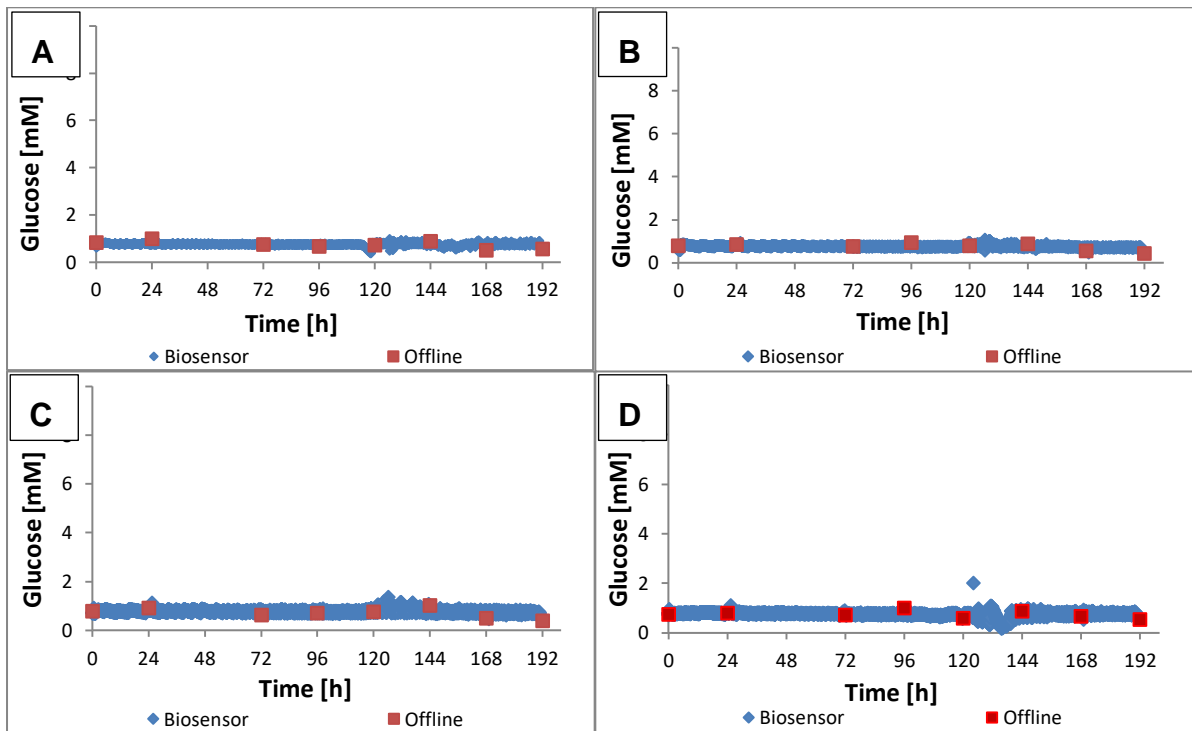
Figure 91 Biosensor and offline measurements of glucose during cell culture at a low glucose level

CHO culture experiment carried out in 50 mL at 37 °C, 130 RPM, 5 % CO_2 and 50 % air saturation. The offline measurements were performed with the Cedex-Bio at an accuracy of 5 % (error bars) according to the manufacturer. The measurements were jointly performed with Mario Lederle.

Figure 92 Biosensor and offline measurements of glucose during cell culture at a high glucose level

CHO culture experiment carried out in 50 mL at 37 ℃, 130 RPM, 5 % CO_2 and 50 % air saturation. The offline measurements were performed with the Cedex-Bio at an accuracy of 5 % (error bars) according to the manufacturer. The measurements were jointly performed with Mario Lederle.
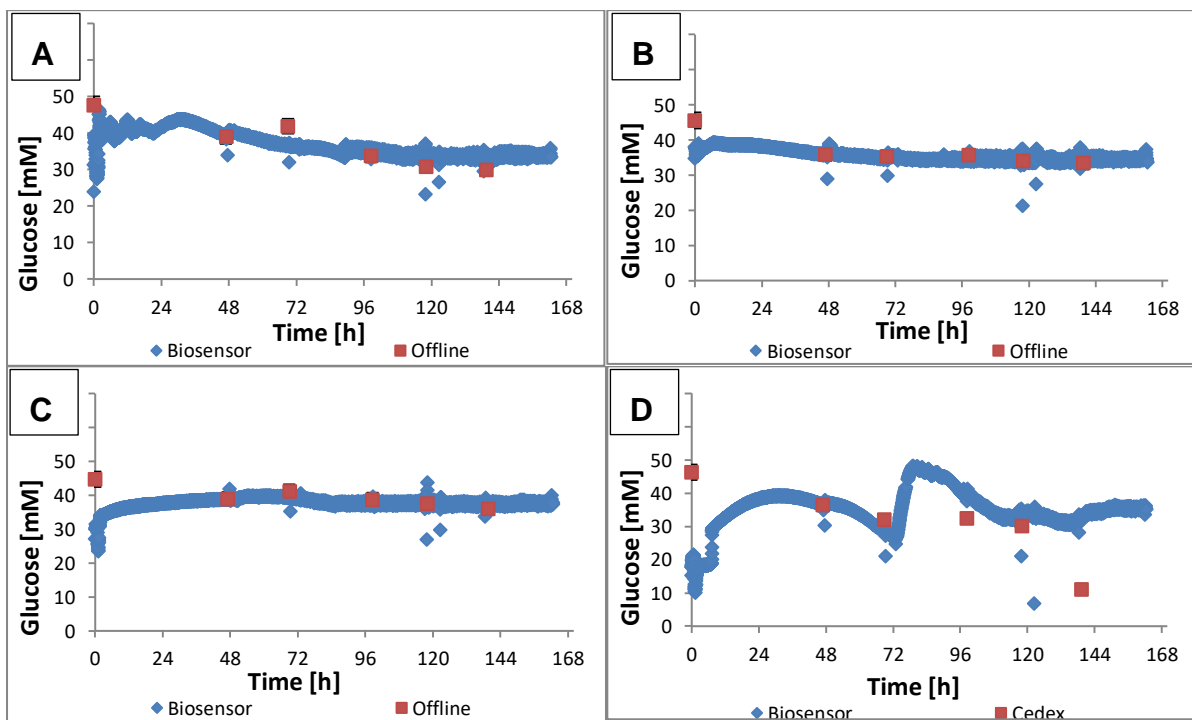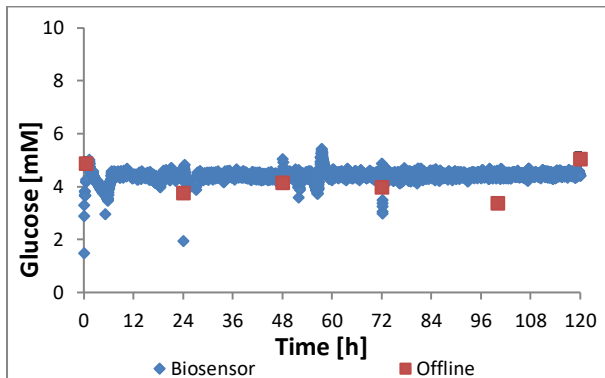

Figure 93 Biosensor and offline measurements of glucose during cell culture

CHO culture experiment carried out in 50 mL at 37 °C, 130 RPM, 5 % CO_2 and 50 % air saturation. 3 mL $NaHCO_3$ was added to the shake flask on day three. The offline measurements were performed with the Cedex-Bio at an accuracy of 5 % (error bars) according to the manufacturer.

Eidesstattliche Versicherung gemäß § 8 der Promotionsordnung für die Naturwissenschaftlich-Mathematische Gesamtfakultät der Universität Heidelberg

1. Bei der eingereichten Dissertation zu dem Thema

………………………………………………………………………………………………

handelt es sich um meine eigenständig erbrachte Leistung.

2. Ich habe nur die angegebenen Quellen und Hilfsmittel benutzt und mich keiner unzulässigen Hilfe Dritter bedient. Insbesondere habe ich wörtlich oder sinngemäß aus anderen Werken übernommene Inhalte als solche kenntlich gemacht.

3. Die Arbeit oder Teile davon habe ich bislang nicht[1] an einer Hochschule des In- oder Auslands als Bestandteil einer Prüfungs- oder Qualifikationsleistung vorgelegt.

Titel der Arbeit: ………………………………………………………………………

Hochschule und Jahr: ………………………………………………………......

Art der Prüfungs- oder Qualifikationsleistung: ……………………………

4. Die Richtigkeit der vorstehenden Erklärungen bestätige ich.

5. Die Bedeutung der eidesstattlichen Versicherung und die strafrechtlichen Folgen einer unrichtigen oder unvollständigen eidesstattlichen Versicherung sind mir bekannt.

Ich versichere an Eides statt, dass ich nach bestem Wissen die reine Wahrheit erklärt und nichts verschwiegen habe.

………………………………………….   ……………………….………

Ort und Datum   Unterschrift

[1] Nicht Zutreffendes streichen. Bei Bejahung sind anzugeben: der Titel der andernorts vorgelegten Arbeit, die Hochschule, das Jahr der Vorlage und die Art der Prüfungs- oder Qualifikationsleistung.